Patient Dosimetry in Nuclear Medicine

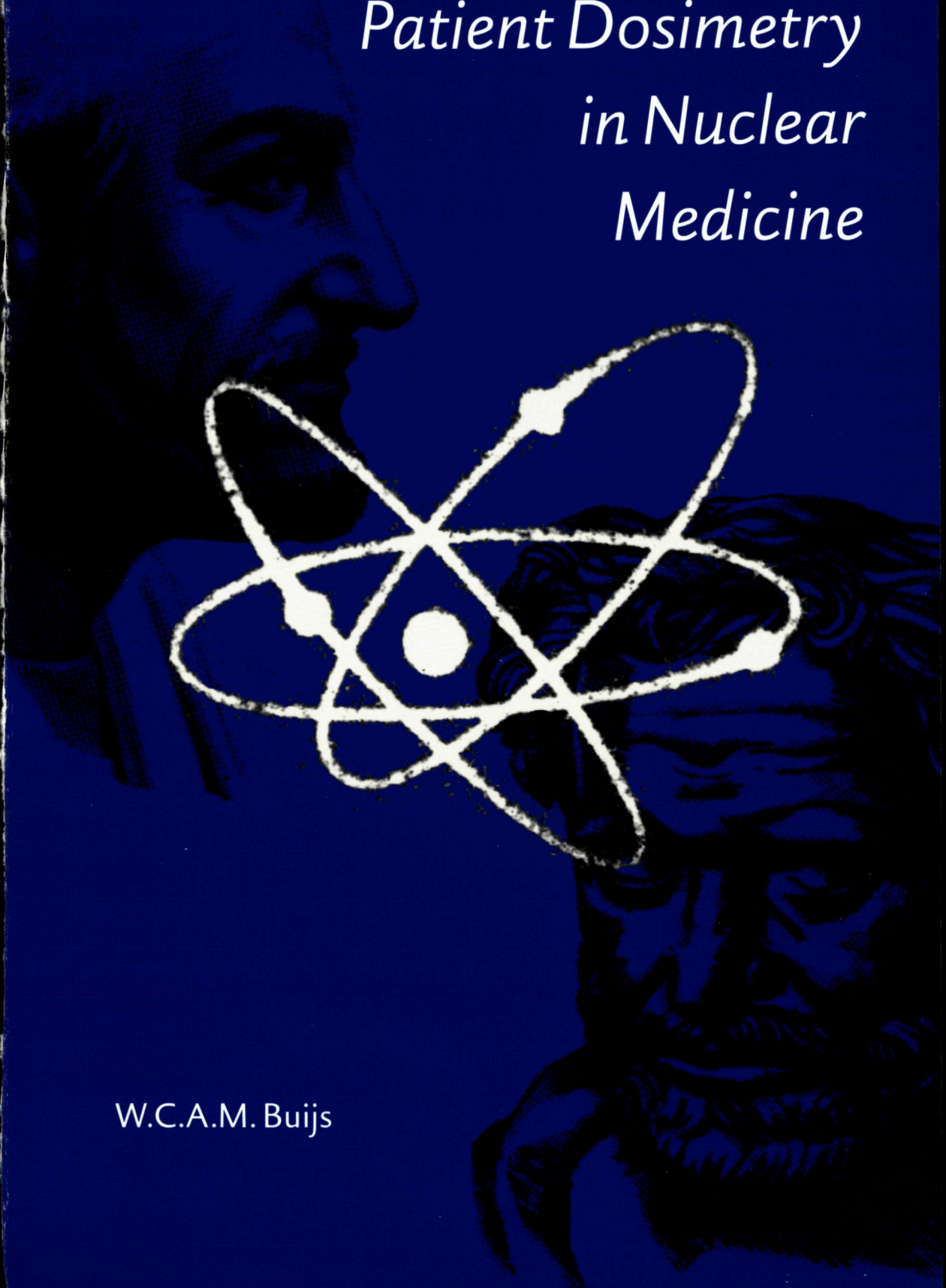

W.C.A.M. Buijs

CIP GEGEVENS KONINKLIJKE BIBLIOTHEEK, DEN HAAG
Buijs, Wilhelmina Clementina Adriana Maria
Patient Dosimetry in Nuclear Medicine / Wilhelmina Clementina Adriana Maria Buijs
Proefschrift Katholieke Universiteit Nijmegen – met literatuuropgave – met samenvatting in het Nederlands
ISBN 90 9012 177 3
NUGI 743
Subject headings: nuclear medicine; dosimetry; ovarian cancer; thyroid cancer; infection

Design & layout: G. Vroon, Grafisch Bureau G&T, Nijmegen
Printing: Drukkerij S.S.N., Nijmegen
Cover illustrations and concept: J. Troost
The application of radionuclides in nuclear medicine, as presented in this thesis, balance at the interface between physics (Democritos, right) and medicine (Hippocrates, left)

Patient Dosimetry in Nuclear Medicine

Een wetenschappelijke proeve
op het gebied van de Medische Wetenschappen

Proefschrift
ter verkrijging van de graad van doctor
aan de Katholieke Universiteit Nijmegen,
volgens besluit van het College van Decanen
in het openbaar te verdedigen op
vrijdag 4 december 1998
des namiddags om 1.30 uur precies

door

Wilhelmina Clementina Adriana Maria Buijs

geboren te Hoeven

Promotor: Prof Dr. F H M. Corstens

Co-promotor Dr O C Boerman

Manuscriptcommissie·

Prof Dr A van der Kogel
Prof Dr J J Broerse (Rijksuniversiteit Leiden)
Prof. Dr P W.C. Kloppenborg

The studies presented in this thesis were performed at the Department of Nuclear Medicine (Head. Prof Dr F H M Corstens), University Hospital Nijmegen, The Netherlands

Table of Contents

List of Abbreviations

AUC	area under the curve
Bq	becquerel
Ci	curie
cMOv18	chimeric monoclonal antibody MOv18
CT	X ray computed tomography
cpm	counts per minute
d	day
DIBF	depth independent buildup factor
DTPA	diethylenetriaminepentaacetic acid
E	effective dose
EDE	effective dose equivalent
^{67}Ga	radionuclide gallium-67
GM	geometric mean
Gy	gray
h	hour
^{131}I	radionuclide iodine 131
ICRP	International Commission on Radiological Protection
IgG	immunoglobuline G
^{111}In	radionuclide indium 111
ID	injected dose
ip	intraperitoneal
iv	intravenous
keV	kiloelectronvolt
L	liter
MAb	monoclonal antibody
MBq	megabequerel
min	minute
MIRD	Medical Internal Radiation Dosimetry
ml	milliliter
^{99}Mo	radionuclide molybdenum 99
MRI	magnetic resonance imaging
MTD	maximum tolerable dose
OV-TL 3	monoclonal antibody OV-TL 3
PET	positron emission tomography
pi	post injection
RIT	radioimmunotherapy
ROI	region of interest
s	second
sd	standard deviation
SEM	standard error of the mean
SPECT	single photon emission tomography
Sv	sievert
^{99m}Tc	radionuclide technetium 99m
^{201}Tl	radionuclide thallium 201
TLD	thermo luminescent dosimeter
y	year

CHAPTER 1

Introduction

AIM OF THE STUDY

Nuclear medicine is a multidisciplinary specialty with growing impact in diagnostic and therapeutic patient care. In the Netherlands each year 250 000 diagnostic examinations and more than 4 000 therapeutic treatments are performed, using in-vivo administration of radionuclides. The development of new radiopharmaceuticals and of new imaging techniques is based on a combined effort of nuclear medicine physicians, chemists, pharmacists, physicists and other scientists.

The absorbed dose from internally deposited radionuclides is a major factor in assessing risk and therapeutic utility when evaluating new radiopharmaceuticals in use or proposed for diagnosis or for treatment. Absorbed dose is a quantity that usually is estimated from the localized uptake and retention of administered radiopharmaceuticals, the radiation decay data of the radionuclide and simulations of radiation transport in anthropomorphic models. Accurate estimation of the absorbed dose in organs, in other tissues and in the whole body after administration of radiopharmaceuticals in patients, is important to assess the radiation risk in nuclear medicine diagnosis. Furthermore it can be used to predict the tumor dose delivered in radionuclide treatment. Both aspects form the basis of the aim of the studies as described in this thesis.

OUTLINE OF THE THESIS

The concepts of the methods in dosimetry are summarized in chapter 2. In chapter 3, the principles of methods to determine the absorbed dose in nuclear medicine are discussed. Quantification of the actual activity present in an organ is a complex matter. One of the important issues that needs to be addressed when the amount of activity in a tissue has to be determined, is the method to correct for activity in the background. A newly developed method for background correction is described in chapter 4. The results obtained with this method are compared with other frequently used methods. In chapter 5, dosimetry analyses in the context of thyroid volume reduction using ^{131}I – a relatively novel treatment modality – is described.

The absorbed dose after administration of commonly used radiopharmaceuticals is relatively well known. In the last decade, research at the Department of Nuclear Medicine of the Nijmegen University, has focussed on the development

of new radiopharmaceuticals for the detection of infection and inflammation and on the optimization of the use of monoclonal antibodies for radioimmunotherapy of cancer. Therefore, the second part of this thesis deals with dosimetry calculations of two new diagnostic radiopharmaceuticals for infection imaging and of two new agents developed for ovarian cancer diagnosis and its treatment. In chapter 6 the absorbed dose after administration of ^{111}In-IgG and of ^{99m}Tc-IgG, both agents for infection detection, was estimated. In chapter 7 a new method for estimating the absorbed dose in the red marrow after injection of ^{111}In-IgG is described and compared with the results as obtained in chapter 6. Using new techniques for quantification of activity in organs, absorbed doses of ^{111}In-OV-TL3 $F(ab')_2$ and of ^{131}I-cMOv18 IgG, two monoclonal antibodies directed against ovarian cancer, are estimated in chapter 8 and 9. In chapter 10 the effective doses for the radiopharmaceuticals as described in this thesis were compared with the effective doses for routinely nuclear medicine diagnostic procedures.

CHAPTER 2

Dose Concept, Radiation Risks and Detrimental Effects

RADIOBIOLOGY

Ionizing radiation, such as emitted by radiopharmaceuticals, may cause changes in atoms or molecules, and may thus damage cells. This may either lead to cell death or to viable but modified cells. These two outcomes may have profoundly different implications for the organism as a whole *(1)*. If the number of lost cells is large enough, there will be obvious damage reflected by loss of tissue function. The probability of causing such harm will be zero at small doses but above a particular dose level (the threshold) it will increase to unity (100%). Above the threshold, the severity of the harm will increase with dose. Such an effect is called "deterministic". Examples are: sterility due to loss of function of the reproductive organs, hypothyroidism due to destruction of thyroid tissue, cataract due to damage of the eye lens, or myelosuppression after red marrow irradiation. These effects may occur immediately or shortly after acute irradiation.

When irradiated cells are modified rather than killed the situation is different. In this situation the cell may acquire a malignant phenotype, or in case of germ cells, cells may fail to transmit genetic information in an appropriate way. The probability of a cancer or genetic defect resulting from radiation usually increases with dose, probably without a threshold. The severity of the effect is not affected by the dose. Such an effect is called "stochastic" meaning "of a random or statistical nature". If damage occurs in a cell whose function is to transmit genetic information to later generations, any resulting effects, which may be of many different kinds and severity, are expressed in the progeny of the exposed person. This type of effect is called "hereditary".

BASIC DOSIMETRIC QUANTITIES

The fundamental dosimetric quantity in radiological protection is the absorbed dose. This is the energy absorbed per unit mass and its unit is joule per kilogram, or gray (Gy). The probability of stochastic effects does not only depend on the absorbed dose, but also on the type and energy of the radiation causing the dose. This is taken into account by weighting the absorbed dose by a factor related to the nature of the radiation. The resulting parameter is called "equivalent dose" and its unit is the sievert (Sv). For the types of radiation used in nuclear medicine (gamma and beta-radiation), the values for absorbed dose and the equivalent dose are equal (1 Sv = 1 Gy).

EFFECTIVE DOSE

The relationship between the pi obability of stochastic effects and equivalent dose depends on the organ or tissue irradiated Therefore, a further quantity, called effective dose (E) is derived from equivalent dose, to indicate the combination of different doses to several tissues in a way which is likely to correlate well with the total of stochastic effects *(1)* The effective dose is the sum of the weighted equivalent doses in all tissues and organs in the body It is calculated by the formula

$$E = \sum_T w_T \; H_T$$

where H_1 is the equivalent dose in organ T and w_T is the weighting factor for tissue T The tissue weighting factor w_1 represents the relative contribution of that organ or tissue to the total detriment due to stochastic effects resulting from uniform irradiation of the whole body The unit of E is joule per kilogram or sievert (Sv)

RISK ESTIMATES

The total health detriment from exposure to ionizing radiation, also called aggregated detriment, includes the fatal cancer rate for each organ, the relative length of life lost, the contribution from nonfatal cancer morbidity and serious hereditary damage for all generations subsequent to the exposure *(1)*

The radiation risk factors are derived from epidemiological information in an exposed study population at high dose rates and high absorbed doses (e g from the Japanese atomic bomb survivors) Applying the risk factors (%/Sv) as found in these studies, to diagnostic medical exposures with low absorbed doses and low dose rates, an overestimation of the risks will occur Therefore, ICRP has introduced a Dose and Dose Rate Effectiveness Factor (DDREF) A DDREF of 2 has been included in the pi obability coefficients foi all equivalent doses resulting from absorbed doses below 0 2 Gy and from higher absorbed doses when the dose rate is less than 0 1 Gy per hour The nominal probability coefficients (also called nominal detriment coefficients), provide a reasonably good indicator of the detriment in a population exposed in diagnostic radiology and nuclear medicine *(2,3)*

The nominal detriment coefficients for individual tissues and organs, are presented in Table 1, together with the tissue weighting factors w_T The tissue weighting factors are defined in relation to the nominal detriment coefficient
The overall risk for radiation damage (nominal detriment coefficient) is 7 3 %/Sv *(1,2)*

TABLE 1

Nominal fatality and detriment coefficients for individual organs and tissues [a] *and tissue weighting factors* [b]

Tissue or organ	Nominal fatality coefficient (10^{-2}/Sv)	Nominal detriment coefficient (10^{-2}/Sv)	Tissue weighting factor w_T
Bladder	0.30	0.29	0 05
Bone marrow	0.50	1.04	0.12
Bone surface	0.05	0 07	0.01
Breast	0 20	0 36	0 05
Colon	0 85	1.03	0 12
Liver	0 15	0.16	0 05
Lung	0 85	0.80	0 12
Oesophagus	0 30	0.24	0 05
Ovary	0.10	0 15	–
Skin	0 02	0.04	0 01
Stomach	1 10	1 00	0 12
Thyroid	0 08	0.15	0 05
Remainder	0.50	0 59	0 05
Sub-total	5.00	5 92	0 80
	Probability of severe hereditary disorders	Hereditary detriment	
Gonads	1 00	1.33	0 2
Total (rounded)	6.0	7.3	1 0

a The values relate to the whole population of equal numbers of both sexes and a wide range of ages The data in column 2 and 3 are obtained from Table 1 in ICRP 73 *(2)*

b The tissue weighting factors in column 4 are obtained from Table 4 in ICRP 60 *(1)*

REFERENCES

1 ICRP Publication 60. 1990 *Recommendations of the International Commission on Radiological Protection* Oxford Pergamon Press, Annals of the ICRP 1991, 21. no 1-3.

2 ICRP Publication 73 *1996 Radiological Protection and Safety in Medicine* Oxford: Pergamon Press, Annals of the ICRP 1996, 26 no 2

3 UNSCEAR (1993) *Sources and Effects of Ionizing Radiation* United Nations Scientific Committee on the Effects of Atomic Radiation, 1993 Report to the General Assembly with Annexes. United Nations, New York

CHAPTER 3

Dosimetric Methods and Quantitative Techniques in Nuclear Medicine: An Overview

Wilhelmina C.A.M. Buijs, Jeffry A. Siegel, Frans H.M. Corstens

INTRODUCTION

Already more than 60 years, radiopharmaceuticals are beneficially applied for medical diagnosis and therapy A potential side-effect of these applications is the radiation risks to patients To estimate the radiation risk for new radiopharmaceuticals, knowledge of the absorbed doses in patients after administration of that radiopharmaceutical is mandatory The radiation risk for a diagnostic procedure should be weighed against the expected benefits of the examination to accurately diagnose the disease in relation to other diagnostic procedures (justification) If treatment with radiopharmaceuticals is considered, the absorbed dose in the pathological site (e g tumor) and in healthy organs should be estimated based on tracer studies in the individual patient Using these data the amount of activity to be administered to reach the therapeutic effect can be calculated and the risk for the healthy organs can be estimated

For accurate estimation of the absorbed dose in the body after administration of a radiopharmaceutical knowledge of the distribution of activity in the total body and the excretion rate of the activity from the body is necessary The most frequently used quantitative techniques are total-body gamma camera imaging at various time points after administration, single probe non-imaging detectors, exposure rate meters and serial measurements of radioactivity concentration in blood, urine and feces After analysis of the activity uptake in organs, whole body, blood and excreta and processing of these data using metabolic models, the absorbed dose can be estimated The standardized techniques for these determinations are described

When estimating the activity uptake from planar images, accurate correction for background activity, attenuation and scatter should be applied The pros and cons of the current methods will be discussed

1 THE MIRD SCHEMA

In the early 1960 s, the Medical Internal Radiation Dose (MIRD) committee, a committee of the Society of Nuclear Medicine from the United States, started to develop a methodology for estimating the absorbed dose from radiopharmaceuticals Since then, the committee has published a large number of pamphlets and reports which described the general dosimetric methods and applications of these methods for a variety of radiopharmaceuticals Currently, the MIRD schema is a widely accepted methodology in nuclear medicine *(1-3)*

The International Commission on Radiological Protection (ICRP), also has a methodology to estimate the absorbed dose in workers who were accidentally contaminated with radioactive agents via inhalation or ingestion The principal goal of the ICRP is to derive absorbed dose limits based on the maximum

amount of activity that can be inhaled or ingested by radiation workers (or members of the public). This has led to the development of occupational dose limits, or dose limits for members of the public. Later on, the ICRP published absorbed dose and effective dose estimates for a large number of radiopharmaceuticals for healthy adults as well as for children *(4,5)*. Dosimetric data were also published for patients with abnormal metabolism due to the presence of disease.

ABSORBED DOSE

An accurate determination of the time dependent activity in tissues of the body is required to calculate the absorbed dose to target organs of the body using the MIRD schema *(1,2)*. Source organs (or regions) are defined as those which contain significant concentrations of the radionuclide. Target organs are those for which the absorbed dose is calculated (source organs should always be considered as target organs as well; however, the dose to other target regions is usually of interest). The absorbed dose is defined as the energy absorbed per unit mass. The mean absorbed dose to tissue is given in the MIRD schema by $D = \tilde{A} \times S$, where D is the mean absorbed dose (Gy or rad [1Gy = 100 rad]), $\tilde{A}$ is the cumulated activity (Bq.s or mCi.h [1Ci = 3.7×10^{10} Bq]), and S is the mean absorbed dose per unit cumulated activity (Gy/Bq.s or rad/mCi.h). The absorbed dose to the target may also be expressed in terms of absorbed dose per unit administered activity. The source organ residence time τ, is defined as $\tau = \tilde{A}/A_0$ where A_0 (Bq or mCi) is the administered activity. Therefore, the mean dose to the target per unit administered activity is given by $D/A_0 = \tau \times S$. The estimation of absorbed dose is thus dependent upon two types of information.

1. Time-dependent factors – those incorporated within $\tilde{A}$ or τ, and
2. Time-independent factors – those represented within S.

The time-dependent factor $\tilde{A}$ incorporates characteristics of both uptake and retention of activity in the organs of interest and includes consideration of the physical half-life of the radionuclide and the biological half-life of the radiopharmaceutical. The time-independent factor S includes consideration of the types and energies of the radiations emitted, geometrical aspects such as the size and shape of the source and target regions and the distance between them, and the composition of the absorbing and intervening media.

To determine the cumulated activity in the desired source regions/organs, serial measurements of region activity must be made following administration of the radiopharmaceutical. A general principle for collecting activity data in vivo is that quantitative procedures or calculations must account for all the activity administered. A minimum number of quantitative measurements must be made for each source region with an appropriate temporal sampling frequency. The latter depends upon the pattern of the uptake and retention of the

activity in the various source organs or regions Serial measurements of activity in the source regions can be performed using quantitative imaging (including planar scintillation camera, SPECT or PET), external non-imaging radiation monitoring, tissue sampling (blood or biopsy) and excreta counting Total body retention may be determined using whole-body quantitative imaging, external probe monitoring (non-imaging), and/or from quantitative total recovery of body excreta Activity in blood is readily obtained by direct sampling The resulting activity-time curve obtained for each source region can be analyzed using several different techniques to provide $\tilde{A}$ or τ, for use in absorbed dose calculations

II. DATA COLLECTION

To determine the activity-time profile of the radioactivity in source regions, four questions need to be answered

1 Which regions are source regions?
2 How fast does the radioactivity accumulate in these source regions?
3 How long does the activity remain in the source regions?
4 How much activity is in the source regions?

The first question concerns identification of the source regions, while the second and third questions relate to the appropriate number of measurements to be made in the source regions as well as the timing of these measurements The fourth question is addressed through quantitative external counting and/or sampling of tissues and excreta

Each source region must be identified and its uptake and retention of activity as a function of time must be determined This provides the data required to calculate cumulated activity or residence time in all source organs Each organ exhibiting significant radionuclide uptake should be evaluated directly where possible The remainder of the body (total body minus the source organs) must usually be considered as a potential source also Compartmental modeling can be used to separate the activities in organs which overlap on imaging studies, such as the renal cortex and renal pelvis or the liver and right colon Some compartmental models are complex and include compartments representing many different biological processes Several computer software packages (SAAM, CONSAM, STELLA, BMDP, a o) are available to solve the equations associated with the different compartmental models *(6-8)*

IDENTIFICATION OF SOURCE REGIONS

The types of measurements required for identifying source regions can be categorized into four basic groups imaging, discrete probe monitoring (whole

body or organ counting), tissue sample (blood or biopsy) counting, and excreta counting. Literature on humans or animal studies along with ex vivo or in vitro data may yield valuable information to assist in identifying tissues that accumulate a particular radiopharmaceutical. This information, if available, may serve as the basis for designing the preliminary data acquisition protocol.

The distribution of a radiopharmaceutical in the body can be determined by sequential imaging methods. Quantitative data can be obtained from planar scintillation camera images or tomographic SPECT or PET images. Because of the time-consuming and more complex nature of quantifying SPECT and PET tomographic image data, conjugate view quantitative planar imaging, using anterior and posterior views, is often the most widely used method *(9,10)*. The whole-body imaging capability of current single- and dual-head scintillation cameras is especially useful for this purpose. Total body measurements may also be obtained with an external non-imaging radiation probe. In addition, source regions can be identified by tissue and excreta sampling. All measurements must provide quantitative results in terms of absolute activity (Bq) or percent or fraction of administered activity within source regions.

For determining source region volume, especially for tumors or abnormal-sized organs where standard phantom geometry may be inadequate, the tomographic capability of SPECT or PET may be required. Independent imaging modalities such as X-ray computed tomography (CT) or magnetic resonance imaging (MRI) may also be used for source volume determination provided a one-to-one correspondence exists between uptake and anatomic structure.

TEMPORAL SAMPLING

After the source regions have been identified, the activity retention in these regions must be determined to answer the questions: How fast does the activity get to the various source regions, and how long does the activity stay there? The calculation of absorbed dose requires that the region and total body uptake, washout and long-term retention be characterized. There are four basic kinetic models:

1. Instantaneous uptake (wash-in) with no biological removal,
2. Instantaneous uptake with removal by both physical decay and biological elimination (washout),
3. Non-instantaneous uptake with no biological removal, and
4. Non-instantaneous uptake with removal by both physical decay and biological elimination.

Selection of optimal time points for sampling radiopharmaceutical biodistributions in humans with the objective of defining the uptake and retention pattern is dependent upon the biokinetic variables to be measured, e.g., effective half-lives

Relevant quantitative data for similar radiopharmaceuticals obtained in animal or human trials may serve as a guide for the initial choice of these time points. The selection of the sampling times can have a significant effect on parameter estimation precision *(11)*.

DATA ACQUISITION

The acquisition of count data for the source regions can be performed with a number of measurement techniques. They include:

1. Quantitative imaging with a planar scintillation camera or tomographic SPECT or PET system,
2. External non-imaging radiation monitoring with a NaI probe or GM survey meter,
3. Tissue sample counting of the blood or biopsy specimen, and
4. Excreta counting (e.g. urine and feces).

The technique employed depends on the nature of the source region. For instance, the total body activity can be measured by whole body monitoring with a non-imaging device, whole body imaging or stationary counting with a scintillation camera, or quantitative recovery of body excretions. Individual tissue activity can be determined by quantitative imaging, blood sampling, and biopsy specimen measurement.

III. DATA ANALYSIS

Estimation of absolute organ activity for the purpose of patient-based dosimetry in radionuclide therapy or radioimmunotherapy (RIT) is of growing interest. The measurement of the biodistribution of radiopharmaceuticals and the use of these data in the Medical Internal Radiation Dose (MIRD) schema *(1,2)* provides a primary means to calculate absorbed doses from internally deposited radionuclides.

A series of physical factors contribute to the difference between measured activity and actual activity in source regions based on planar scintigraphy. Accurate estimation of the activity in an organ from the measured count rate, requires correction for the system calibration factor (measured count rate per MBq), attenuation, scatter, overlying tissue, background activity, organ- and patient thickness and physical decay of the radionuclide used. Because activity in under- or overlying organs and irregular distribution of background may interfere with accurate quantification, SPECT imaging has the potential to improve the accuracy of planar imaging measurements. However, because of the time-consuming and more complex nature of quantifying SPECT image data, there is a need for an accurate and simple quantification method based on planar

imaging A number of techniques for activity quantification of planar images have been reported most of them dealing with attenuation correction using the conjugate view counting method *(9 27)*

CONJUGATE VIEW COUNTING

The most commonly employed imaging method for quantitation of radioactivity in vivo utilizes 180° opposed planar images (known as the conjugate view approach) in combination with transmission data through the subject and a system calibration factor *(10,13 15)* This technique offers an improvement over the single view procedures involving comparison with a standard phantom under fixed geometry in that the rigorous mathematical formalism for conjugate view quantitation provides correction for source thickness, inhomogeneity, and attenuation Of significance is the fact that calculational results are theoretically independent of the source depth in tissue The transmission scan which involves counting an external source of activity through the source region of interest to correct for attenuation, is generally performed at one time point either at the beginning of the study before the administration of the radiopharmaceutical, or at a later time with appropriate correction made for activity in the body

The conjugate view image pair is typically an anterior and posterior (A/P) image of the source region, although any true 180° opposed set might be utilized (e g , right and left lateral) This conjugate image pair is acquired at the selected sampling times post-administration for which quantitative data is desired, in cases where source region activity is not time dependent, a single conjugate view measurement may be adequate Modern dual headed scintillation cameras provide a convenient means for simultaneous acquisition of the two images and commonly allow capability for whole body A/P scans The latter represents an efficient protocol for obtaining total body data as required for biodistribution studies However, single head camera systems may be used with repositioning and re-imaging as necessary to obtain the conjugate view The system calibration factor is required to convert the source region count rate into absolute activity The calibration factor should be measured at each acquisition time point to document that the system response remains constant or to account for any change in performance which might affect the observed count rate

MATHEMATICAL FORMULATION OF THE CONJUGATE VIEW METHOD

The activity A_j of a single uniform source, embedded in a non-radioactive medium consisting of n regions of thickness, t_i, with differing linear attenuation coefficients, $\mu_i(cm^{-1})$, is given by the expression *(10)*

$$A_j = \sqrt{\frac{IAIP}{e^{\mu_e t}} \frac{f_j}{C}} \qquad (1)$$

where

$$f_j \equiv \frac{(\mu_j t_j / 2)}{\sinh (\mu_j t_j / 2)} \qquad (2)$$

$$\mu_e = (1/t) * \sum_1^n \mu\, t_i = \mu_j + (1/t) * \sum_1^n (\mu - \mu_j)t \qquad (3)$$

and I_A and I_p (counts per time) refer to the external conjugate view counting pair (anterior/posterior) across the overall patient thickness The factor f_j represents a correction for the source region attenuation coefficient (μ_j) and source thickness (t_j) (i e , source self-attenuation correction) The expression $e^{\mu_e t}$ represents the transmission factor (T) across the patient thickness t through the region of interest with overall effective linear attenuation coefficient μ_e and may be determined directly by measuring the ratio of the count rates I/I_o obtained using the appropriate radioisotope both with (I) and without (I_o) the patient in position The system calibration factor C (count rate per unit activity) is obtained by counting a known activity for a fixed period of time within a standardized geometry in air relative to the scintillation camera using designated camera acquisition settings

The conjugate view technique allows determination of activity within the volume of interest without requiring knowledge of the depth of the source region and without dependence upon assumptions inherent in single view phantom simulations The factor f_j (≤ 1.0) involves only the source region characteristics and will not deviate significantly from 1 0 until μ_j or t_j become large The thickness of an organ may be estimated by acquiring a scaled orthogonal view (e g , a lateral image) and taking direct measurements from the image

SCATTER CORRECTION

The above analytical methods have been derived under the model of narrow-beam geometry in which scatter effects are negligible The investigator must verify that these conditions are met for his/her experimental data acquisition configuration before applying these methods High resolution collimators and narrow, asymmetric energy window settings assist in approximating these conditions However, in most nuclear medicine imaging applications, broad-beam geometry predominates and scatter effects are significant The presence of scat-

tered photons originating from outside the source organ region-of-interest will artificially inflate the ROI count-density and introduce errors in the quantification of radioactivity. The following approaches are designed to correct for scatter:

a. Pseudoextrapolation Number *(28)*
b. Buildup Factor Method *(15, 21-24)*
c. Multiple Energy Window Techniques (dual and triple) *(29-34)*
d. Digital Filtering Techniques and Energy Weighted Acquisition *(35-43)*

At present none of the correction methods has been adopted as the standard method for clinical use *(44)*.

BACKGROUND SUBTRACTION

In practice the primary source region of interest is frequently surrounded by radioactivity residing in adjacent tissues. This so-called "background" activity may arise from radionuclide concentration in blood, extracellular fluid, or soft tissue. Utilization of conjugate view data to determine the absolute activity in the source volume according to the analytical method described in Equation 1 would overestimate the activity because the overlying and underlying background activity contribute counts to each view. Conventional background subtraction, i.e., subtraction of the background count rate from the source region count rate, does not consider the portion of the background equivalent to the source region volume and may underestimate the source region activity due to oversubtraction of background *(25,27,45)*. In addition, defining background ROIs is sometimes difficult as care must be taken to avoid hot or cold areas, such as major blood vessels.

SINGLE PHOTON EMISSION COMPUTED TOMOGRAPHY (SPECT) TECHNIQUES

Because activity in under- or overlying regions and irregular distribution of background may interfere with accurate quantification, SPECT imaging has the potential for improving the accuracy of planar imaging measurements. Quantitative SPECT *(46-51)* enables the determination of actual tissue activity concentration (e.g., MBq/cm^3) and the associated total volume (e.g., cm^3) over which the activity is distributed. Although attenuation correction schemes, non-optimal statistics, collimator resolution, and scatter result in some limitations to the accuracy of quantitative SPECT determinations of radioactivity, SPECT imaging can provide major advantages over planar conjugate pair imaging for selectively detecting and discriminating activity in source tissues from surrounding structures. The use of SPECT is particularly advantageous for measuring activity in regions where activity in contiguous overlying, underlying, or adjacent structures limit the accuracy of the conjugate pair planar view

measurements The use of appropriate SPECT acquisition parameters a suitable reconstruction algorithm for image reconstruction and image processing, a properly calibrated imaging system and a constant distribution of radiopharmaceuticals during the imaging procedure can all provide an accurate assay of radioactivity in vivo *(46-51)*

To date, the majority of reports have involved the use of a single rotating scintillation camera for SPECT image acquisition to determine activity in regions and tissues The relatively low sensitivity of these systems has held-back development of correction techniques that would allow improved accuracy for quantificating non-uniform activity distributions in inhomogeneous and irregularly-shaped attenuation media *(46 48,51 55)* Numerous approaches have been implemented to correct for the limited counting statistics available from conventional SPECT imaging Multiple detector SPECT systems either multi-camera or ring systems and utilization of fanbeam and conebeam collimators have each contributed to the improvement of the counting statistics available for SPECT The use of filter functions with cutoff frequencies matched to the system spatial resolution has proven to be useful for reducing the effects of statistical uncertainty *(56-58)*

In spite of the limitations, SPECT has been used to measure activity levels in source tissues with acceptable accuracy and precision The SPECT system must be properly calibrated to ensure acceptable reconstructed uniformity sensitivity, spatial resolution, linearity, and count rate performance Acquisition variables must be selected to provide adequate counts per view, appropriate spatial and angular sampling, and the desirable imaging orbit Selection takes into consideration the intrinsic and system performance properties, *in vivo* activity levels at the time of measurement and the determination of imaging times based on subject comfort as well as the uptake and clearance properties of the radiopharmaceutical In addition suitable software for image reconstruction and image processing is necessary *(46 50)* Research into new methods for improving SPECT quantitation is underway, and the approaches for activity quantification in vivo are expected to change as new methods are validated for scatter and attenuation correction

Quantitative SPECT scans can be used for all imaging time points if the tomograph has sufficient sensitivity to keep acquisition time to reasonable intervals so that patients will tolerate the procedure Alternatively, the sequential images can be acquired by planar procedures, with a SPECT image taken at one time point during the study The result from the SPECT scan can be used to constrain the planar data at that point Then, assuming that the image contrast is time invariant, one can apply the correction factor required for that constraint to the earlier and later planar-imaging results *(59)*

Reasonably accurate and precise quantitative SPECT imaging is clinically

feasible, even without sophisticated scatter corrections, at least in uniformly attenuating parts of the body such as the abdomen and pelvis *(47)* With Chang s first order postprocessing method of attenuation compensation *(60)*, the most commonly used approach in commercial SPECT systems, investigators have obtained fairly accurate activity estimates using a semi-automated processing method employing thresholding *(61 62)* The attenuation-corrected reconstructed slices are used to obtain source region activity based on a fixed threshold method Briefly, all the reconstructed slices spanning the object of interest typically are analyzed to determine the maximum voxel count Only voxels containing more than a predetermined percentage of this maximum count, as derived from phantom studies, are included for the activity calculation The activity is determined from the sum of the counts in the included voxels divided by the acquisition time and an independently acquired count rate per unit activity system calibration factor In addition to threshold methods *(63 64)* image segmentation has also been based on edge detection

It should be pointed out that any technique which does not specifically compensate for scatter will not be rigorously correct especially in the presence of low-energy photons which are known to contribute a significant amount of scatter In areas of nonuniform density, such as the thorax, it is necessary to incorporate a nonuniform attenuation map in the Chang attenuation compensation method *(60)* Also the use of a fixed threshold method to distinguish between source and background voxels is based on a global maximum and can be incorrect if the activity in the selected volume of interest changes rapidly with time In addition, Mortelmans et al *(64)* reported that a single fixed threshold value may not be accurately enough because the threshold value was found to be dependent upon object size and image contrast

QUANTITATIVE MEASUREMENT TECHNIQUES: NON-IMAGING

A EXTERNAL NON-IMAGING RADIATION MONITORING

Whole body retention can be estimated by placing a shielded NaI detector or other suitable survey meter 3 to 7 meters from the patient and recording the number of counts detected *(65)* A source of known activity is used to calibrate the detector Initial measurements for the total body must be made within a short time after administration, defined as within the "no patient excretion" period, so that later measurements may be easily and more accurately compared to initial body content of the administered activity and to the reference standard The use of a reference standard measured at each time corrects for radioactive decay and for instrumental drifts Whole body counters with dual-opposed NaI(Tl) detectors have also been used to measure whole body radioactivity *(20,26,66,67)*

B. TISSUE SAMPLE COUNTING

The most frequently sampled tissue is blood *(68)*. The temporal variation of activity in blood may be important for assessing bone marrow dose and providing input functions and central compartments for some compartmental models. If bone marrow dosimetry is desired, the hematocrit and the red marrow extracellular fluid fraction for the patient should also be obtained *(69)*. Activity may be determined using a variety of instruments including dose calibrators, gamma well counters, and liquid scintillation counters. A calibrated (through the use of appropriate standards) gamma well counter is commonly used to obtain serial blood activity concentration (Bq/ml). Typically, 1-3 ml of blood are withdrawn by peripheral venipuncture from the patient at various times post administration such as 5, 10, 15, 30, 60, 120 min, 24 h, 48 h, and 72 h. Samples may need to be taken at later times postinjection depending on the half-life of the radionuclide and the blood retention rate.

An estimate of the activity retained in tissues and regions may be obtained through serial biopsy sampling of the tissue of interest *(70)*. Most frequently, this is not a viable option. However, in therapeutic radionuclide protocols, biopsy samples or tissue samples might be obtained after surgical resection from one or more tissues of interest, such as tumor, liver, lymph node, etc. Also a tissue may be biopsied for other clinical reasons and a sample obtained (or portion thereof) for quantification in a calibrated well counter. The biopsy sample may be useful in deriving an empirical conversion factor (count rate/activity) for scintigraphic images of the same tissue in vivo.

C. EXCRETA COUNTING

Characterization of the total amount (or fraction) of activity excreted, excretory rates and routes of excretion are essential for estimating absorbed doses *(68)*. However, direct measurement of excretion rates per se is rarely performed. Total body retention as determined from imaging or radiation monitoring may be used to assess excreted activity The four major routes of excretion are urine, feces, perspiration and exhalation. Of the excretory pathways, the fraction of the administered activity excreted in the urine is most easily determined. Urine collection is the method of choice.

IV DATA PROCESSING

CURVE FITTING AND DETERMINATION OF $\tilde{A}$ AND τ

The activity (number of nuclear transitions per unit time) in region h is a function of time t and is symbolized as $A_h(t)$. From serial activity measurements (obtained from external counting, tissue sampling, or excreta sampling), one can

determine the area under the activity-time curve, $\tilde{A}$ (2) The cumulated activity, $\tilde{A}_h$, is the sum of all nuclear transitions in region h during the time interval of interest. The residence time, τ_h, is obtained by dividing $\tilde{A}_h$ by the administered activity, A_0.

Several methods are available for determining $\tilde{A}_h$ from graphical representations of A_h (t). Among these are numerical methods such as the trapezoidal rule *(71)* and Simpson's rule *(72)*, and analytical methods *(73)*, based on the assumption that some fitting function can adequately describe the data.

A potential problem in estimating the area under the activity-time curve concerns the segment of the curve beyond the period of data sampling. Large under- or over-estimation errors may occur, if extrapolation beyond the data set is based on the observed biological removal from earlier phases of the curve or based on the conservative assumption that removal from the body is only by physical decay, respectively *(74)* For example, in radioimmunotherapy, there may be complete tumor retention of the antibody. However, image data points are often obtained only up to 96 or 120 hours post injection, making extrapolation of the terminal portion of the curve necessary *(75,76)*. Fitting a flat curve beyond the measured data (this means that no radiolabeled antibody is cleared from the tumor) can result in 100% overestimation of the absorbed dose to the tumor compared to the curve resulting from a curve fit using an exponential function over the measured data range *(76)*.

V. ABSORBED DOSE ESTIMATES

Within the MIRD schema, software phantoms have been developed for adults, newborn and children of 1, 5, 10 and 15 years of age (3). Also, software phantoms were developed for the adult female during various stages of pregnancy: at 3, 6 and 9 months *(77)*. Using the PC computer program MIRDOSE3, developed by the Oak Ridge group for internal dosimetry, S-factors for all these phantoms can be calculated for a combination of 26 source organs and 25 target organs for 223 different radionuclides *(78)*. The residence times, in hours, calculated for the source organs and for the remainder of the body in a patient, or from any biokinetic model, can be entered in this computer program. After selecting the relevant software phantom and radionuclide and then entering the appropriate source organ residence times, target organ absorbed doses, effective dose and effective dose equivalent are determined. These results are given in conventional units, rad/mCi and rem/mCi, as well as in mGy/MBq and mSv/MBq, for organ doses and effective dose, respectively.

FETAL DOSE

The calculation of absorbed dose estimates to the fetus is often important in nuclear medicine. The simplest method of estimating the dose to the embryo or fetus after administration of a radiopharmaceutical to the mother is to use the absorbed dose to the maternal uterus. Data for specific absorbed fractions of photon energy in pregnant women are published by Stabin et al. *(79)*. For some radiopharmaceuticals data for placental transfer are available, so that dose estimates can be calculated more accurately. Most of the information concerning placental crossover of radiopharmaceuticals has been obtained in animal experiments. Recently Russell et al published data for placental crossover for a variety of radiopharmaceuticals *(80)*. Fetal dose estimates, including maternal and fetal self dose contributions, from 90 of the most commonly used nuclear medicine procedures in women of childbearing age, have been tabulated for 4 stages of pregnancy *(81)*. In general the doses tend to decrease throughout pregnancy This occurs because the increase in mass of the fetus is usually greater than the increase in absorbed fractions of photon energy for the fetus being irradiated by the maternal organs, with exceptions for liver, lungs and spleen *(79)*. In contrary the dose to the fetus may increase throughout pregnancy if the fetal and/or placental uptake increase throughout pregnancy (e.g. ^{131}I-sodium-iodide) *(82)* The dose which the embryo or fetus receives from common diagnostic nuclear medicine procedures is less than 10 mGy and the risk of detrimental effects on the embryo is negligible *(83)* In the case of therapeutic use of internally administered radiopharmaceuticals, however, the risks are greater, and therefore extreme care should be taken to ensure that pregnant woman are not inadvertently given therapeutic quantities of ^{131}I *(82)*.

RED MARROW DOSE

In most diagnostic or therapeutic nuclear medicine procedures the red marrow is the organ at risk *(84-89)*. The red marrow dose is considered to be one of the best predictors of myelotoxicity after radioimmunotherapy *(88)*. Therefore accurate estimation of the red marrow dose is very important. If red marrow is visible on the gamma camera images, the uptake of activity in the red marrow at diverse time points can be calculated. In this case the red marrow is one of the source organs. The residence time of the activity in the red marrow can be calculated and entered in the MIRDOSE3 program *(78)*, together with the other source organs. However, if no accumulation of activity in the skeleton is seen on the gamma camera images, the estimated dose to the red marrow can be calculated from the penetrating photon radiation emitted by activity in other organs or from the rest of the body. Usually, this will give an underestimation of the real absorbed dose to the red marrow *(84)*. When no accumulation of activity in the red marrow is visualized, a better estimate of red marrow dose can be obtained

from blood samples *(84)* Using a blood volume of 5000 ml, a red marrow mass of 1120 gram, and the assumption that the red marrow-to-blood activity concentration is 25%, it can be shown that the red marrow residence time is 5.6% of the blood residence time *(85)*. Recently, Dunn et al reported that the patient-specific marrow to blood ratios ranged from 0.26 to 0.76 in patients with medullary thyroid carcinoma treated with ^{131}I-murine MN-14 F(ab)2 anti-CEA MAb *(88)*. For bone marrow 2 Gy is considered to be the maximum tolerated dose that can be administered safely without bone marrow support *(89)*.

NONUNIFORM DOSE DISTRIBUTION

The various approaches in radionuclide dosimetry depend on the size and spatial relation of the sources and targets considered in conjunction with the emission range of the radionuclides used *(90)*. For whole organs, or for sources or targets larger than the range of the radionuclide emissions, the approach used by MIRDOSE3 *(78)* is widely accepted. The program calculates a mean absorbed dose and assumes a uniform distribution of the radioactivity in the organ of interest. At this level, the most important computational effort is for photons (since the absorbed fractions for particles are assumed to be unity).

However, the distribution of the radiopharmaceutical in the organ is sometimes very nonuniform, leading to high focal doses in the tissues Also the characteristics of the emitted radiation may cause a non-uniform distribution of the absorbed dose in the organs *(90)*. At the millimeter level, photons can often be disregarded, since the absorbed dose due to β-particles or electrons predominate. The commonly used radionuclides in diagnostic nuclear medicine emit low energy Auger and Coster-Kronig electrons *(91)*. The average yield of these low energy electrons per decay varies from 3 to 20, e.g. 4 for ^{99m}Tc , 8 for ^{111}In and 20 for ^{201}Tl *(92)*. If these radionuclides are incorporated in the cell nucleus and/or bound to DNA, all the energy of the Auger-electrons will be deposited in the cell nucleus due to their short range in tissue. In these cases, micro-dosimetric methods should be used *(90-101)*.

ERRORS IN ABSORBED DOSE ESTIMATES

There are many sources of error in an absorbed dose estimate. They include:

1. Variation between individuals: organ size, metabolism, changes due to disease,
2. Limited accuracy in estimation of absolute organ activity from gamma camera images,
3. Missing data,
4. Appropriate selection of sampling times,
5. Curve fitting,

6. Extrapolation of the activity-time curve beyond the period of data sampling
7. Non-uniform activity distribution.

Many of these issues have already been discussed. In dose estimation studies a combination of individual sampled data and data for standard man are used. In estimating the organ dose the S-factors and residence times are multiplied. The residence times are often derived from data measured in individuals, the S-factors are derived from tables using software phantoms for standard man, or other groups of individuals. Due to the large variation of organ sizes, total body weight, etc., the estimated absorbed dose using mean S-factors can give errors on the order of a factor of 2, even if the metabolism is assumed to be the same for all individuals.

Larger variations can occur due to differences in metabolism between individuals. The standard deviation for absorbed dose in the organ per MBq, has been shown to vary from 10 to 30 % *(26)*, or is as high as 50% *(102)* in organs of patients which are not affected by disease. In 5 healthy volunteers the standard deviation of the estimated dose/MBq varied from 15% for the urinary bladder wall to 65% for the spleen *(67)*. Similar or larger variations of absorbed organ doses have also been reported *(12,103,104)*.

A summary of the methods used for activity quantification and their associated errors has been reported by Miller et al. *(44)*. The errors in activity quantification depend on the method used and the organ of interest. Using the depth dependent build-up factor method for scatter correction in a phantom results in errors of < 5% *(22)*. The depth dependent build-up factor method for scatter correction used for quantification for lung uptake after administration of ^{99m}Tc MAA generates an estimated activity uptake of 100% ± 3% *(105)*. Van Rensburg et al. have demonstrated a 43.3% and 50.9% overestimation of activity in liver and spleen phantoms filled with ^{111}In using the geometric mean approach and 0.8 and 1.2 % using the depth independent build up factor method *(15)*. Using the geometric mean approach for liver, spleen and distributed sources, Myers et al. have shown that this approach results in a 20% overestimation of activity *(106)*. Accurate tumor radiation dosimetry is potententially useful to predict tumor response after radioimmunotherapy provided that over- or underestimation of activity in the organ is low. The accuracy of tumor quantification based on gamma camera images may be enhanced using a contrast-dependent threshold method in combination with the conjugate view method, or, in some circumstances preferable, the effective point source method *(107)*.

REFERENCES

1 Loevinger R, Berman M. A Revised Schema for Calculating the Absorbed Dose from Biologically Distributed Radionuclides. *MIRD Pamphlet No 1 (Revised)*. New York: The Society of Nuclear Medicine, 1976.

2 Loevinger R, Budinger, TF, Watson, EE. *MIRD Primer for Absorbed Dose Calculations* (Revised Edition). New York: The Society of Nuclear Medicine, 1991.

3 Cristy M. Active bone marrow distribution as a function of age in humans. *Phys Med Biol* 1981, 26: 389-400.

4 ICRP Publication 53. *Radiation Dose to Patients from Radiopharmaceuticals*. Oxford: Pergamon Press, 1988.

5 ICRP Publication 62. Radiological protection in biomedical research. Includes addendum 1 to publication 53-*Radiation Dose to Patients from Radiopharmaceuticals*. Oxford: Pergamon Press, 1993.

6 Foster DM, Boston RC. The Use of Computers in Compartmental Analysis: The SAAM and CONSAM Programs. In: Robertson JS, Colombetti LG, eds. *Compartmental Distribution of Radiotracers*. Boca Raton, Florida: CRC Press, 1983: 73-142.

7 Bogen DK. Simulation Software for the Macintosh. *Science* 1989, 246: 138-142.

8 Ralston ML, Jennrich RI, Sampson PF, Uno FK. Fitting Pharmacokinetic Models with BMDPAR, BMDP Technical Report No. 58. Los Angeles: UCLA *Health Sciences Computing Facilities*, 1979.

9 Leichner PK, Koral KF, Jaszczak RJ, Green AJ, Chen GTY, Roeske JC. An Overview of Imaging Techniques and Physical Aspects of Treatment Planning in Radioimmunotherapy. *Med Phys* 1993, 20: 569-577.

10 Thomas SR, Maxon HR, Kereiakes JG. In Vivo Quantitation of Lesion Radioactivity Using External Counting Methods. *Med Phys* 1976, 3: 253-255.

11 Landaw EM, DiStefano JJ. Multiexponential, Multicompartmental, and Noncompartmental Modeling II. Data Analysis and Statistical Considerations. *Am J Physiol* 1984, 246: R665-R677.

12 Breitz HB, Fisher DR, Weiden PL, et al. Dosimetry of Rhenium-186-Labeled Monoclonal Antibodies: Methods, Prediction from Technetium-99m-Labeled Antibodies and Results of Phase I Trials. *J Nucl Med* 1993, 34: 908-917.

13 Fleming JS. A Technique for the Absolute Measurement of Activity Using a Gamma Camera and Computer. *Phys Med Biol* 1979, 24: 176-180.

14 Early JF, Appelbaum FA, Durack L and Brown P. Preliminary validation of the opposing view method for quantitative gamma camera imaging. *Med Phys* 1989, 16: 382-387.

15 Van Rensburg AJ, Lotter MG, Heyns AP, et al. An Evaluation of Four Methods of ^{111}In Planar Image Quantitation. *Med Phys* 1988, 15: 853-861.

16 Sorenson JA. *Methods for Quantitating Radioactivity In Vivo by External Counting Measurements*, Ph D Thesis. University of Wisconsin, Madison, WI, 1971.

17 Beekhuis H, Nieweg O. Radiation Absorbed Doses from Co-57- and Co-55 Bleomycin. *J Nucl Med* 1984, 25: 478-485.

18 Reenen v R, Lotter M, Heyns A du P, Kock F de, Herbst C, Kotze H et al. Quantification of the Distribution of ^{111}In Labbelled Platelets in Organs. *Eur J Nucl Med* 1982, 7: 80-84.

19 Macey DJ, Marshall R. Absolute Quantitation of Radiotracer Uptake in the Lungs using a Gamma Camera. *J Nucl Med* 1982, 23: 731-734.

20 Tsui BMW, Chen C-T, Yasillo NJ, et al. *A Whole-Body Scanning System for Collection of Quantitative In Vivo Distribution Data in Humans*. In: Watson, EE, Schlafke-Stelson, AT, Coffey JL, et al (eds). Third International Radiopharmaceutical Dosimetry Symposium.

Proceedings of a Conference Held at Oak Ridge, TN, October 7-10 1980. HHS Publication FDA 81-8160, 1981 138
21. Thomas SR Maxon RH, Kereiakes JG *Techniques for Quantitation of In Vivo Radioactivity* In Effective Use of Computers in Nuclear Medicine Editors M J Gelfand and S R Thomas McGraw-Hill, New York, 1988 468 484
22 Wu RK, Siegel JA Absolute Quantitation of Radioactivity Using the Buildup Factor *Med Phys* 1984, 11 189-192
23 Siegel JA, Wu RK, Maurer AH The Buildup Factor Effect of Scatter on Absolute Volume Determination *J Nucl Med* 1985, 26 390-394
24 Siegel JA The Effect of Source Size on the Buildup Factor Calculation of Absolute Volume *J Nucl Med* 1985, 26 1319-1322
25 Kojima M Takaki Y, Matsumoto M, et al A Preliminary Phantom Study on a Proposed Model for Quantification of Renal Planar Scintigraphy *Med Phys* 1993, 20 33-37
26 Buijs WC AM, Massuger L Claessens RAMJ Kenemans P, Corstens FH Dosimetric Evaluation of Immunoscintigraphy Using Indium 111-Labeled Monoclonal Antibody Fragments in Patients with Ovarian Cancer *J Nucl Med* 1992, 33 1113-1120
27 Buijs WCAM, Siegel JA and Corstens FHM Estimation of absolute organ activity using five different methods for background correction a phantom study *Eur J Nucl Med* 1997, 24 931(abs)
28 Thomas SR, Gelfland MJ Burns GS et al Radiation Absorbed-dose Estimates for the Liver, Spleen and Metaphyseal Growth Complexes in Children Undergoing Gallium-67 Citrate Scanning *Radiology* 1983, 146 817-820
29 Jaszczak RJ, Floyd CE, Coleman RE Scatter Compensation Techniques for SPECT *IEEE Trans Nucl Sci* 1985, 32 786-793
30 Koral KF, Clinthorne NH, Rogers WL Improving Emission-Computed Tomography Quantification by Compton-Scatter Rejection through Offset Windows *Nucl Inst Meth Phys Res* 1986, A242 610-614
31 Pretorius PH, Van Rensburg AJ, Van Aswegen AI et al The Channel Ratio Method of Scatter Correction for Radionuclide Image Quantitation *J Nucl Med* 1993, 34 330-335
32 King MA, Hademenon GJ, Glick SJ A Dual-Photopeak Window Method for Scatter Correction *J Nucl Med* 1992, 33 605-612
33 Ogawa K Harata Y, Ichihara T, Kubo A, Hashimoto S A Practical Method for Position-Dependent Compton-Scatter Correction in Single Emission CT *IEEE Trans Med Imag* 1991, 10 408-412
34 Macey DA, Grant EF, Bayouth JE, et al Improved Conjugate View Quantitation of I-131 by Subtraction of Scatter and Septal Penetration Events with a Triple Energy Window Method *Med Phys* 1995, 22 1637-1643
35 King MA Doherty PW, Schwinger RB A Wiener Filter for Nuclear Medicine Images *Med Phys* 1983, 10 876-880
36 King MA, Schwinger PW, Doherty PW, Penney BC Two-Dimensional Filtering of SPECT Images Using the Metz and Wiener Filters *J Nucl Med* 1984, 25 1234-1240
37 Penney BC, Glick SJ, King MA Relative Importance of the Error Success in Wiener Restoration of Scintigrams *IEEE Trans Med Imag* 1990; 9:60-70
38 Clarke LP, Cullom SJ, Shaw R, Reece C, Penney BC, King MA, Silbiger M Bremsstrahlung Imaging Using the Gamma Camera Factors Affecting Attenuation *J Nucl Med* 1992, 33 161-166
39 Shen S DeNardo GL, DeNardo S Quantitative Bremsstrahlung Imaging of Yttrium-90 Using a Wiener Filter *Med Phys* 1994, 21 1409 1417
40 Halama, JR, Henkin RE, Friend LE Gamma Camera Radionuclide Images Improved Contrast with Energy-Weighted Acquisition *Radiology* 1988, 169 533-538

41 DeVito RP, Hamill JJ, Treffert J, Staub EW. Energy-Weighted Acquisition of Scintigraphic Images Using Finite Spatial Filters *J Nucl Med* 1989; 30 2029-2035
42. Hamill, JJ, DeVito RP Scatter Reduction with Energy-Weighted Acquisition *IEEE Trans Nucl Sci* 1989; NS-36:1334-1339
43 DeVito RP, Hamill JJ. Determination of Weighting Functions for Energy-Weighted Acquisition. *J Nucl Med* 1991, 32:343-349
44 Miller C, Filipow L and Jackson S A review of Activity Quantification by Planar Imaging Methods. *J Nucl Med Technol* 1995; 23:3-9
45 Buijs WCAM, Siegel JA and Corstens FHM Absolute Organ Activity Estimated by Five Different Methods of Background Correction. *J Nucl Med* 1998, 39 in press.
46 Rosenthal MS, Cullom J, Hawkins W, Moore SC, Tsui BMW, Yester M. Quantitative SPECT Imaging A Review and Recommendations by the Focus Committee of the Society of Nuclear Medicine Computer and Instrumentation Council. *J Nucl Med* 1995; 36:1489-1513
47 Zanzonico PB, Bigler RE, Sgouros G, Strauss A Quantitative SPECT in Radiation Dosimetry. *Semin Nucl Med* 1989, 19 47-61.
48. Tsui BMW, Zhao X, Frey EC, McCartney WH. Quantitative Single-Photon Computed Tomography: Basics and Clinical Considerations. *Semin Nucl Med* 1994; 24:38-65
49 Tsui BMW, Frey EC, Zhao X, Lalush DS, Johnson RF, McCartney WH The Importance and Implementation of Accurate 3D Compensation Methods for Quantitative SPECT *Phys Med Biol* 1994, 39:509-530
50 Schold Jr SC, Zalutsky MR, Coleman RE, et al Distribution and Dosimetry of I-123 Labeled Monoclonal Antibody 81C6 in Patients with Anaplastic Glioma *Invest Radiol* 1993, 28:488-496.
51. Parker JA. Quantitative SPECT: Basic Theoretical Considerations *Semin Nucl Med* 1989; 19.3-12
52. Budinger TF Physical Attributes of Single Photon Tomography *J Nucl Med* 1980, 21.579-592
53. Gullberg GT, Budinger TF. The Use of Filtering Methods to Compensate for Constant Attenuation in Single Photon Emission Computed Tomography. *IEEE Trans Biomed Eng* 1981; 28:142-157
54. Jaszczak RJ, Coleman RE, Whitehead FR Physical Factors Affecting Quantitative Measurements Using Camera-Based Single Photon Emission Computed Tomography *IEEE Trans Nucl Sci* 1981, 28 69-80.
55 Tanaka E, Toyama H, Murayama H Convolutional Image Reconstruction for Quantitative Single Photon Emission Computed Tomography. *Phys Med Biol* 1984, 29.1489-1500.
56 Mas J, Ben-Younes R, Bidet R. Improvement of Quantification in SPECT Studies by Scatter and Attenuation Compensation *Eur J Nucl Med* 1989, 15:351-356
57. King MA, Schwinger RB, Doherty PW, Penney BC Variation of the Count-Dependent Metz Filter with Imaging System Modulation Transfer Function. *Med Phys* 1986; 25:139-149.
58 Gilland DR, Tsui BMW, Perry JR, et al Optimum Filter Function for SPECT Imaging *J Nucl Med* 1988, 29:643-650.
59. Koral KF, Zasadny KR, Kessler ML, et al A Method Using CT-SPECT Fusion Plus Conjugate Views for Dosimetry in ^{131}I-MoAb Therapy of Lymphoma Patients. *J Nucl Med* 1994; 35 1714-1720
60. Chang LT A Method for Attenuation Correction in Radionuclide Computed Tomography. *IEEE Trans Nucl Sci* 1978; NS-25:638-642.
61 Iosilevsky G, Israel O, Frenkel A, et al. A Practical SPECT Technique for Quantitation of Drug Delivery to Human Tumors and Organ Absorbed Radiation Dose. *Semin Nucl Med* 1989; 19:33-46.
62 Pretorius PH, van Aswegen AI, Herbst CP, Lotter MG The Effects of Different Correction Techniques on Absolute Volume Determination with SPECT Using a Threshold Edge Detection Method. *Med Phys* 1991;18 390-393.

63. Gilland DR, Jaszczak RJ, Turkington TG, Greer KL, Coleman RE. Volume and Activity Quantitation with Iodine-123 SPECT. *J Nucl Med* 1994; 35:1707-1713.
64. Mortelmans L, Nuyts J, Van Pamel G, Van den Maegdenbergh V, De Roo M, Suetens P. A New Thresholding Method for Volume Determination by SPECT. *Eur J Nucl Med* 1986; 12:284-290.
65. Leichner PT, Klein JL, Garrison LB, et al. Dosimetry of 131I-labeled anti-ferritin in Hepatoma: A Model for Radioimmunoglobulin Dosimetry. *Int J Radiat Oncol Biol Phys* 1981; 7:323-333.
66. Cohn SH. *Whole Body Counters.* In: Principles of Nuclear Medicine. Second Edition. Editors: Wagner HN, Szabo Z, Buchanan JW. W.B. Saunders, Philadelphia, 1995:298-305.
67. Buijs WCAM, Oyen WJG, Dams EThM, Boerman OC, Siegel JA, Claessens AMJ, van der Meer JWM and Corstens FHM. Dynamic Distribution and Dosimetric Evaluation of Human Nonspecific Immunoglobulin G labelled with In-111 or Tc-99m. *Nucl Med Commun* 1998; 19:743-751.
68. Lathrop KA, Harper PV, Charleston DB, Atkins FB, Mock BH. *Acquisition of Quantitative Biologic Data in Humans for Radiation Absorbed Dose Estimates.* In: Radiopharmaceutical Dosimetry Symposium. Proceedings of a Conference held at Oak Ridge, TN, April 26-29, 1976: 164-173.
69. Sgouros G. Bone Marrow Dosimetry for Radioimmunotherapy: Theoretical Considerations. *J Nucl Med* 1993; 34:689-694.
70. Fisher DR. Radiation Dosimetry for Radioimmunotherapy. *Cancer Suppl* 1994; 73:905-911.
71. Bers L. *Calculus.* New York: Holt, Rinehelt, and Winston, Inc; 1969:413-416.
72. Macon N. *Numerical Analysis.* New York: Wiley; 1963.
73. Riggs DS. *The Mathematical Approach to Physiological Problems.* Cambridge, Massachusetts: The M.I.T. Press; 1976.
74. Selikson MH, Jaggi J, Mozley PD, McCue J, Vu H and Forrest R. A proposal for minimum detectable compartment in MIRD dosimetry modelling. *Phys Med Biol* 1997;42:1605-1617.
75. Eary JF, Press OW, Badger CC et al. Imaging and Treatment of B-cell Lymphoma. *J Nucl Med* 1990; 31:1257-1268.
76. Wahl RL, Zasadny K and Kaminski M. Importance of the Terminal Portion of Tumor Time-Activity Curve in Determining Tumor Dosimetry in Radioimmunotherapy. *J Nucl Med* 1991; 32:1314-1315.
77. Stabin M, Watson E, Cristy M et al. *Mathematical models of the adult female at various stages of pregnancy.* ORNL Report ORNL/TM-12907. Oak Ridge, TN: Oak Ridge National Laboratory; 1995.
78. Stabin MG. MIRDOSE: Personal Computer Software for Internal Dose Assessment in Nuclear Medicine. *J Nucl Med* 1996; 37:538-546.
79. Stabin M, Watson E, Cristy M et al. *Mathematical Models and Specific Absorbed Fractons of Photon Energy in the Nonpregnant Adult Female at the End of Each Trimester of Pregnancy.* Oak Ridge, TN: Oak Ridge National Laboratory; ORNL Report ORNL/TM-12907; 1995.
80. Russell JR, Stabin MG and Sparks RB. Placental Transfer of Radiopharmaceuticals and Dosimetry in Pregnancy. *Health Phys* 1997; 73:747-755
81. Russell JR, Stabin MG, Sparks RB and Watson Evelyn. Radiation Absorbed Dose to the Embryo/Fetus from Radiopharmaceuticals. *Health Phys* 1997; 73:756-769.
82. Stabin MG, Watson EE, Marcus CS and Salk RD. Radiation dosimetry for Adult Female and fetus from Iodine-131 Administration in Hyperthyroidism. *J Nucl Med* 1991; 32:808-813.
83. Steenvoorde P, Pauwels EK, Harding LK, Bourguignon M, Marière B and Broerse JJ. Diagnostic Nuclear Medicine and risk for the fetus. *Eur J Nucl Med* 1998; 25:193-199.
84. Siegel JA, Wessels BW, Watson EE et al. Bone marrow dosimetry and toxicity for radioimmunotherapy. *Antibody Immunoconj Radiopharm* 1990; 3:213-233.
85. Buijs WCAM, Steffens MG, Boerman OB, Oosterwijk E, Siegel JA and Corstens FHM. Estimation of absorbed red marrow dose after administration of ^{131}I-cG250. *Eur J Nucl Med* 1997; 24:868 (abs).

86 Zanzonico P and Sgouros G Editorial Predicting Myelotoxicity in Radioimmunotherapy What does Dosimetry contribute? *J Nucl Med* 1997 38 1753-1754
87 Sgouros G Bone Marrow Dosimetry for Radioimmunotheraphy Theoretical Considerations *J Nucl Med* 1993, 34 689-694
88 Dunn RM, Juweid M, Sharkey RM and Goldenberg DM Patient Specific (PS) estimates of red marrow dose result in improved correlation with myelotoxicity *J Nucl Med* 1998 39 112P-113P (suppl)
89 Larson SM Carrasquillo JA, Colcher DC et al Estimates of radiation absorbed dose for intraperitoneally administered iodine 131 radiolabeled B72 3 monoclonal antibody in patients with peritoneal carcinomatoses *J Nucl Med* 1991, 32 1661-1667
90 Bardies M and Myers MJ Computational methods in radionuclide dosimetry *Phys Med Biol* 1996 41 1941 1955
91 Mountfort PJ Internal dosimetry Developments and limitations Editorial *Eur J Nucl Med* 1996, 23 491 493
92 Sastry KSR, Howell RW, RAO DV et al *Dosimetry of Auger emitters Physical and phenomenological approaches* In Baverstock KF and Charlton DE eds DNA Damage by Auger Emitters London Taylor and Francis, 1988 27 38
93 Makrigiorgos GM, Adelstein SJ and Kassis AI Cellular radiation dosimetry and its implications for estimation of radiation risks Illustrative results with technetium 99m-labeled microspheres and microaggregates *Jama* 1990, 264 592 595
94 Faraggi M, Gardin I de Labriolle-Vaylet C, Moretti J L, Nok BD The influence of tracer localisation on the electron dose rate delivered to the cell nucleus *J Nucl Med* 1994, 35 113-119
95 Kassis AI Adelstein SJ Does nonuniformity of dose have implications for radiation protection? *J Nucl Med* 1992, 33 384 387
96 Gardin I, Linhart NC, Petiet A, and Bok B Dosimetry at the Cellular Level of Kupffer Cells After Technetium-99m-Sulphur Colloid Injection *J Nucl Med* 1992, 33 380 384
97 Howell RW The MIRD-schema from organ to celular dimensions *J Nucl Med* 1994, 35 531-533
98 Hofer KG Biophysical aspects of Auger processes A review *Acta Oncologica* 1996 35 789 796
99 Stepanek J, Larsson B and Weinreich R Auger-electron spectra of radionuclides for therapy and diagnostics *Acta Oncologica* 1996, 35 863-868
100 Goddu SM, Howell RW and Rao DV Calculation of Equivalent Dose for Auger electron emitting radionuclides distributed in human organs *Acta Oncologica* 1996, 35 909-916
101 Gardin I Faraggi M, Huc E and Bo BD Absorbed fraction to the cell nucleus for low energy electrons *Acta Oncologica* 1996 35 953-958
102 Steffens MG Boerman OC Oosterwijk-Wakka JC et al Targetting of renal Cell carcinoma With Iodine-131 Labeled Chimeric Monoclonal Antibody G250 *J Clin Oncology* 1997 15 1529 1537
103 Castronovo FP ^{201}Tl-labeled TlCl dosimetry revisited *Nucl Med Commun* 1993, 14 104-107
104 Fisher DR Radiation Dosimetry for Radioimmunotherapy An Overview of Current Capabilities and Limitations *Cancer Supplement* 1994, 73 905 911
105 Forge NJ Mountfort PJ, O Doherty MJ Quantification of technetium 99m lung radioactivity from planar images *Eur J Nucl Med* 1993, 20 10-15
106 Myers BM, Lavender AR, Oliveira JB Maseri A A simplified method of quantitating organ uptake using a gammacamera *Br J Radiol* 1981, 54 1062 1067
107 DeNardo GL, Shen S DeNardo SJ et al Quantification of iodine-131 in tumors using a threshold based on image contrast *Eur J Nucl Med* 1998 25 497-502

CHAPTER 4

Estimation of Absolute Organ Activity Using Five Different Methods of Background Correction

Wilhelmina C.A.M. Buijs, Jeffry A. Siegel, Otto C. Boerman and Frans H.M. Corstens.

J Nucl Med 1998, in press

ABSTRACT

Accurate absorbed dose estimates in radionuclide therapy requires patient-specific dosimetry In patient-based dosimetry estimation of absolute organ uptake is essential The methods used should be reasonably accurate as well as easy to perform in routine clinical practice One of the major sources of uncertainties in quantification of organ or tumor activity from planar images is the activity present in tissue surrounding the source

Method To estimate organ activity as a function of organ-to background activity concentration ratio, a cylindrical phantom, filled with 5 6 liters of water was used to simulate the abdomen of a patient Two other cylinders of 150 ml each representing the kidneys, were each filled with 19 MBq of ^{99m}Tc and were positioned in the abdomen phantom The phantom was imaged with a dual headed gamma camera with the kidneys placed at posterior depths of 1, 5 and 10 cm at kidney-to-background activity concentration ratios of infinity, 10 1, 5 1 and 2 1 The conjugate view geometric mean counting method was used to quantify activity Five methods for background correction were applied 1 no correction 2 conventional background correction (simple subtraction of the background count rate from the source region count rate) 3 Kojima method (background corrected for organ thickness and depth) 4 Thomas method (analytical solution), and 5 Buijs method (background corrected for organ and total body thickness)

Results Since the results were identical for both kidneys only the left kidney activity measurements are presented The accuracy of the five background correction methods is given as the % difference between the actual and measured activity in the left kidney For method 1 the percent difference ranged from -2% with an infinite kidney-to-background activity concentration ratio to +413% with a 2 1 ratio For method 2 these values ranged from -1% to -80%, for method 3 from +11% to -18% for method 4 from -2% to +120% and for method 5 from -4% to +39%

Conclusion Even though quantitative SPECT is the most rigorous method for activity quantification in conditions of low organ-to-background activity concentration ratio planar scintigraphy can be accurately applied if appropriate attention is paid to background correction Using relatively simple background subtraction methods the quantitative planar imaging technique can result in reasonably accurate activity estimates (methods 3 and 5)

The use of Kojima's method is preferable especially at very low source-to-background activity concentration ratios

INTRODUCTION

Estimation of absolute organ activity for the purpose of patient-based dosimetry in radionuclide therapy, particularly radioimmunotherapy (RIT), is of growing interest. The measurement of the biodistribution of radiopharmaceuticals and the use of these data in the Medical Internal Radiation Dose (MIRD) schema *(1,2)* provide a primary means to calculate absorbed doses from internally deposited radionuclides.

A series of physical factors contribute to the difference between measured activity and actual activity in source regions based on planar scintigraphy. Accurate estimation of the activity in an organ from the measured count rate requires correction for the system calibration factor (measured count rate per MBq), attenuation, scatter, background activity, organ- and patient thickness and physical decay of the radionuclide used. Because activity in surrounding organs and non-uniform distribution of background may interfere with accurate quantification, SPECT imaging has the potential to improve the accuracy of planar imaging measurements *(3-7)*. However, because of the time-consuming and more complex nature of quantifying SPECT image data, there is a need for a reasonably accurate and simple quantification method based on planar imaging.

A number of techniques for activity quantification of planar images have been reported, most of them dealing with attenuation and other corrections using the conjugate view counting method *(8-18)*. In situations with low target-to-background activity concentration ratios, such as in radioimmunotargeting, accurate background correction is very important. Different methods of background correction have been described *(9,19,20)*.

In the present study the accuracy of five different methods for background correction are compared at various organ-to-background activity concentration ratios.

MATERIALS AND METHODS

PHANTOM

A cylindrical phantom with an inner diameter of 21.5 cm was filled with 5.6 liters of water to simulate the abdomen of a patient (Figure 1). The thickness of the acrylate (density 1.18 g/cm^3) cylinder wall was 0.3 cm. The length of the large cylinder (H) was 18 cm (Figure 1B). Two other cylinders with an inner diameter of 5.2 and an outer diameter of 5.5 cm (t_m), representing the kidneys, were each filled with a solution of 19 MBq of ^{99m}Tc-pertechnetate in 150 ml water (Figure 1A). The height of the water-level in the small phantoms was 7 cm (h, Figure 1B). The thickness of the part of the large cylindrical phantom that include the kidney

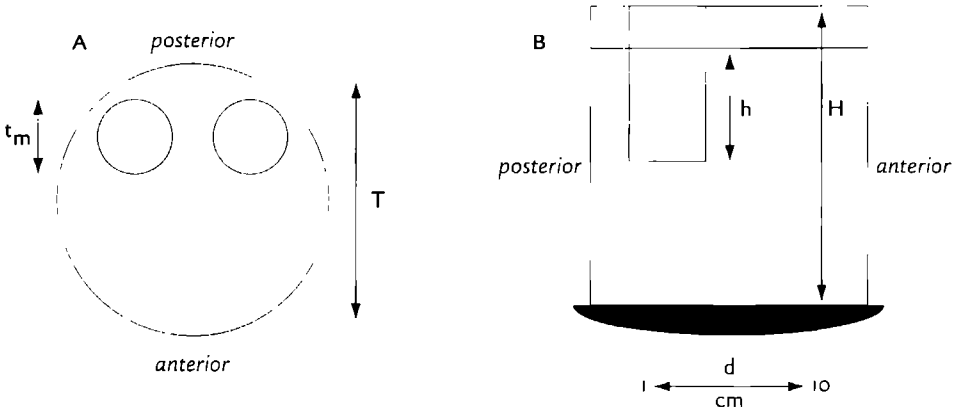

Figure 1. *Top (A) and side (B) views of the phantom with the two kidney cylinders inserted in the large abdomen cylinder. (A) T is the thickness of the part of the large cylindrical phantom that include the kidney cylinders (18.5 cm), and t_m is the diameter of the small cylinder (5.5 cm). (B) H is the length of the large cylinder (18 cm), h is the height of the activity-solution in the small kidney cylinders (7 cm), and d is the depth of the kidney phantoms (1, 5 and 10 cm from the posterior wall of the large cylinder). The large cylinder was not filled to the top of the cylinder, in order to make it possible to stir the solution in the cylinder after each new addition of activity to reach a uniform distribution of activity in the background compartment.*

cylinders (T) was 18.5 cm (Figure 1A). The kidneys were positioned in the abdomen phantom at three different depths (d). The distances between the posterior kidney surface and the posterior abdominal cylinder wall in these three positions were approximately 1, 5 and 10 cm (Figure 1B). The axis between the centers of the two kidney cylinders was parallel to the detector and the distance between the centers was 10.5 cm.

In some of the background correction methods described in this study, the thickness of the source, measured in the direction perpendicular to the gamma camera surface, must be known. Because the shape of the cross section in a cylindrical phantom is circular, the "thickness" would vary along the direction parallel to the gamma camera surface. In order to get a constant (virtual) thickness along the direction parallel to the gamma camera surface an effective thickness was calculated (t). This effective thickness was defined as the height of a rectangle, which has a width equal to the diameter of the cylinder and an area equal to the area of the circular cross section of the small cylinder. The height of that rectangular is then: $^1/_4 \pi t_m^2/t_m$, where t_m is the diameter of the small cylinders (5.5 cm). Thus the effective thickness t is equal to 4.3 cm.

Various kidney-to-background activity concentration ratios were obtained by adding ^{99m}Tc-pertechnetate to the background (abdomen cylinder), while

keeping the activity in the kidneys constant. Kidney-to-background activity concentration ratios of infinity (no background activity), and approximately 10:1, 5:1, and 2:1 were achieved. After the activity was uniformly distributed in the various compartments, a sample of 2 ml was taken from each kidney phantom at the start of the study; 2 ml samples were also taken from the solution in the large cylinder for each of the kidney-to-background activity concentration ratios. The purpose of taking the initial 2-ml sample from the abdominal phantom (when no background activity was present) was to ensure that the kidney cylinders were not leaking activity. At the end of the imaging study, 0.5 ml aliquots from each 2-ml-kidney and -background sample were measured in a well counter and activity concentration in cpm/g was calculated. Exact kidney-to-background activity concentration ratios were determined by comparing the activity concentration in the samples taken from the kidney cylinders to the activity concentration in the samples taken from the abdominal phantom for the four different background situations.

IMAGING

The phantom was imaged with a dual headed gamma camera (MultiSPECT2, Siemens, Hoffman Estates, IL) equipped with parallel-hole low-energy high-resolution collimators, connected to a computer (ICON, Siemens). A symmetric 15% window was set at 140-keV photopeak. The phantom was placed upright on the scanning table and the detectors were placed in vertical positions 180 degrees opposed to each other. For each of the four kidney-to background activity concentration ratios, the kidneys were moved from the 1 to 5 to 10 cm depths. Anterior and posterior static images were acquired during five minutes and stored in a 256 x 256 matrix. For each of the two detectors, the system calibration factor for ^{99m}Tc was determined in cpm/MBq.

ANALYSIS AND BACKGROUND CORRECTION

On the posterior image with no background activity in the large cylinder, a rectangular ROI (28 by 36 pixels) was drawn manually around the left kidney, which was positioned at a depth of one centimeter from the background surface of the large cylinder. The same ROI was positioned on the right kidney and on the background area beneath the left kidney. These ROIs were then superimposed on the images with background activity (Figure 2). The measured ROI count rates (counts per minute) were corrected for physical decay.

To quantify the activity in the kidney cylinders the conjugate view counting method was used *(9)*:

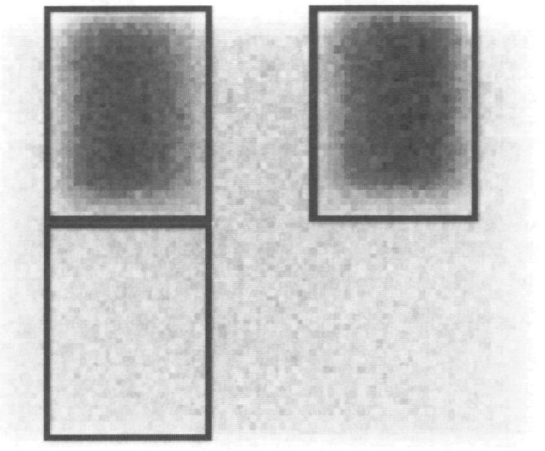

Figure 2. *Posterior image of the phantom at a kidney-to-background activity concentration ratio of 10:1. The kidney cylinders are positioned at a depth of five cm from the posterior wall of the large cylinder. The rectangular ROIs used for the kidneys and the background are shown.*

$$A = \left(\frac{I_A I_P}{e^{-\mu_e T}} \right)^{1/2} \frac{f}{C}, \qquad (1)$$

where A is the kidney activity in MBq, I_A and I_P are the anterior and posterior view count rates, respectively (counts per minute), T (cm) is the thickness of the abdominal cylinder at the position of the kidney cylinders (18.5 cm), μ_e (cm^{-1}) is the effective total linear attenuation coefficient (for the abdomen phantom an experimentally derived effective attenuation coefficient for ^{99m}Tc of 0.143 cm^{-1} was used), f is equal to $(\mu_e t/2)/\sinh(\mu_e t/2)$ and represents a correction for the source region attenuation coefficient (μ_e) and source thickness (t) (i.e., source self-attenuation correction); it was determined to be 0.98, and C is the system calibration factor (count rate per unit activity). The system calibration factor used in this study (5540 cpm/MBq) was obtained by counting a known activity of ^{99m}Tc for a fixed period of time in air using the same camera, collimators, and camera acquisition settings as for the phantom study.

The effective linear attenuation coefficient was determined using a transmission phantom consisting of a series of acrylic plates (tissue-equivalent material) each with a diameter of 42 cm and a thickness of 2 – 3 cm (density 1.18 g/cm^3). A hollow circular phantom of diameter 8.5 cm, was filled with a solution of 30 MBq ^{99m}Tc to a height of 2.5 mm. Images of 5 minutes were acquired for the

source in air and then with consecutive thicknesses of tissue-equivalent material in steps of 2 cm up to 23 6 cm Transmission factors were measured using a ROI size equal to the size of the ROIs in the kidney phantom study Curve fitting the resulting transmission factor versus depth curve resulted in an attenuation coefficient of 0 143 cm $^{-1}$ (μ_e) and a buildup factor of 1 07 *(21)* For small ROI sizes the buildup factor is small and was not used in our analysis

The following five methods of background correction were applied to estimate the absolute kidney activity

1 No background subtraction

Equation *(1)* is applied with measured I_A and I_P without correction for background activity

2 Conventional background subtraction

The count rate measured in an adjacent ROI was subtracted from the count rate in the kidney ROI according to

$$I_A = I'_A - I_{BGA}, \text{ and}$$

$$I_P = I'_P - I_{BGP} \qquad (2)$$

where I_A (I_P) is the background corrected count rate in the anterior (posterior) kidney ROI, I'_A (I'_P) is the measured count rate in the anterior (posterior) kidney ROI, and I_{BGA} (I_{BGP}) is the count rate in the anterior (posterior) background ROI These I_A (I_P) count rates are used in Equation *(1)* The activity in the background ROI was expressed as counts per minute (cpm) per pixel This count rate was multiplied by the number of pixels in the kidney ROI and then subtracted from the total counts in the kidney ROI

3 Kojima method

This method corrects for over-subtraction of background activity by taking into account the size of the kidney and assuming a uniform background activity concentration *(19)*

$$I_A = I'_A - I_{BGA} \times C_A, \text{ and}$$

$$I_P = I'_P - I_{BGP} \times C_P \qquad (3)$$

where C_A (C_P) is the multiplication factor for the anterior (posterior) background count rate defined as

$$C_A = 1 - \frac{e^{-\mu_0(T-d-t)} \cdot \left[1 - e^{-\mu_0 t}\right]}{1 - e^{-\mu_0 T}}, \text{ and}$$

$$C_P = 1 - \frac{e^{-\mu_0 d} \cdot \left[1 - e^{-\mu_0 t}\right]}{1 - e^{-\mu_0 T}} \qquad (4)$$

The second term in each of these Equations is the correction for the background count rate equivalent to the volume of the kidney at depth d from the background surface to the posterior aspect of the kidney, t is the effective thickness of the kidney, T is the thickness of the abdomen phantom, and μ_0 is the narrow beam linear attenuation coefficient (equal to 0.15 cm^{-1} for ^{99m}Tc). The correction factors C_A and C_P were calculated using a BASIC program with the appropriate values of d (i.e., 1, 5, and 10 cm), t (effective) = 4.3 cm and T = 18.5 cm. These I_A (I_P) count rates determined from Equations *(3)* and *(4)* are used in Equation *(1)*.

4. Thomas method

Quantification using the conjugate view counting method in combination with an analytical method for background correction was applied *(9)*:

$$A = \left(\frac{I_A I_P}{e^{-\mu_1 T}} \right)^{1/2} \frac{f}{C} * k(\gamma) \qquad (5)$$

Equation *(1)* was multiplied by $k(\gamma)$, where $k(\gamma)$ is the background correction factor defined as:

$$\begin{aligned} k(\gamma) \equiv \{ & 1 + (\gamma_2 f_3/f_2)^2 + (\gamma_4 f_3/f_4)^2 \\ & + 2\gamma_2\gamma_4 (f_3^2/f_2 f_4) \cosh\left[(\mu_2 t_2 + 2\mu_3 t_3 + \mu_4 t_4)/2\right] \\ & + 2\gamma_2 f_3/f_2 \cosh\left[(\mu_2 t_2 + \mu_3 t_3)/2\right] \\ & + 2\gamma_4 f_3/f_4 \cosh\left[(\mu_3 t_3 + \mu_4 t_4)/2\right] \}^{-1/2} \end{aligned} \qquad (6)$$

The subscripts 2, 3, and 4 represent the anterior background region, the kidney region, and the posterior background region, respectively. The individual f-factors are as previously defined according to $(\mu_j t_j/2)/\sinh(\mu_j t_j/2)$, while $\gamma_2 \equiv A_2/A_3$ and $\gamma_4 \equiv A_4/A_3$ represent the ratios of the activity in the adjacent regions to that in the source volume.

The value of the factor $k(\gamma)$ thus depends on the organ-to-background activity concentration ratio, thickness of the source organ, thicknesses of the background volumes anterior and posterior to the kidneys, and the attenuation coefficients for tissue layers with different densities. The $k(\gamma)$ factors were calculated for all three positions of the kidney in the abdomen phantom, thus for three pairs of background thicknesses, and for the four kidney-to-background activity concentration ratios (infinity, 10:1, 5:1 and 2:1), using a software program written in BASIC.

5. Buijs method

A simple geometrically-based subtraction technique was applied to correct for over-subtraction of background activity, as a consequence of the volume occupied by the organ *(20)*:

$$I_A = I'_A - I_{BGA} \times F, \text{ and}$$

$$I_P = I'_P - I_{BGP} \times F \qquad (7)$$

where I_A, I'_A, I_{BGA} and I_P, I'_P and I_{BGP} are the same as in Equation *(2)*. F is the fraction of the total background activity I_{BGA} (I_{BGP}) to be subtracted from the measured activity in the source organ ROI, I'_A (I'_P) and is defined as:

$$F = 1 - (t/T) \qquad (8)$$

where t is the thickness of the source organ and T is the thickness of the abdomen cylinder through the source ROI. In this study, t is the effective diameter of the kidney (4.3 cm) and T is 18.5 cm. Therefore F was calculated to be 0.76 (1-[4.3/18.5]). The I_A (I_P) count rates determined from Equations *(7)* and *(8)* are used in Equation *(1)*.

RESULTS

Because the results for both kidney cylinders were virtually identical, only results for the left kidney are presented here. The measured activity in the left kidney at the start of the phantom study was 19.3 MBq ^{99m}Tc. The actual activity concentration ratios between the left kidney and the background (abdominal volume) were 10.1:1, 5.01:1 and 2.15:1, respectively. The total counts per five-minute-image are presented in Table 1. The maximum count rate found during the measurements was 11.3 kcps; therefore, deadtime did not play a role.

The exact depths of the kidneys and the related background correction

TABLE 1

Total counts in five-minute-images

Activity concentration ratio	Posterior depth (cm)	Anterior image	Posterior image
infinity	1	199816	656483
	5	303157	400016
	10	553473	224559
10 1	1	991048	1301297
	5	1033779	1057713
	10	1217281	898773
5 1	1	1633057	1816363
	5	1669148	1631166
	10	1788251	1463417
2 1	1	3342533	3275677
	5	3320268	3120964
	10	3331846	2984341

TABLE 2

Background correction factors at different depths (Kojima method)

Distance between kidney and posterior abdomen (cm)	Kidney anterior depth (cm)	Kidney posterior depth (cm)	Background correction factor (anterior) C_A	Background correction factor (posterior) C_P
1	12 6	1 6	0 92	0 61
5	8 6	5 6	0 86	0 78
10	3 6	10 6	0 71	0 89

TABLE 3

k(γ) for background correction (Thomas method)

Posterior depth (cm)	Kidney-to-background activity concentration ratio: Infinity	10 1	5 1	2 1
1	1	0 76	0 63	0 42
5	1	0 78	0 64	0 44
10	1	0 77	0 63	0 43

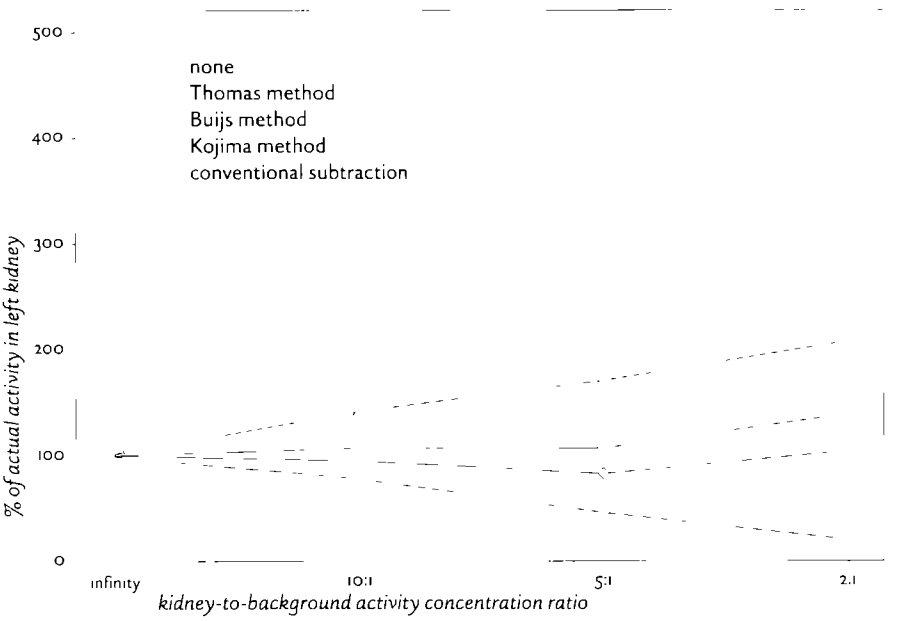

Figure 3. *Percentage of actual activity in the left kidney, at depth 1 cm from the background surface to the posterior aspect of the kidney, as a function of kidney-to-background activity concentration ratio, for all five methods of background correction*

factors for the Kojima method are presented in Table 2. The correction factors were calculated using Equation *(4)*.

The Thomas k(γ) background correction factors were calculated for the three different kidney depths and for the four kidney-to-background activity concentration ratios (Table 3).

The relation between estimated activity in the left kidney and the kidney-to-background activity concentration ratio was different for the five methods of background correction (Figure 3). When no background activity was present, the difference between the estimated activity in the left kidney and the actual activity for all five background correction methods at all three positions of the kidney cylinders, ranged from -4 to +1 % (Table 4). If no background correction was applied, overestimation from 77% for the kidney-to-background activity concentration ratio of 10:1, up to 413% in the case of the lowest kidney-to-background activity concentration ratio of 2:1 was found (Table 4). Conventional background subtraction resulted in an underestimation of the actual activity, ranging from -22 to -80% with decreasing kidney-to-background activity concentration ratios. For the Kojima method, the differences in estimated activity and actual activity varied from -18 to +11%. Using Thomas' method, the activity was overestimated, gradually increasing with decreasing kidney-to-

TABLE 4
Percentage difference between estimated and actual activity in left kidney

Activity concentration ratio	Posterior depth (cm)	No background correction	Conventional background correction	Kojima method	Thomas method	Buijs method
infinity	1	1	-1	-1	1	0
	5	-2	-4	-4	-2	-4
	10	-1	-3	-2	-1	-2
10:1	1	88	-22	-5	42	7
	5	77	-22	-4	38	2
	10	81	-24	-6	40	2
5 1	1	171	-54	-17	71	7
	5	168	-35	2	71	14
	10	166	-56	-18	68	3
2:1	1	396	-80	4	108	39
	5	400	-75	11	118	39
	10	413	n d	-11	120	32

n d Not determined

background activity concentration ratios, to a difference of 120% between the estimated activity and the actual activity at the 2:1 ratio. For the Buijs method, the differences in estimated activity and actual activity ranged from +2 to +39%. The overall differences between kidney activity estimated from the phantom measurements and the actual activity in the kidney ranged from -80 to +413 % (Table 4).

DISCUSSION

Biodistribution data for radiopharmaceuticals within the body and specific organs may be obtained from planar scintillation camera views using the conjugate view geometric mean technique. The accuracy of this method will be greatest for radiopharmaceuticals distributed in a single organ or isolated organs which do not overlap in the planar projection. However, in most nuclear medicine examinations background activity will be present in adjacent tissues. For planar gamma camera imaging, subtraction of background activity present in surrounding tissue from activity measured in the organ of interest is routinely performed. Background subtraction is required to allow accurate estimation of the organ activity or for comparisons of relative activity uptakes or retentions

between tissues. The adequacy of background subtraction is especially important for the accurate estimation of the activity in the red marrow (22,23), since red marrow is the dose-limiting toxicity in most, if not all, radionuclide therapy and radioimmunotherapy.

This phantom study was carried out to determine the optimal method of background correction. The accuracy of the absolute activity determination in the kidney phantom was evaluated using five different methods of background correction and planar imaging, for three different organ depths and four organ-to-background activity concentration ratios: infinity (meaning no activity in the background at all), 10:1, 5:1 and 2:1. Two kidney inserts were used in order to simulate the clinical situation where cross scatter between activity in the kidneys may occur. The results were virtually identical for both kidneys, therefore only the results for the left kidney were presented.

As all images were uniformly acquired for five minutes each, the counting statistics will differ between the images at different source-to-background activity concentration ratios (achieved by adding different amounts of activity to the abdominal phantom). This may somewhat affect the results due to the statistical uncertainties (i.e., noise) in the resulting images. However, if fixed counts per image would have been acquired, the results could also be affected since most of the counts will come from the background as the background activity is raised and the image acquisition time is shortened. As the acquisition time is shortened for the same number of counts, the statistical uncertainty in the count rate (defined as the square root of the number of counts divided by the acquisition time) will increase. So, irrespective of the methods used to acquire the data, some statistical uncertainty would result.

Application of the conjugate-view method to actual patients generally involves some sort of transmission imaging for estimation of the attenuation term. In this phantom-study the attenuation coefficient (μ_e) was estimated by transmission measurements in a tissue-equivalent phantom using the same camera, collimators, and camera acquisition parameters as in the kidney-phantom study.

In the absence of background activity, the difference between the estimated activity in the left kidney and the actual activity for all five background correction methods at all three positions of the kidney cylinders, was highly accurate and ranged from -4 to +1 % (Table 4). These results indicate that the method of attenuation correction applied in this study is reliable and yields accurate results in a zero-background situation.

Obviously, in the presence of background activity, background correction must be performed (Table 4). The most common method used for background correction is to subtract the counts in a selected background ROI from the counts in the ROI drawn over the organ of interest (representing the sum of

activity in the organ and in the surrounding background). Such a conventional background correction method leads inevitably to an over-correction since the volume of the organ of interest is not taken into account, thus leading to a large underestimation of the true activity in the organ. In our phantom model the underestimation rose with increasing background activity from 22% to 80%.

The no-background-correction method and the conventional method for background correction do not correct for source volume, in contrast to the Kojima, the Thomas and the Buijs methods.

Kojima's background correction method corrects for source volume *(19)*, and was originally used with the depth-independent buildup factor method (DIBF) for attenuation correction *(19,21,24,25)*. However, in this study the geometric mean method (Equation *(1)*) was used for attenuation correction, instead of the DIBF method, in combination with Kojima's background correction method for estimating the organ activity. This modified Kojima method is easy to perform and provides reliable results, if organ thickness, derived from CT images or from anatomical atlas data, are available and patients' thickness is measured as well (Table 4 and Figure 3). Recently, Kojima et al *(26)* refined their method for quantitative planar imaging, using a combination of a transmission image and a conjugate view emission image. The triple energy window (TEW) method for scatter correction of the emission and transmission images was used. Applying this method to their kidney phantom, they found differences of less than 5% between estimated and actual activity for source-to-background activity concentration ratios from 40:1 to 5:1. These results are better than the results of our study using their earlier described method *(19)*, where differences of 5% and 17% for source-to-background activity concentration ratios of 10:1 and 5:1, respectively, were found.

Thomas' method does not use a background subtraction technique, but introduces a multiplication factor $k(\gamma)$ for background correction, in combination with Equation *(1)*. The results of Thomas' method were not very accurate, with a maximum difference of 120% between estimated and actual activity in the kidney at a kidney-to-background activity concentration ratio of 2:1. This may be explained by the fact that this method does not correct for scatter since the formula for $k(\gamma)$ was derived under the condition of narrow-beam geometry. The method may therefore be inadequate for low organ-to-background activity concentration ratios, since as the background activity is increased, more scatter radiation will be present in the source ROI. This analytical method is not based on the measurement of actual background activity, but needs a priori global knowledge of the source-to-background activity concentration ratio. This may be a disadvantage.

The Buijs method also requires a correction factor for the source volume. This factor is simply the ratio between the source thickness and the patient

thickness *(27)* To use this method for quantitative organ uptake in clinical practice, a one-time estimation of the broad beam (effective) attenuation coefficient (μ_e, cm^{-1}) must be calculated from phantom-based transmission curve measurements, for each combination of radionuclide, window settings, collimator and camera

For all five methods of background correction the differences between estimated and actual activity in the kidney varied only slightly with source depth

At low kidney-to-background activity concentration ratios (2 1), Kojima's method is more accurate than Buijs' method However, both methods yield results of estimated activity that are reasonably accurate and reliable for use in routine clinical practice

Finally, it must be stated that the results of any phantom-based study represent a "best-case" scenario Phantom-based studies of radionuclide quantitation, including the current study, generally have limitations, including the inability to accurately simulate the irregularity and non-uniformity of background activities and the irregular sizes, shapes, compositions, and, therefore, linear attenuation coefficients of source and non-source regions In patient studies less accurate activity estimations may result due to variations in background activity concentrations, the size of the ROIs used in the data analysis, variations in and inaccurate estimates of body thickness, organ thicknesses and organ depths

CONCLUSION

This phantom study shows that the use of the Kojima or Buijs methods for background correction combined with quantitative planar imaging, provides more accurate results for the estimation of actual activity in an organ, compared to methods without background subtraction or to conventional background correction The use of Kojima's method is preferable, especially at very low source to background activity concentration ratios

ACKNOWLEDGMENTS

The authors thank Mr A Meeuwis for technical assistance

REFERENCES

1 Loevinger R, Berman M A Revised Schema for Calculating the Absorbed Dose from Biologically Distributed Radionuclides *MIRD Pamphlet No 1 (Revised)* New York. Society of Nuclear Medicine, 1976.

2 Loevinger R, Budinger TF, Watson, EE. *MIRD Primer for Absorbed Dose Calculations (Revised Edition)* New York· Society of Nuclear Medicine; 1991.

3. Rosenthal MS, Cullom J, Hawkins W, Moore SC, Tsui BMW, Yester M Quantitative SPECT Imaging. A Review and Recommendations by the Focus Committee of the Society of Nuclear Medicine Computer and Instrumentation Council *J Nucl Med* 1995; 36 1489-1513.

4 Zanzonico PB, Bigler RE, Sours G, Strauss A. Quantitative SPECT in Radiation Dosimetry. *Semin Nucl Med* 1989; 19:47-61.

5. Tsui BMW, Zhao X, Frey EC, McCartney WH. Quantitative Single-Photon Computed Tomography. Basics and Clinical Considerations *Semin Nucl Med* 1994; 24·38-65

6 Tsui BMW, Frey EC, Zhao X, Lalush DS, Johnson RE, McCartney WH The Importance and Implementation of Accurate 3D Compensation Methods for Quantitative SPECT *Phys Med Biol* 1994, 39 509-530.

7 Parker JA Quantitative SPECT· Basic Theoretical Considerations. *Semin Nucl Med* 1989; 19·3-12.

8 Graham LS, Neil BA In Vivo Quantitation of Radioactivity Using the Anger Camera *Radiology* 1974; 112:441-442.

9. Thomas SR, Maxon HR, Kereiakes JG. In Vivo Quantitation of Lesion Radioactivity Using External Counting Methods *Med Phys* 1976, 3 253-255

10. Sorenson JA. Methods for Quantitating Radioactivity In Vivo by External Counting Measurements. *Ph D Thesis* University of Wisconsin, Madison, WI, 1971

11 Fleming JS A Technique for the Absolute Measurement of Activity Using a Gamma Camera and Computer. *Phys Med Biol* 1979; 24·176-180.

12 Reenen O van, Lotter MG, Heyns A du P, Kock F de, Herbst C, Kotze H et al. Quantification of the distribution of ^{111}In-labeled platelets in organs *Eur J Nucl Med* 1982, 7:80-84

13. Macey DJ, Marshall R Absolute Quantitation of Radiotracer Uptake in the Lungs using a Gamma Camera. *J Nucl Med* 1982; 23:731-734.

14 Eary JF, Appelbaum FL, Durack L,Braun P Preliminary validation of the opposing view method for quantitative gamma camera imaging *Med Phys* 1989, 16:382-387

15. Gainey MA, Siegel JA, Smergel M, Jara BJ Indium-111-labeled white blood cells dosimetry in children. *J Nucl Med* 1988; 29:689-694

16. Rensburg AJ, Lotter MG, Heyns AP, Minnaar PC An evaluation of four methods of ^{111}In planar image quantification *Med Phys* 1988, 15.853-861

17. Hammond N, Moldofsky P, Beardsley M, Mulhern C Jr. External imaging techniques for quantitation of distribution of 1-131 F (ab')2 fragments of monoclonal antibody in humans. *Med Phys* 1984, 11:778-783

18. Ott RJ. Imaging technologies for radionuclide dosimetry. *Phys Med Biol* 1996, 41·1885-1894.

19 Kojima M, Takaki Y, Matsumoto M, Tomiguchi S, Hara M, Shimomura O et al. A Preliminary Phantom Study on a Proposed Model for Quantification of Renal Planar Scintigraphy. *Med Phys* 1993; 20:33-37

20. Buijs WCAM, Massuger L, Claessens RAMJ, Kenemans P, Corstens FH. Dosimetric Evaluation of Immunoscintigraphy Using Indium-111-Labeled Monoclonal Antibody Fragments in Patients with Ovarian Cancer. *J Nucl Med* 1992; 33.1113-1120

21. Wu RK, Siegel JA. Absolute Quantitation of Radioactivity Using the Buildup Factor *Med Phys* 1984; 11·189-192

22 Siegel JA, Lee RE, Pawlyk DA, Horowitz JA, Sharkey RM, Goldenberg DM. Sacral Scintigraphy for Bone Marrow Dosimetry in Radioimmunotherapy. *Nucl Med Biol* 1989; 16: 553-559.
23 Siegel JA, Wessels BW, Watson EE, Stabin MG, Vriesendorp HM, Bradley EW, et al. Bone Marrow Dosimetry and Toxicity for Radioimmunotherapy. *Antibody, Immunoconjug Radiopharm* 1990; 3: 213-233.
24 Siegel JA, Wu RK, Maurer AH. The Buildup Factor: Effect of Scatter on Absolute Volume Determination. *J Nucl Med* 1985; 26: 390-394.
25 Siegel JA. The Effect of Source Size on the Buildup Factor Calculation of Absolute Volume. *J Nucl Med* 1985; 26: 1319-1322.
26 Kojima A, Ohyama Y, Tomiguchi S, Kira M, Matsumoto M, Takahasi M. Quantitative Planar Imaging Method for measuring renal activity using a conjugate-emission image and transmission data. *J Nucl Med* 1997; 38: 208P (abs).
27 Buijs WCAM, Siegel JA, Corstens FHM. Estimation of Absolute Organ Activity Using Five Different Methods of Background Correction: A Phantom Study. *Eur J Nucl Med* 1997; 24: 931 (abs).

CHAPTER 5

Dosimetry and Risk Estimates of Radioiodine Therapy for Large, Multinodular Goiters

Dyde A.K.C. Huysmans, Wilhelmina C.A.M. Buijs, Marjo T.P. van de Ven, Wim J.M. van den Broek, Peter W. C. Kloppenborg, Ad R.M.M. Hermus and Frans H.M. Corstens

J Nucl Med 1996, 37 2072-2079

ABSTRACT

In patients with a large multinodular goiter (>100g), absorbed doses in the thyroid, surrounding tissues and remainder of the body were estimated after therapeutic administration of ^{131}I (3.7 MBq or 100 μCi/g of thyroid tissue retained at 24 h)

Methods Thermoluminescent dosimeter (TLD) measurements were performed on 23 patients (12 euthyroid and 11 hyperthyroid, thyroid weight 222 ± 72 g, 2.1 ± 0.9 GBq ^{131}I) on the skin over the thyroid, over the submandibular gland and over the parotid gland. Thyroid radioactivity measurements were done daily in 6 euthyroid- and 6 hyperthyroid patients (thyroid weight 204 ± 69 g, 1.9 ± 0.9 GBq ^{131}I). An iodine biokinetic model and the MIRD methodology were used to estimate absorbed doses in organs. Cancer risks were calculated using ICRP Publication 60.

Results Cumulated absorbed doses on the skin (TLD measurements) were 4.2 ± 1.4 Gy (thyroid), 1.2 ± 0.6 Gy (submandibular) and 0.4 ± 0.2 Gy (parotid). All these values were significantly correlated with the amount of radioiodine retained in the thyroid at 24 h (euthyroid versus hyperthyroid not significant). Absorbed doses in the thyroid of 94 ± 25 Gy for euthyroid and 93 ± 17 Gy for hyperthyroid patients were calculated (thyroid radioactivity measurements). Extrathyroidal absorbed doses (means of 12 patients) were 0.88 Gy in the urinary bladder, 0.57 Gy in the small intestine, 0.38 Gy in the stomach, and ranged from 0.05 to 0.30 Gy in other organs (euthyroid versus hyperthyroid not significant). A 1.6% life-time risk of development of cancer outside the thyroid gland was calculated. When applied to people of 65 y and older the estimated risk is approximately 0.5%.

Conclusions These data may help in choosing the treatment regimen for individual patients with a large, multinodular goiter, who have to be treated for hyperthyroidism or compressive problems. In younger patients surgery may be preferred. However, for elderly patients and patients with cardiopulmonary disease, the advantages of non-invasive radioiodine treatment will outweigh the life-time risk of this mode of therapy.

INTRODUCTION

Surgery is standard therapy for patients with a large, toxic or nontoxic compressive goiter. However it is not without risk, especially in elderly patients with cardiopulmonary disease *(1,3)*. Radioiodine, a widely accepted treatment for patients with toxic non-compressive goiters is an alternative for these patients. In a recent study we have shown that radioiodine therapy can induce an average reduction in thyroid volume of 40% after one year and a significant widening of the tracheal lumen in patients with a large compressive multinodular goiter *(4)*. However reluctance to treat these patients with radioiodine may be due to a concern for exessive absorbed doses. Many commonly used dosage schedules for radioiodine therapy are aimed at delivering a certain amount of radioiodine per gram of thyroid tissue retained in the thyroid gland at 24 h. The use of such a dosage schedule implies that large amounts of radioiodine are administered to patients with a large nodular goiter.

The present study is focussed on the dosimetric aspects of radioiodine therapy in patients with large goiters. We have estimated absorbed doses in the thyroid, in tissues directly near the thyroid and in tissues and organs in the remainder of the body after therapeutic administration of radioiodine in hyperthyroid and in euthyroid patients with a large, multinodular goiter. Thermoluminescent dosimetry was used to estimate the radiation burden of tissues directly near the thyroid gland. Estimations of absorbed doses in the thyroid and in the remainder of the body were made using thyroid radioactivity measurements and a model of iodine kinetics in the body as described by Robertson and Gorman *(5)*. Risks of radiation-induced cancer were assessed based on the 1990 Recommendations of the International Commission on Radiological Protection *(6)*.

MATERIAL AND METHODS

PATIENTS AND RADIOIODINE TREATMENT

Twenty three consecutive patients with a multinodular goiter of more than 100 g as estimated from palpation and planar thyroid scintigraphy *(7)*, were treated with radioiodine. The diagnosis of multinodular goiter was based on the presence of one or more thyroid nodules at palpation and an irregular distribution of [^{123}I] or [^{131}I] sodium iodide on a thyroid scan. Patients with a solitary hot nodule were excluded. In the 11 patients with toxic multinodular goiter the primary aim of radioiodine therapy was to treat hyperthyroidism. Eight of them had compressive symptoms. All euthyroid patients (n=12) sought treatment for compressive symptoms. In these patients, radioiodine therapy was chosen because of contraindications for surgery (n=8, mainly because of cardiopulmo-

nary disease) or refusal of the patient to undergo surgery (n=4). Patients were classified as euthyroid when they had serum free thyroxine (fT_4) and tri-iodothyronine (T_3) levels within the normal range of our laboratory (fT_4, 9.0-17.0 pmole/liter; T_3, 1.5-3.5 nmole/liter) and were not taking antithyroid or thyromimetic drugs. The serum level of thyroid stimulating hormone (TSH) was subnormal (<0.4 mU/l) in 7 of them. In two euthyroid patients, prior TSH suppressive treatment with L-thyroxine had failed to diminish goiter size. L-thyroxine had been withdrawn 2 months before radioiodine treatment in these patients. All hyperthyroid patients used methimazole and L-thyroxine. They did not receive methimazole for 3 days before and 3 days after radioiodine therapy. Radioiodine was given as a single intravenous dose on an in-patient basis. The administered activity was aimed at delivering 3.7 MBq (100 μCi) of ^{131}I per gram of thyroid tissue retained at 24 h, according to the following formula *(8)*:

$$\text{Administered activity (GBq)} = \frac{\text{thyroid weight (g)} \times 0.37}{\text{24-h thyroid radioactive iodide uptake (\%)}}$$

Thyroid radioactive iodide uptake (RAIU) was measured 24 h after oral ingestion of 7.4 MBq (200 μCi) ^{131}I (normal range 10%–59%). Since gastrointestinal absorption of radioiodine is rapid and complete it is unlikely that the oral route of administration of the diagnostic activity may result in different values for 24-h RAIU compared with the intravenous route. The thyroid weight was estimated from the planimetric surface on a rectilinear thyroid scintigram using the formula of Doering and Kramer: thyroid weight (g) = 0.326 x (surface in cm^2)$^{3/2}$ *(7)*.

THERMOLUMINESCENT DOSIMETER MEASUREMENTS AND DOSIMETRIC CALCULATIONS

Thermoluminescent dosimeter (TLD) measurements were performed following the therapeutic administration of radioiodine in 12 euthyroid and in 11 hyperthyroid patients. Two freshly annealed TLDs sealed in a thin polyethylene bag were positioned with sticking plaster on the skin on each of the following three locations: directly over the thyroid gland, over the submandibular gland and over the parotid gland. The TLD on the thyroid gland was placed over the center of the most prominent nodule, which was checked not to be cold on thyroid scintigraphy. Distances between the TLDs on the salivary glands and the palpated ipsilateral top of the thyroid were measured. The TLDs were left in position for 24 h, and replaced daily for 5 to 15 days after the therapeutic administration of radioiodine. After preannealing, TLDs were read for light output (in nanocoulombs) on a TLD reader under dry N_2. The calibration factor of TLDs for the gamma irradiation of ^{131}I, as checked in vitro, was 100 microgray per nanocoulomb (μGy/nC). Data from a previous study *(4)* in patients with a large

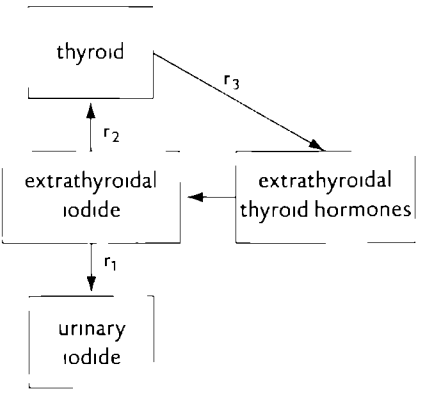

Figure 1 *Simplified model for iodine biokinetics (5)* $r_1 = 0.072\ h^{-1}$ *based on a normal renal function* r_2 *and* r_3 *were calculated from thyroid radioactivity measurements. A total of 15% of the extrathyroidal iodide compartment is located in the stomach, 17% in the small intestine, and 40% of the extra thyroidal thyroid hormone compartment is located in the liver. The remaining parts are evenly distributed throughout the body.*

multinodular goiter (nine of whom also participated in the present study) suggest that the distance between the surface of the thyroid and the surface of the skin, as determined from axial magnetic resonance imaging slices, was more than 5 mm. Therefore, the contribution of beta irradiation was assumed to be negligible on the surface of the skin.

TLD measured values from Day 2 onward were fitted monoexponentially and extrapolated to infinity. The measured values and the integral of the extrapolated function were summed for each location in order to determine cumulated absorbed doses on the skin (Gy).

THYROID RADIOACTIVITY MEASUREMENTS, DOSIMETRIC CALCULATIONS, RISK ESTIMATES

In six euthyroid and in six hyperthyroid patients, thyroid radioactivity measurements were performed every 24 h after the therapeutic administration of radioiodine for 7 to 14 days. A 2 in. x 2 in. NaI(Tl) detector with a diverged-lead collimator connected with an analyzer (type ST 6, Nuclear Enterprises, Reading, UK) was used. The collimator was provided with a lead collimator diaphragm complying with recommendations of the International Atomic Energy Agency (neck-tot-detector distance 26 cm). An 18-mm thick lead-shield was placed in front of the detector in order to reduce the count rate and avoid dead-time effects. Measurements were corrected for a 10-ml test tube standard with a known activity of ^{131}I and all values were corrected for background radioactivity in the room and for physical decay. The mean of three measurements of 1 min duration was used.

Thyroid radioactivity measurements were implemented in a simplified model for iodine biokinetics as described by Robertson and Gorman, diagrammatically represented in Figure 1 *(5)*. In this model, intravenously administered

radioiodide is removed from the extrathyroidal iodide compartment by excretion into the urinary iodide compartment, with fractional removal rate r_1 (in h^{-1}), and by uptake into the thyroid, with fractional uptake rate r_2 (in h^{-1}). In the thyroid radioiodide is incorporated in thyroglobulin. A 24-h delay in the secretion of radioiodinated thyroid hormones is assumed *(5)*. After that time, the loss of radioactivity from the thyroid into the compartment of extrathyroidal radioiodinated thyroid hormone is indicated by the fractional secretion rate r_3 (in h^{-1}). Degradation of the radioiodinated thyroid hormone is assumed to be instantaneous *(5)*. The rate of (renal) excretion of radioiodide resulting from thyroid hormone degradation is supposed to equal that of the administered iodide. The model does not take into account re-uptake into the thyroid of radioiodide resulting from thyroid hormone degradation outside the thyroid. A system of differential equations, using the three rate constants, r_1, r_2 and r_3, and the physical decay constant λ (0.00359 h^{-1}) describes the rates of changes of radioactivity in the four compartments. The solutions of the differential equations describe the fractional activities, i.e., the fractions of the administered activity at time t in each of the compartments. These fractional activities are integrated in order to obtain the cumulated (time-integrated) fractional activities (cumulated activity per MBq of administered activity in MBq·h/MBq, i.e., in h; this parameter is also referred to as residence time) in each of the four compartments. Time-integrated activities resulting from the total administered activities of radioiodine are referred to as cumulated activities (in MBq·h).

Serum creatinine levels were within the normal range in all patients. Therefore, an r_1 of 0.072 h^{-1} based on a normal renal function was assumed for all patients in our study *(9)*. The r_2 was calculated from the radioactivity measurement at 24 hours and from r_1 (24-h RAIU = $RAIU_{max}$ $[1\text{-}e^{-24(r_1+r_2)}]$ in which $RAIU_{max}$ is the theoretical maximal thyroid radioactive iodide uptake). Thyroid radioactivity measurements from Day 2 onward (corrected for physical decay) were fitted as a monoexponential function. The rate constant of this function was used as r_3.

In the biokinetic model of Robertson and Gorman *(5)*, the extrathyroidal iodide and extrathyroidal thyroid hormone compartments are combined and assumed to be evenly distributed throughout the body, outside the thyroid and urinary bladder. We made the following amendments to the biokinetic model based on data in MIRD pamphlet No. 12 and MIRD report No. 5 *(10, 11)*. Of the extrathyroidal iodide compartment 15% was assumed to be located in the stomach and 17% in the small intestine. Of the extrathyroidal thyroid hormone compartment, 40% was assumed to be located in the liver (and, proportional to the weight of the liver, 2.4% of the iodide compartment). Corresponding percentages of the residence times in the extrathyroidal iodide and thyroid hormone compartments were assigned to the stomach, small intestine and liver.

The remaining parts of these residence times were assigned to the total body (i.e., evenly distributed throughout the body outside the thyroid, urinary bladder, stomach, small intestine and liver). To obtain the residence time in the urinary bladder, the cumulated fractional activity in the urine was corrected for voiding with a voiding interval of 4 h *(5)*. Only the urine that enters the bladder during a voiding interval is used in calculating the fractional activity in the bladder during that interval. A constant bladder volume was assumed.

Radiation absorbed doses (1 Gy = 100 rad) in organs were calculated using the MIRD method with tabulated S values for adults (i.e. the mean absorbed dose in a target organ per unit cumulated activity in a source organ) *(12)*. The calculated residence times in the source organs thyroid, urinary bladder, stomach, small intestine, liver and restbody were entered in the MIRDOSE2 computer program (Oak Ridge, TN). In all patients, absorbed doses in the thyroid, as calculated in the MIRDOSE2 program, were corrected for differences in thyroid mass between Standard Man *(12)* and patients using the Standard Man thyroid mass (20 g)-to-patient thyroid mass ratio and for the increasing absorbed fraction of beta particles and photons with increasing thyroid volume, based on S-values for ^{131}I uniformly distributed in spheres of increasing volumes of 1 g/cm^3 density *(13)*.

ICRP Publication 60 *(6)* was used to estimate the risk of radiation-induced cancer in our patients. In ICRP 60, absorbed doses weighted by a radiation factor (which is 1 for radiopharmaceuticals) are called equivalent doses (H; in sievert, Sv; 1 Sv = 100 rem) *(6)*. The sum of the fatal cancer risk (estimated at 5%/Sv whole-body irradiation), nonfatal cancer risk (estimated at 1%/Sv whole-body irradiation) and the risk of severe hereditary effects (estimated at 1.3%/Sv whole-body irradiation) is 7.3% per sievert total body irradiation and is called the total health detriment. The total health detriment is a measure of the adverse health effects that would eventually be experienced by an exposed group and its descendants as a result of the group's exposure to a radiation source *(6)*. These probability coefficients (in %/Sv) are applicable to equivalent doses resulting from absorbed doses below 0.2 Gy and from higher absorbed doses when the dose rate is less than 0.1 Gy per hour. The relative importance of each of the various organs in contributing to this detriment *(4)* is expressed by its weighting factor (w_T) *(6)*. The detriment for each organ is expressed as w_T x 7.3%/Sv organ dose. The fatal and nonfatal cancer risk is extracted from the total health detriment by excluding 90% of the weighting factor for the gonads because this weighting factor applies for 90% to the risk of severe hereditary effects and for only 10% to the gonadal (especially ovarian) cancer risk. For other organs the weighting factor only applies to the cancer risk. Furthermore, the values for tissue weighting factors were used to determine the effective dose which is the sum of the weighted equivalent doses in all the tissues and organs of the body

(effective dose = $\Sigma w_T \times H_T$) *(6)* Only the contributions of the organs and tissues outside the thyroid were summed, because equivalent and effective doses are not applicable to high doses as received by the thyroid during radioiodine therapy

STATISTICAL ANALYSES

The mean values ± s d are given Statistical analyses were done using the Mann-Whitney U test for unpaired observations (p-values denoted as p), the Wilcoxon sign-rank test for paired observations (p-values denoted as p*) and the Spearman rank correlation test (p-values denoted as p**) The level of significance was 0 05

RESULTS

No increases of compressive symptoms were observed after radioiodine treatment One hyperthyroid patient complained about some further swelling of his goiter from the third until the sixth day after radioiodine therapy For detailed information on the effectiveness of radioiodine treatment for large, multinodular goiters the reader is referred to a recently published study from our group *(4)* in which a 20% to 70% reduction of thyroid volume (mean 40%) and significant decompression of the trachea was demonstrated using MRI one year after radioiodine treatment In the present group of patients no MRI measurements of thyroid volume reduction and decompression of vital structures were done

THERMOLUMINESCENT DOSIMETER MEASUREMENTS

Table 1 shows patient characteristics and data of TLD measurements on the skin over the thyroid, the submandibular and the parotid gland in 12 euthyroid and 11 hyperthyroid patients The thyroid weight was similar in both groups of patients The 24-h thyroid radioactive iodide uptake was significantly lower in euthyroid patients ($p < 0\ 02$) The total administered activity was higher in euthyroid than in hyperthyroid patients, although the difference was not significant No significant differences in cumulated absorbed doses between euthyroid and hyperthyroid patients were observed at any of the three locations on the skin

Cumulated absorbed doses at all three locations were significantly correlated with the total activity retained in the thyroid at 24 hours (administered activity x 24-h RAIU/100) ($r=0\ 642$, $p^{**}<0\ 001$ for the thyroid location, $r = 0\ 696$, $p^{**} < 0\ 001$ for the submandibular location, $r = 0\ 579$, $p^{**} < 0\ 005$ for the parotid location) (Figure 2) The correlation of the cumulated absorbed dose on the skin with the total administered activity was only significant for the location over the thyroid gland ($r = 0\ 557$, $p^{**} < 0\ 01$) and no correlation of cumulated absorbed doses

TABLE 1

Patient characteristics and data of TLD measurements after radioiodine treatment of euthyroid and hyperthyroid patients with large multinodular goiters (>100 g)

	Euthyroid	Hyperthyroid
Number of patients	12	11
Age (y)	62 ± 12 (44 – 81)	71 ± 8 (57 – 82)
Female Male ratio	11 1	8 3
Serum level of thyroid-stimulating hormone [a]	0 33±0 39 (<0 01–1 20)	(on thyroid medication)
Serum level of free thyroxine [a]	11 9 ± 1 9 (6 9 – 14 2)	(on thyroid medication)
Serum level of total tri-iodothyronine [a]	2 2 ± 0 5 (1 6 – 3 3)	(on thyroid medication)
Thyroid weight (g)	221 ± 81 (122 – 351)	224 ± 65 (130 – 312)
24h RAIU (%)	36 ± 11 (21 – 56)	51 ± 14 (32 – 78)[b]
Administered activity of ^{131}I (GBq)	2 3 ± 0 8 (1 2 – 4 0)	1 8 ± 0 8 (0 8 – 3 3)
Cumulated dose on skin thyroid (Gy)	4 4 ± 1 5 (2 4 – 7 2)	4 1 ± 1 4 (2 0 – 6 3)
Cumulated dose on skin submandibular gland (Gy)	1 2 ± 0 6 (0 5 – 2 4)	1 3 ± 0 6 (0 5 – 2 0)
Cumulated dose on skin parotid gland (Gy)	0 3 ± 0 1 (0 2 – 0 8)	0 4 ± 0 1 (0 2 – 0 7)
Distance thyroid – submandibular gland (cm)	4 7 ± 2 0 (2 5 – 7 5)	4 3 ± 1 7 (2 5 – 7 5)
Distance thyroid – parotid gland (cm)	10 7 ± 1 8 (8 5 – 13 5)	10 5 ± 2 0 (8 0 – 13 5)
TLD measured effective half-life thyroid (days)	6 1 ± 0 8 (4 4 – 7 3)	5 5 ± 0 7 (4 2 – 6 5)[c]

The mean values ± s d are given, ranges are given in parentheses

a Normal ranges thyroid-stimulating hormone, 0 4 – 4 0 mU/l, free thyroxine, 9 0 – 17 0 pmole/liter, total tri-iodothyronine, 1 5 – 3 5 n mole/liter

b $p < 0\ 02$ euthyroid versus hyperthyroid patients

c $p < 0\ 03$ euthyroid versus hyperthyroid patients

on the skin with 24-h RAIU was found ($p^{**} > 0.1$) The effective half-life of ^{131}I in the thyroid gland, as measured by TLDs, was significantly higher for euthyroid patients (6.1 ± 0.8 days) than for hyperthyroid patients (5.5 ± 0.7 days) ($p < 0.03$).

THYROID RADIOACTIVITY MEASUREMENTS, DOSIMETRIC CALCULATIONS AND RISK ESTIMATES

Table 2 shows patient characteristics and data of thyroid radioactivity measurements in six euthyroid and six hyperthyroid patients. The thyroid weight was similar for euthyroid and hyperthyroid patients. There were no significant differences in administered activity, 24-h RAIU or effective half-life of ^{131}I in the thyroid (thyroid radioactivity measurements) between both groups. Residence times in source organs, as calculated from thyroid radioactivity measurements and the aforementioned biokinetic model *(5)* with modifications *(10,11)*, did not differ significantly between euthyroid and hyperthyroid patients, except for the residence time in the liver, which was significantly higher for hyperthyroid patients ($p < 0.03$) (Table 2). Effective half-lives of ^{131}I in the thyroid resulting from thyroid radioactivity measurements were not significantly different from

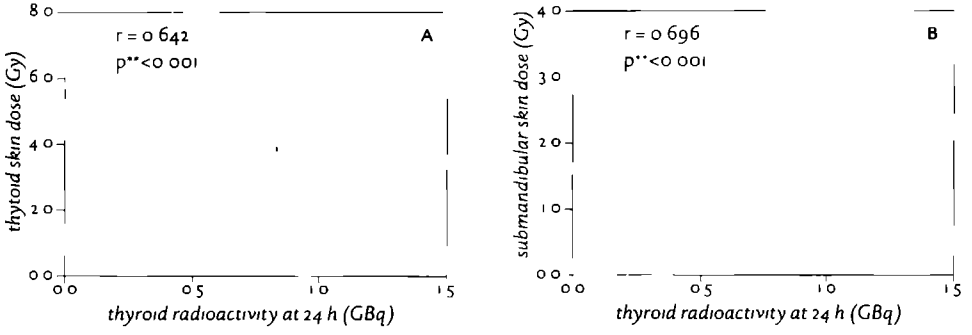

those measured with TLDs in the same 12 patients (Wilcoxon sign-rank test, $p^* = 0.7$). Moreover, a highly significant correlation was found between the cumulated activity (in GBq.h) in the thyroid and the cumulated absorbed dose on the skin overlying the thyroid as measured with TLDs in the same 12 patients ($r = 0.748$, $p^{**} < 0.01$).

Table 3 shows the calculated absorbed doses in the tissues and organs for

TABLE 2

Patient characteristics and data of thyroid radioactivity measurements after radioiodine treatment of euthyroid and hyperthyroid patients with large multinodular goiters (>100 g)

	Euthyroid	Hyperthyroid
number of patients	6	6
age (years)	65 ± 10(52-81)	70 ± 6 (63-80)
Female Male ratio	5 1	3 3
Thyroid weight (g)	203 ± 84 (126-351)	206 ± 59 (130 274)
24-h RAIU tracer activity (%)	37 ± 11 (21-48)	51 ± 11 (35-63)[a]
24-h RAIU therapeutic activity (%)	37 ± 16 (17-58)	52 ± 5 (47-59)[a]
Therapeutic activity of ^{131}I (GBq)	2 2 ± 1 1 (1 2-4 0)	1 6 ± 0 6 (0 8-2 2)
Effective half life of ^{131}I in thyroid (d)	5 7 ± 0 4 (5 1-6 1)	5 3 ± 0 5 (4 7-6 1)
Biological half life of ^{131}I in thyroid (d)	21 ± 6 (14-31)	18 ± 5 (11-25)
Cumulated activity in thyroid (GBq h)	160 ± 110 (67-377)	155 ± 57 (82-215)
Residence time thyroid (h) [b]	77 ± 34 (37-120)	99 ± 11 (82-116)
Residence time stomach (h) [c]	1 23 ± 0 31 (0 84-1 62)	0 96 ± 0 08 (0 82 1 04)
Residence time small intestine (h) [c]	1 40 ± 0 35 (0 95-1 83)	1 09 ± 0 10 (0 93-1 18)
Residence time liver (h) [c]	0 70 ± 0 17 (0 47-0 90)	1 00 ± 0 16(0 71-1 16)[d]
Residence time rest body (h) [c]	6 3 ± 1 1 (4 9-7 6)	5 5 ± 0 4 (5 0-6 0)
Residence time urinary bladder (h) [c]	1 5 ± 0 2 (1 2-1 7)	1 3 ± 0 1 (1 2-1 4)

The mean values ± s d are given, ranges are given in parentheses

a p<0 02 euthyroid versus hyperthyroid patients

b Calculated from thyroid radioactivity measurements

c Calculated using thyroid radioactivity measurements and the biokinetic model of Robertson and Gorman *(5)* with amendments based on MIRD pamphlet no 12 *(10)* and MIRD report no 5 *(11)*

d p<0 03 euthyroid versus hyperthyroid patients

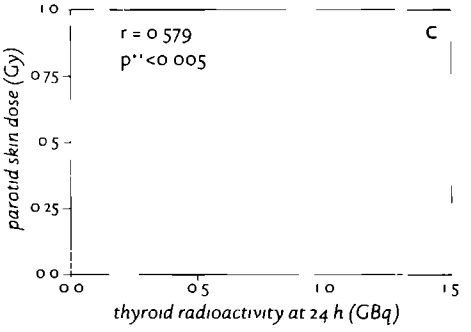

Figure 2 *Cumulated absorbed doses on the skin over the thyroid (A), over the submandibular gland (B) and over the parotid gland (C) plotted against the total radioactivities retained in the thyroid at 24 hours (administered activity x 24 h RAIU(%) / 100)*

which a tissue weighting factor has been determined *(6)*, expressed as dose per unit of administered radioiodine (in mGy/MBq) and as dose resulting from the total administered activities of radioiodine (in Gy). Outside the thyroid gland the highest absorbed doses per MBq of administered ^{131}I were calculated for the urinary bladder, followed by the stomach and small intestine. Inverse correla-

TABLE 3

Radiation absorbed doses in target organs after radioiodine treatment of euthyroid and hyperthyroid patients with large multinodular goiters (>100 g) calculated with the MIRD method

	Absorbed Dose per Unit Administered Activity (mGy/MBq)		Absorbed Dose (Gy)	
Target Organ	Euthyroid (n-6)	Hyperthyroid (n=6)	Euthyroid (n=6)	Hyperthyroid (n=6)
Thyroid [a]	51 ± 23	64 ± 19	94 ± 25	93 ± 17
Red bone marrow	0 092 ± 0 024	0 108 ± 0 008	0 19 ± 0 11	0 16 ± 0 08
Ovaries	0 044 ± 0 008	0 039 ± 0 002	0 10 ± 0 06	0 06 ± 0 02
Testes	0 025 ± 0 004	0 023 ± 0 001	0 06 ± 0 03	0 04 ± 0 01
Colon [b]	0 044 ± 0 008	0 038 ± 0 002	0 10 ± 0 06	0 06 ± 0 02
Lung	0 089 ± 0 028	0.107 ± 0 009	0 19 ± 0 11	0 17 ± 0 06
Stomach	0 33 ± 0 08	0 26 ± 0 02	0 74 ± 0 49	0 41 ± 0 16
Urinary bladder	0 48 ± 0 08	0 43 ± 0 03	1 06 ± 0 63	0 71 ± 0 30
Breast	0 045 ± 0 010	0 051 ± 0 003	0 10 ± 0 05	0 08 ± 0 03
Liver	0 078 ± 0 012	0 099 ± 0 011 [c]	0 17 ± 0 08	0 16 ± 0 06
Skin	0 056 ± 0 015	0 066 ± 0 005	0 12 ± 0 07	0 11 ± 0 03
Bone surface	0 116 ± 0 037	0 140 ± 0 013	0 24 ± 0 14	0 22 ± 0 09
Remainder [d]	0 085 ± 0 006	0 088 ± 0 003	0 18 ± 0 09	0 14 ± 0 05
Effective dose outside thyroid (Sv)			0 27 ± 0 14	0 19 ± 0 07

The mean values ± s d are given

a Thyroid absorbed doses as calculated with MIRDOSE2 are corrected for differences in thyroid mass between Standard Man *(12)* and patients using the Standard Man thyroid mass (20 g)-to-patient thyroid mass ratio and for the increasing absorbed fraction of beta particles and photons with increasing thyroid volume

b 0 57 x dose upper large intestine + 0 43 x dose lower large intestine *(6)*

c $p < 0\ 03$ euthyroid versus hyperthyroid patients

d The absorbed dose in the "remainder of the body" is the average dose in the following organs and tissues adrenals, brain, upper large intestine, small intestine, kidney, muscle, pancreas, spleen, thymus and uterus *(6)*

tions were found between the 24-h RAIU and the absorbed doses per MBq in the stomach ($r = -0.97$, $p < 0.001$), small intestine ($r = -0.98$, $p < 0.001$) and urinary bladder ($r = -0.85$, $p < 0.01$). The absorbed dose in the liver was positively correlated with the 24-h RAIU ($r = 0.83$, $p < 0.001$). The absorbed dose in the liver (mGy/MBq) was significantly higher in hyperthyroid than in euthyroid patients ($p < 0.03$). There were no other significant differences for organ doses between euthyroid and hyperthyroid patients.

Extrathyroidal doses resulting from the total administered activities ranged between 0.06 Gy (testes) and 1.06 Gy (urinary bladder) in euthyroid patients and between 0.04 Gy (testes) and 0.71 Gy (urinary bladder) in hyperthyroid patients (average values of six patients in both groups). No significant correlations of absorbed doses (Gy) with 24-h RAIU were found. The mean absorbed doses in most tissues were about similar for euthyroid and hyperthyroid patients ($p > 0.3$). The mean absorbed doses in stomach, small intestine and urinary bladder were higher for euthyroid than for hyperthyroid patients. However, these differences were not significant.

The effective dose for the combined organs and tissues outside the thyroid gland was not significantly different for euthyroid (0.27 ± 0.14 Sv) and hyperthyroid patients (0.19 ± 0.07 Sv). Using the total health detriment of 7.3% / Sv given in ICRP Publication 60 *(6)* and excluding the risk of severe hereditary effects, the life-time risk of cancer for the combined organs and tissues outside the thyroid can be estimated as $1.8\% \pm 1.0\%$ for euthyroid patients and $1.3\% \pm 0.5\%$ for hyperthyroid patients in the present study (difference euthyroid versus hyperthyroid not significant). A total health detriment of 7.3 % / Sv is, however, an average for a population of all ages. For people of 45 y or older the probability of radiation-induced cancer is less than half of the average for a population of all ages and for people of 65 y and older it is only about one-third of the average *(6,14,15)*. Because 8 of 12 patients in the present study were older than 65 years and only one patient was younger than 60 years an estimate of approximately 0.5% life-time risk of cancer (outside the thyroid gland) seems more appropriate.

DISCUSSION

In the present study thermoluminescent dosimeter (TLD) measurements showed cumulated (i.e. time-integrated) absorbed doses of 4.2 ± 1.4 Gy on the skin directly overlying the thyroid, of 1.2 ± 0.6 Gy on the skin over the submandibular gland and of 0.4 ± 0.2 Gy on the skin over the parotid gland, after therapeutic administration of radioiodine in patients with a large, multinodular goiter (mean thyroid weight 222 ± 72 g). There were no significant differences between euthyroid and hyperthyroid patients. Absorbed doses at all three

locations were significantly correlated with the amount of radioiodine retained in the thyroid at 24 h. Absorbed doses in the spinal cord must have been lower than the doses measured on the skin over the thyroid because the distance between the posterior edge of the thyroid and the spinal cord is considerably larger than the distance between the anterior edge of the thyroid and the surface of the skin. This implies that the cervical spinal cord has absorbed less than one tenth of the dose which in external radiation therapy is considered the threshold dose above which necrosis of the spinal cord may be induced (approximately 55 Gy delivered in 30 fractions over 5 to 6 weeks) *(15)*. On the other hand, it is likely that in a number of our patients the esophageal and tracheal mucosa at the level of the thyroid gland have absorbed higher doses of gamma radiation than those measured with thermoluminescent dosimeters (TLDs) on the skin, because in many patients with a large goiter, thyroid tissue is immediately adjacent to the trachea and esophagus on the anterior as well as on the right and left side. However, it is not to be expected that significant doses of beta radiation have been absorbed in the esophageal and tracheal mucosa, because the maximal range of beta particles of ^{131}I in tissues is 3 mm and the average range only 0.3 mm.

The significant correlation between absorbed doses on the skin overlying the salivary glands and the amount of radioiodine in the thyroid at 24 h suggests that these doses were for a large part caused by gamma radiation from radioiodine in the thyroid gland. Absorbed doses within the salivary glands will have been higher than those measured on the skin, because of beta irradiation from radioiodide concentrated in these glands. The methods we used do not permit further quantification of the absorbed doses within the salivary glands.

In accordance with earlier studies *(16, 17)* TLD measurements proved an effective method of monitoring effective half-lives of ^{131}I in the thyroid. For this purpose TLDs may be applied by the patients themselves at home, thus eliminating the need for frequent thyroid radioactivity measurements in the clinic *(17)*. Our TLD measurements in 23 patients showed a small but significant difference in effective half-lives of ^{131}I in the thyroid between euthyroid and hyperthyroid patients (6.1 ± 0.8 days and 5.5 ± 0.7 days, respectively). Thyroid radioactivity measurements with a NaI detector in 12 patients showed similar effective half-lives of ^{131}I in the thyroid. Using this method, the difference between euthyroid and hyperthyroid patients was not significant (5.7 ± 0.4 days and 5.3 ± 0.5 days, respectively). The effective half-life of about 5.5 days for hyperthyroid patients found in our study is comparable to other reports on hyperthyroid patients *(18–21)*. However, the observed effective half-life in hyperthyroid as well as in euthyroid patients are considerably lower than those reported in the dose estimate reports for radioiodine in ICRP Publication 53 (7.3 days) *(22)* and MIRD report no. 5 (6.9 days) *(11)* which apply to tracer doses of ^{131}I in euthyroid adults. The fast release of radioiodine from the thyroid found in our study may have

been caused by radiation-induced damage to thyroid cells from therapeutic activities of radioiodine *(5,21,23)* or may be related to the state of iodine sufficiency. In view of the small difference between euthyroid and hyperthyroid patients, the elimination rate of a therapeutic activity of ^{131}I from the thyroid appears to be less dependent on the functional state of the thyroid at the time of therapy.

A highly significant correlation between the cumulated dose on the skin overlying the thyroid and the cumulated activity within the thyroid as measured with a NaI detector was found. However, TLD measurements depend too much on thyroid mass, depth and geometry to warrant their use in estimating absorbed doses within the thyroid *(24)*. Therefore, we used radioactivity measurements with a NaI detector to estimate absorbed doses in the thyroid. The absorbed dose in the thyroid of approximately 95 Gy for both euthyroid and hyperthyroid patients, found in our study, is in the lower range of doses commonly used for the treatment of toxic multinodular goiter (80-200 Gy) *(25-28)*. This is explained by the combination of a relatively low administered activity per gram of thyroid tissue and a short effective half-life in the thyroid. Uncertainty in our calculations of thyroid absorbed doses is caused by the inaccuracy of thyroid weight estimations by planar scintigraphy *(29,30)*. Furthermore, the calculated absorbed dose in the thyroid is an average value for the whole thyroid gland. In a nodular goiter, considerable regional differences in absorbed doses are caused by inhomogeneous radioiodine uptake within the goiter.

Using radioactivity measurements and the biokinetic model of Robertson and Gorman *(5)*, the mean values for absorbed doses in extrathyroidal tissues and organs ranged from 0.023 to 0.48 mGy/MBq of administered radioiodine. Absorbed doses per MBq in the urinary bladder, stomach and small intestine were inversely correlated with 24-h RAIU, because a larger uptake of iodide into the thyroid gland reduces the residence time of ^{131}I-iodide in the urinary bladder and other extrathyroidal organs. The liver, unlike stomach, small intestine and urinary bladder, is the organ where ^{131}I incorporated in thyroid hormones is collected and metabolized. This was accounted for by assigning 40% of the extrathyroidal thyroid hormone compartment to the liver *(10,11)*. This explains why the absorbed dose per MBq in the liver was positively correlated with the 24-h RAIU, which is an indicator of the synthesis of thyroid hormones. Furthermore, the residence time and the absorbed dose per MBq in the liver were significantly higher in hyperthyroid than in euthyroid patients, reflecting the higher metabolism of radioiodinated thyroid hormones in hyperthyroidism. However, for the absorbed doses resulting from the total administered activities of radioiodine neither significant correlations with the 24-h RAIU nor a significant difference between hyperthyroid and euthyroid patients were found, because in our dose calculations the total administered activity is inversely related with 24-h RAIU.

The absorbed doses per MBq of administered ^{131}I found in our study are in accordance with data in the literature, obtained by other techniques of measurement and other biokinetic models *(11,22,31-33)*. However, our patients with large, multinodular goiters and a low thyroid radioiodide uptake received considerably larger total activities of radioiodine than the amounts that are commonly used in patients with Graves' disease. Therefore, extrathyroidal absorbed doses (in Gy) were about four times as high as those reported for patients with Graves' disease in the literature *(5,34-37)*.

The risk of induction of thyroid cancer by external radiation is dose dependent *(38)*. Absorbed doses in the thyroid during radioiodine therapy are more than 10 times as high as doses reported for external radiation exposure *(38)*. However, in studies with a long-term follow-up of large numbers of patients treated with radioiodine for hyperthyroidism no significantly increased risk of thyroid cancer was found *(33,37,39,40)*. It has been suggested that high doses, as absorbed in the thyroid during radioiodine therapy for hyperthyroidism, lead to substantial cell killing and cell sterilization instead of the production of carcinogenic mutations in the cell's DNA *(36,38,41)*. Although our patients with large goiters received higher total amounts of radioiodine than the patients in the aforementioned follow-up studies *(36,37,39,40)* absorbed doses in the thyroid were similar. Therefore, an elevated risk of thyroid cancer is not to be expected in these patients with a large goiter.

From studies with follow-up till 35 y, there is no evidence that the overall cancer incidence and cancer mortality in patients with Graves' disease treated with radioiodine are elevated *(36,37,42,43)*. Literature on cancer incidences after radioiodine therapy relating specifically to patients with nodular goiter is sparse. In one study, a slightly elevated overall cancer incidence was reported in patients with toxic nodular goiter treated with radioiodine (average administered activity 700 MBq or 19 mCi), possibly related to higher administered activities than in patients with Graves' disease (average administered activity 360 MBq or 10 mCi) *(36)*. This is still to be confirmed in other studies. With respect to the incidence of cancers of individual extrathyroidal organs and tissues in patients treated with radioiodine for hyperthyroidism (Graves' disease or nodular goiter), the risk of leukemia appears not to be elevated *(44-46)*. The risk of cancer of the stomach may be slightly increased *(36,37)*. In some studies, the incidences of bladder cancer and of breast cancer have been reported to be increased *(45,47,48)*. However, these findings have not been confirmed by other studies *(36,37,45)*.

In our study, patients with a large, multinodular goiter were treated with considerably larger amounts of radioiodine (1900 MBq or 51 mCi on average) than the average doses administered in the aforementioned studies. Using a total health detriment of 7.3%/Sv for a population of all ages *(6)* and excluding the risk

of severe hereditary effects, we calculated a 1 6% life-time risk of fatal and non-fatal cancer for the combined organs outside the thyroid By comparison, the life-time risk of fatal cancer for an unexposed population of all ages is approximately 20% *(49)* and this percentage is of course higher when non-fatal cancers are included In older people the full incidence of radiation-induced cancer is not expressed because their life expectancy is shorter than the average latent period *(14,49)* Accordingly, we calculated a lower risk (0 5%) for people over 65 years of age This figure is in the same order of magnitude as that reported for the surgical mortality of subtotal thyroidectomy *(1,3)* The risks of surgery are of course higher in elderly patients, in patients with a large goiter and in those with cardiopulmonary disease (2) Furthermore, the morbidity of thyroid surgery, including non-fatal complications, is considerably larger *(1-3)*

Until now, no follow-up data on cancer incidence in patients with a large goiter treated with high doses of radioiodine are available It has to be stressed that the risk of radioiodine therapy calculated in our study is only a rough estimate of risk Because radiation risk estimates are predominantly based on epidemiological data of populations after instantaneous external irradiation (mostly survivors of the atomic bombs) they comprise a number of uncertainties, e g uncertainties inherent in dose estimations, in the selection of an appropriate risk model, and in the applicability of risk estimates measured in one population to other exposed groups *(6,49,50)* In the case of radioiodine therapy the cancer risk may be overestimated because the carcinogenic effectiveness per gray of gamma and beta radiation is reduced at the low dose rates which are delivered by the internally deposited ^{131}I with its physical half life of 8 days *(49)*

CONCLUSION

The estimated risks of both surgery and radioiodine should be carefully weighed in all patients with a large, multinodular goiter who have to be treated for hyperthyroidism or compressive problems In younger patients surgery may be preferred, especially when the amount of radioiodine to be administered, as calculated from a radioiodine tracer study, is high or whenever there is any suspicion of thyroid malignancy However, for elderly patients and patients with cardiopulmonary disease, the profits of noninvasive radioiodine treatment will outweigh the life-time risk of this mode of therapy

ACKNOWLEDGMENTS

The authors thank Mr A de Leeuw from the Department of Health Physics for handling the TLDs

REFERENCES

1 Studley JGN Lynn J Surgical anatomy of the thyroid gland and the technique of thyroidectomy In Lynn J Bloom SR eds *Surgical Endocrinology* Oxford Butterworth Heinemann 1993 231 240

2 Weitensfelder W Lexer G Aigner H Fellinger H Trattnig J Grunbacher G Die langfristige laryngoskopische Nachkontrolle bei Einschrankung der Stimmbandmotilitat nach Strumaoperation *Chirurg* 1989 60 29 32

3 Foster RS Morbidity and mortality after thyroidectomy *Surg Gynecol Obstet* 1978 146 423 429

4 Huysmans DAKC Hermus ARMM Barentsz JO Corstens FHM Kloppenborg PWC Large compressive goiters treated with radioiodine *Ann Intern Med* 1994 121 757-762

5 Robertson JS Gorman CA Gonadal radiation dose and its genetic significance in radioiodine therapy of hyperthyroidism *J Nucl Med* 1976 17 826 835

6 ICRP Publication 60 *1990 Recommendations of the International Commission on Radiological Protection* Oxford Pergamon Press 1991

7 Doering P Kramer K Die Bestimmung des Schilddrusengewichtes mit der Szintigraphie nach Gabe von Radiojod Ein Beitrag zur Dosierung des Radioisotopes *Strahlentherapie* 1958 105 245 259

8 DeGroot LJ Graves disease diagnosis and treatment Multinodular goitre In DeGroot LJ Stanbury JB eds *The Thyroid and Its Diseases* 4th ed New York Wiley 1975 314 367 637 665

9 Keating FR Power MH Berkson J et al The urinary excretion of radioiodine in various thyroid states *J Clin Invest* 1947 26 1138 1151

10 Berman M Appendix B Iodine kinetics In Cloutier RJ Smith EM eds *Kinetic models for absorbed dose calculations* (MIRD pamphlet No 12) New York Society of Nuclear Medicine 1977 11 13

11 Berman M Braverman LE Burke J DeGroot L McCormack KR Oddie TH Rohrer RH Wellman HN Smith EM MIRD dose estimate report no 5 Summary of current radiation dose estimates to humans from ^{123}I ^{124}I ^{125}I ^{126}I ^{130}I ^{131}I and ^{132}I as sodium iodide *J Nucl Med* 1975 16 857-860

12 Loevinger R Berman M A revised schema for calculating the absorbed dose from biologically distributed radionuclides *MIRD pamphlet no 1* revised New York Society of Nuclear Medicine 1975

13 Siegel JA Stabin MG Absorbed fractions for electrons and beta particles in spheres of various sizes *J Nucl Med* 1994 35 152 156

14 Land CE Sinclair WK The relative contribution of different organ sites to the total cancer mortality associated with low dose radiation exposure *Annals of the ICRP* 1991 22 31 57

15 Misadministrations of radioactive material in medicine Scientific background NCRP *Commentary no 7* Bethesda NCRP 1991

16 Malone JF Cullen MJ A thermoluminescent method for estimation of effective thyroidal half life of therapeutic ^{131}I in toxic goitre *Br J Radiol* 1975 48 762 764

17 O Connor MK Cullen MJ Malone JF The influence of thyroid geometry on the response of LiF and $CaSO_4$ thermoluminescent discs to ^{131}I and ^{125}I irradiation *Phys Med Biol* 1978 23 712 722

18 DeGroot LJ Kinetic analysis of iodine metabolism *J Clin Endocr* 1966 26 149 173

19 Werner SC Johnson PM Goodwin PM Wiener JD Linderboom GA Long-term results with iodine 125 treatment for toxic diffuse goitre *Lancet* 1970 ii 681 685

20 Muller B Bares R Bull U Untersuchungen zur effektiven Halbwertzeit des ^{131}J bei der Radiojodbehandlung der Schilddrusenautonomie *Nuklearmedizin* 1991 30 71-76

21 Bockisch A, Jamitzky T, Derwanz R, Biersack HJ. Optimized dose planning of radioiodine therapy of benign thyroidal diseases. *J Nucl Med* 1993; 34: 1632-1638.

22 Iodide ^{123}I, ^{124}I, ^{125}I, ^{131}I. In: ICRP Publication 53. *Radiation Dose to Patients from Radiopharmaceuticals*. New York: Pergamon Press; 1987: 259-278.

23 Maloof F, Dobyns BM, Vickery AL. The effects of various doses of radioactive iodine on the function and structure of the thyroid of the rat. *Endocrinol* 1952; 50: 612-638.

24 O'Connor MK, Cullen MJ, Malone JF. The influence of thyroid geometry on the response of LiF and $CaSO_4$ thermoluminescent discs to ^{131}I and ^{125}I irradiation. *Phys Med Biol* 1978; 23: 712-722.

25 Glanzmann Ch, Kaestner F, Horst W. Therapie der Hyperthyreose mit Radio-Isotopen des Jods. Erfahrungen bei über 2000 Patienten. *Klin Wochenschr* 1975; 53: 669-678.

26 Holm LE, Lundell G, Israelsson A, Dahlqvist I. Incidence of hypothyroidism occurring long after iodine-131 therapy for hyperthyroidism. *J Nucl Med* 1982; 23: 103-107.

27 Hoeschel M, Heinze HG. 131-J-Therapie des Morbus Basedow und der nicht immunogenen Hyperthyreose. *Nuklearmedizin* 1984; 23: 143-149.

28 Berding G, Schicha H. Ergebnisse der Radiojodtherapie der manifesten Hyperthyreose und der autonomen Struma mit Euthyreose. *Nuklearmedizin* 1990; 29: 158-165.

29 Farzakas S, Balazs G, Petranyi G, Szeleczky G. Zur Bestimmung des Schilddrusengewichtes mittels einer szintigraphischen Methode. *Nuklearmedizin* 1964; 4: 56-62.

30 Brown MC, Spencer R. Thyroid gland volume estimated by use of ultrasound in addition to scintigraphy. *Acta Radiol Oncol* 1978; 17: 337-341.

31 Philippon B, Briere J. Absorbed dose to ovaries and uterus during ^{131}I-treatment of hyperthyroidism: comparison between in vivo TLD measurements and calculations. *Health Phys* 1979; 36: 727-729.

32 McEwan AC. Absorbed doses in the marrow during ^{131}I therapy. *Br J Radiol* 1977; 50: 329-331.

33 Stabin MG, Watson EE, Marcus C S, Salk RD. Radiation dosimetry for the adult female and fetus from iodine 131 administration in hyperthyroidism. *J Nucl Med* 1991; 32: 808-813.

34 Halnan KE. Risks from radioiodine treatment of thyrotoxicosis. *Br Med J* 1983; 287: 1821-1822.

35 Graham GD, Burman KD. Radioiodine treatment of Graves' disease: an assessment of its potential risks. *Ann Intern Med* 1986; 105: 900-905.

36 Holm LE, Hall P, Wiklund K, Lundell G, Berg G, Bjelkengren G, Cederquist E, Eriesson UB, Hallquist A, Larsson LG, Lidberg M, Lindberg S, Tennvall J, Wicklund H, Boice JD. Cancer risk after iodine-131 therapy for hyperthyroidism. *J Natl Cancer Inst* 1991; 83: 1072-1077.

37 Hall P, Berg G, Bjelkengren G, Boice JD, Eriesson UB, Hallquist A, Lidberg M, Lundell G, Tennvall J, Wiklund K, Holm LE. Cancer mortality after iodine 131 therapy for hyperthyroidism. *Int J Cancer* 1992; 50: 886-890.

38 Shore RE. Issues and epidemiological evidence regarding radiation-induced thyroid cancer. *Radiat Res* 1992; 131: 98-111.

39 Van Middlesworth L. Effects of radiation on the thyroid gland. In: Siperstein MD, ed. *Advances in Internal Medicine* no 34. Year Book Medical Publishers; 1989: 265-284.

40 Dobyns BM, Sheline GE, Workman JB, Tompkins EA, McConahey WM, Becker DV. Malignant and benign neoplasms of the thyroid in patients treated for hyperthyroidism: a report of the Cooperative Thyrotoxicosis Therapy Follow-up Study. *J Clin Endocrinol Metab* 1974; 38: 976-998.

41 Holm LE, Dahlqvist I, Israelsson A, Lundell G. Malignant thyroid tumors after iodine-131 therapy: a retrospective cohort study. *N Engl J Med* 1980; 303: 188-191.

42 Hoffman DA. Late effects of I-131 therapy in the United States. In: Boice JD, Fraumeni JR, eds. *Progress in Cancer Research and Therapy: Radiation Carcinogenesis: Epidemiology and Biological Significance*. Vol 26. New York: Raven Press; 1984: 273-280.

43 Hennemann G, Krenning EP, Sankaranarayanan K Place of radioactive iodine in treatment of thyrotoxicosis *Lancet* 1986, 1 1369-1372
44 Saenger EL, Thoma GE, Tompkins EA Incidence of leukemia following treatment of hyperthyroidism *JAMA* 1968 205 855-862
45 Hoffman DA, McConahey WM, Fraumeni JF, Kurland LT Cancer incidence following treatment of hyperthyroidism *Int J Epidemiol* 1982, 11 218-224
46 Hall P, Boice JD, Berg G, Bjelkengren G Ericsson UB, Hallquist A, Lidberg M, Lundell G, Mattsson A, Tennvall J, Wiklund K, Holm LE Leukaemia incidence after iodine-131 exposure *Lancet* 1992 340 1-4
47 Hoffman DA, McConahey WM Breast cancer following iodine-131 therapy for hyperthyroidism *J Natl Cancer Inst* 1983,70 63-67
48 Goldman MB, Maloof F, Monson RR, et al Radioactive iodine therapy and breast cancer a follow-up study of hyperthyroid women *Am J Epidemiol* 1988, 127 969-980
49 Health effects of exposure to low levels of ionizing radiation *BEIR V report* Washington DC National Academy Press, 1990
50 Genetic and somatic effects of ionizing radiation *UNSCEAR report E 86 IX 9* New York United Nations, 1986

CHAPTER 6

Dynamic Distribution and Dosimetric Evaluation of Human Nonspecific Immunoglobulin G labeled with In-111 or Tc-99m

Wilhelmina C.A.M. Buijs, Wim J.G. Oyen, Els Th.M. Dams, Otto C. Boerman, Jeffry A. Siegel, Roland A.M.J. Claessens, Jos W.M. van der Meer and Frans H.M. Corstens

Nucl Med Commun 1998, 19:743-751

ABSTRACT

This study presents data on the dynamic distribution and dosimetry of In-111 and Tc-99m labeled human nonspecific immunoglobulin G (IgG), two recently developed radiopharmaceuticals for detection of infection and inflammation.

Methods Five healthy volunteers were injected with 20-75 MBq ^{111}In-IgG and seven patients were injected with 740 MBq ^{99m}Tc-hydrazinonicotinamide derivative (HYNIC)-IgG. Blood samples, urine and feces were collected. Total body gamma camera imaging studies were performed. The activity in source organs was quantified using the conjugate view counting method and a partial background subtraction technique. Dosimetric calculations were performed using the MIRD technique.

Results For ^{111}In-IgG, the mean biological half-lifes in the blood were 0.90 and 46 h for the a- and b-phase, respectively. For ^{99m}Tc-HYNIC-IgG, these parameters were 0.46 and 45 h. For ^{111}In-IgG the mean cumulative urinary excretion in the first 48 h was 18% of the injected dose, while excretion in the feces was less than 2% of the injected dose. For ^{99m}Tc-HYNIC-IgG, the total body retention was always 100% up to 24 h. The mean absorbed doses in the liver, spleen, kidneys, red marrow and testes from ^{111}In-IgG were 0.8, 0.7, 1.2, 0.3 and 0.4 mGy/MBq, respectively. The mean absorbed doses for ^{99m}Tc-HYNIC-IgG to these organs were 16, 24, 15, 10 and 22 μGy/MBq, respectively. The mean effective dose was 0.25 mSv/MBq and 8.4 μSv/MBq for ^{111}In-IgG and ^{99m}Tc-HYNIC-IgG, respectively.

Conclusion The absorbed doses for both ^{111}In-IgG and ^{99m}Tc-HYNIC-IgG are low, and therefore, these radiopharmaceuticals can be administered safely from a radiation risk perspective.

INTRODUCTION

Localization of infection often presents a diagnostic problem. Since the currently available scintigraphic imaging techniques show limitations in diagnosing infections with regards to imaging characteristics (^{67}Ga) or preparation (labeled white blood cells), new radiopharmaceuticals are being developed *(1,2)*.

Recent studies have demonstrated the utility of ^{99m}Tc-hydrazinonicotinamide labeled human nonspecific immunoglobulin G (^{99m}Tc-HYNIC-IgG) and ^{111}In-IgG as imaging agents to detect focal inflammation *(2-5)*. These studies have been performed in bone, joint, soft tissue, intra-abdominal and vascular infections, in both animals and humans. Both methods have shown to be effective for the detection of infection and inflammation.

In this study we describe the dynamic distribution of both ^{111}In-IgG and ^{99m}Tc-HYNIC-IgG in volunteers and in patients, the calculated uptake of radioactivity in the organs and the absorbed dose to these organs and to the whole body. The radiation burden was compared with that of other radiopharmaceuticals commonly used for the detection of infection.

MATERIALS AND METHODS

RADIOPHARMACEUTICALS

^{111}In-IgG. Human nonspecific polyclonal IgG (Sandoglobulin, Sandoz AG, Nurnberg FRG), conjugated to diethylenetriaminepentaacetic bicyclic anhydride (bicyclic DTPA), was radiolabelled with 20-75 MBq ^{111}In (Indium chloride, Amersham International Ltd., Buckinghamshire, UK) as described previously *(6)*.

^{99m}Tc HYNIC-IgG. Human polyclonal IgG (Gammacard, Baxter/ Hyland, Lessines, Belgium) was conjugated to the hydrazinonicotinamide derivative (HYNIC) and radiolabelled with 740 MBq ^{99m}Tc *(5,7)*.

SUBJECTS

Five healthy volunteers (3 males, 2 females), mean age of 29 years (range 21 to 45 years) received an intravenous injection of 20-75 MBq ^{111}In-IgG. Seven patients (3 males, 4 females), mean age 48 years (range 29 to 75 years), were injected intravenously with 740 MBq ^{99m}Tc-HYNIC-IgG. All patients had possible infectious or inflammatory foci. Two patients were suspected of having joint prosthesis infection, two patients had possible bone infection and three patients had fever of unknown origin. The studies were approved by the Institutional Review Board of the University Hospital Nijmegen. Written informed consent was obtained.

BLOOD CLEARANCE AND URINE AND FECES MEASUREMENTS

In the volunteers receiving ^{111}In-IgG multiple blood samples were taken during the first 48 hours post injection (p i) and up to 24 hours p i in the patients receiving ^{99m}Tc HYNIC IgG Whole-blood data were analyzed by non-linear least-squares fit using a bi-exponential model For ^{111}In-IgG, urine was collected at 12-h intervals for 48 h Feces were also collected for 48 h and each defecation was collected in a separate container After homogenization, whole sample activity was measured on a well-type gamma counter in a configuration of reproducible geometry The activity was expressed as a percentage of the injected dose (%ID)

IMAGING PROCEDURE

For the ^{111}In IgG study planar imaging was performed with a single head gamma camera (Orbiter-ZLC-Digitrac, Siemens, Hoffmann Estates, IL) equipped with a parallel-hole medium-energy collimator, connected to a computer for subsequent data analysis (A2, Medical Data Systems/ Medtronic, Ann Arbor MI) Symmetric 15% windows were used over both the 173 and 247 keV energy peaks The data were stored digitally in a 128 x 128 matrix Anterior and posterior images of the chest, abdomen and pelvis were recorded at 4, 24 and 48 h p i with a preset time of 5, 7 5 and 10 minutes, respectively All images were recorded with the patient in the supine position At least 300,000 counts per image were acquired

For the ^{99m}Tc-HYNIC-IgG study whole body images were recorded at 10 min, 4 h and 24 h p i using a dual-head gamma camera (MultiSPECT2, Siemens, Hoffman Estates, IL) equipped with parallel-hole low energy high resolution collimators A symmetric 15% window was used at 140-keV photopeak The data were stored in a computer (ICON, Siemens) with a 256 x 1024 matrix The speed of the patient pallet was 7 cm/min for the measurements on the first day and 3 cm/min at 24 h At least 750,000 counts were recorded per image

CALCULATION OF QUANTITATIVE ORGAN UPTAKE

Rectangular regions of interest (ROIs) were drawn around the total body on both anterior and posterior views Irregular ROIs were drawn manually over liver, spleen, left kidney and left and right iliac crest on the anterior and posterior abdominal images A background region in the abdomen was drawn just caudally and medially of the left kidney Due to superposition of the right kidney over the liver, the liver ROI on the posterior images excluded the kidney and only ROIs over the left kidney were used Uptake in the kidneys was determined as twice the calculated uptake in the left kidney Counts in the liver and spleen ROIs were corrected for the abdominal body contour *(8)*

Estimates of absolute activity uptake in these organs were made using the

conjugate view counting method by calculating the geometric mean of the background corrected counts in an organ ROI on the anterior and posterior views *(9-11)*. The geometric mean of the anterior and posterior counts in the whole body ROIs of the first scan was defined as 100% of the injected dose. For each subsequent scan, the whole body retention was determined relative to the first scan as % ID, using the geometric mean of the anterior and posterior counts in the whole body ROIs at that time, corrected for physical decay and for differences in scanning time for ^{111}In-IgG or scan speed for ^{99m}Tc-HYNIC-IgG. The percent injected dose in the organs at each time point was estimated from the ratio of the geometric mean of ROI counts in the respective organ divided by the geometric mean of ROI counts in the whole body and multiplied by the whole body retention at that point in time. For ^{111}In-IgG, imaged with the single-head gamma camera, the total counts in the whole body ROI was calculated as the sum of the counts measured in adjacent overlying spot views of the thorax, abdomen and pelvis ROIs *(12)*. For that part of the body not imaged with the gamma camera, a correction factor was measured with a shadow shield total body counter in profile scanning mode *(13)*. If the patient had voided or defecated in the interval between injection and the first scan, the container with excreted urine or feces was measured together with the patient at the time of the first whole-body scan.

BACKGROUND CORRECTION

The partial background subtraction method was used. In this method, ROI counts in the liver regions were not corrected for background activity because the liver occupies almost the entire thickness of the patient's abdomen *(14)*. For background correction in the spleen and left kidney regions, only a fraction of the counts in the abdominal background ROI was subtracted. This fraction *(F)* was calculated using the formula *(13)*

$$F = \frac{\text{abdomen thickness} - \text{organ thickness}}{\text{abdomen thickness}}$$

The organ thickness was estimated from computed tomographic (CT) data or from anatomical atlas data, and the thickness of the abdomen was measured with a ruler while the patient was in the supine position on the imaging table.

RED MARROW

Red marrow uptake was estimated from anterior and posterior gamma camera images. Regions of interest were drawn over a part of the left and right iliac crests. The sum of these areas represented 25% of the pelvic bones, as determined from X-ray CT measurements *(13)*. Background ROIs were drawn lateral

to the iliac crest The activity in the iliac crest ROIs was calculated using the same method as for the abdominal organs The total activity in the red marrow was then calculated via extrapolation from the activity in the pelvic bones, assuming that 17 5% of the total red marrow mass is present in the pelvic bones and that the red marrow is distributed homogeneously throughout the skeleton *(15)*

TESTES

Radioactivity in the testes was measured using the anterior gamma camera images only A region of interest was drawn around the testes and a background region was drawn on both upper legs The testes counts were corrected for the mean counts in both upper leg ROIs An overlying layer of 1 5 cm soft tissue was assumed for attenuation correction The uptake of the radioactivity in the testes was determined using a calibration standard with a known activity of ^{111}In-IgG or ^{99m}Tc HYNIC-IgG

CALCULATION OF THE ABSORBED DOSE

The absorbed dose to the organs was calculated using the MIRD scheme *(16)* Liver, spleen, kidneys, bone marrow, urinary bladder, testes and the rest of the body (remainder) were considered as source organs For the bladder, a voiding interval of 4 h was assumed The activity in the remainder of the body was calculated at each time point either by subtracting the sum of excreted activity and activity in the source organs from the injected activity, or by subtracting the sum of the activity in all source organs from the activity in the whole body at each point in time The residence time in a source organ is defined as the cumulated fractional activity in that organ, which is determined from the area under the fractional activity-time curve between time of injection and infinity For the period between time of injection and the end of data collection (4 - 48 h for ^{111}In-IgG and 0-24 h for ^{99m}Tc-HYNIC-IgG), the area under the source organ activity-time curves was calculated with the trapezoidal method, using a linear extrapolation between the assumed uptake fraction of 0 at time of injection, and the measured fractional uptake at the time of the first image, not corrected for physical decay The remaining area under the source organ curves (i e , from the end of data collection out to infinity) was determined by considering only physical decay of the radionuclide The absorbed doses in the organs and the effective doses were computed using the MIRDOSE3 computer program *(17)*, using the reference adult software phantom for males and the adult female phantom for females

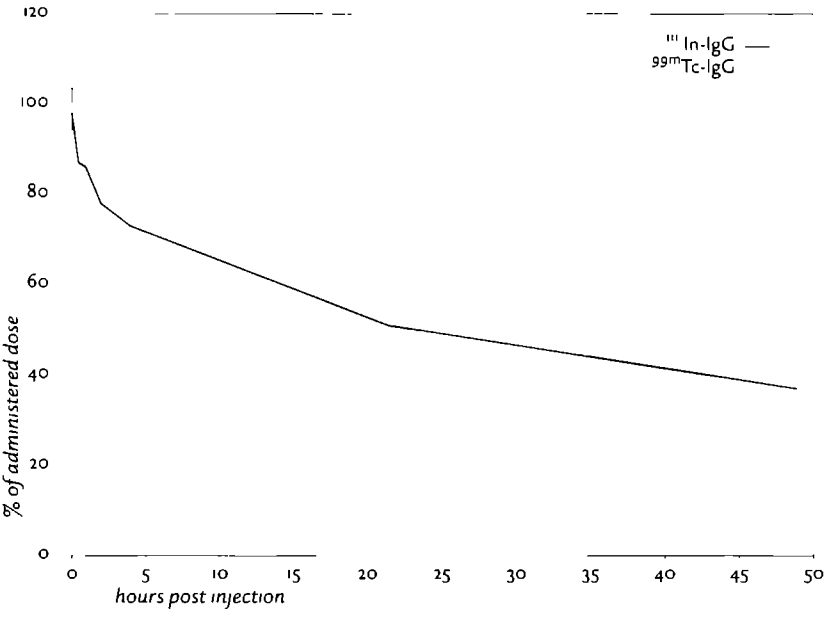

Figure 1. *Blood activity-time curves for ^{111}In-IgG and ^{99m}Tc-HYNIC-IgG. Data are expressed as percent administered dose. Error bars represent one s d.*

RESULTS

BLOOD CLEARANCE

Analysis of the ^{111}In-IgG data resulted in a distribution phase (24 ± 5%) with a $t_{1/2a}$ of 0.90 ± 0.76 h and an excretion phase (77 ± 5%) with a $t_{1/2b}$ of 46 ± 9 h (Figure 1).

For ^{99m}Tc-HYNIC-IgG, these parameters were similar: $t_{1/2a}$ = 0.46 ± 0.20 h (17 ± 7%) and $t_{1/2b}$ = 45 ± 18 h (85 ± 7%) (Figure 1).

EXCRETION IN URINE AND FECES

The mean cumulative urinary excretion of ^{111}In-IgG after 24 and 48 h was 13.7 ± 3.8% ID (range 8.9 - 18.4% ID) and 18.1 ± 3.1% ID (range 13.9 - 21.7% ID), respectively (Figure 2). The fecal excretion was 0.3 ± 0.3% ID (range 0 - 0.9% ID) after 24 h and 0.9 ± 0.4% ID (range 0.5 - 1.6% ID) after 48 h (Figure 2).

WHOLE BODY RETENTION

The mean retention of the ^{111}In-IgG in the body measured with the shadow shield whole body counter after 24 and 48 h was 88 ± 2% and 84 ± 2% ID, respectively. The biologic half-life of ^{111}In-IgG in the body was 830 h, corresponding to an effective half-life of 63 h. The activity in the body not imaged with the spot views was 16.1 ± 0.4, 16.6 ± 3.3 and 16.2 ± 4% ID after 1, 24 and 48 h, respectively.

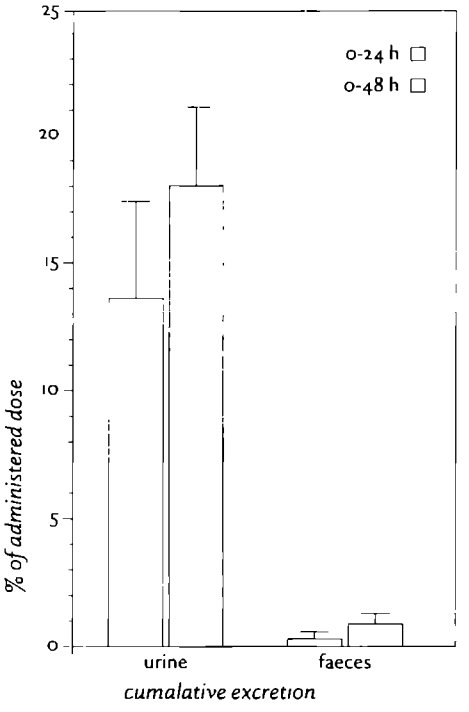

Figure 2. *Excretion of ^{111}In-IgG in urine and feces. Data are expressed as percent administered dose. Error bars represent one s.d.*

The whole body retention in patients receiving ^{99m}Tc-HYNIC-IgG was 100% during the first 24 h.

ORGAN UPTAKE

The gamma camera images indicated that ^{111}In-IgG accumulated in liver, spleen, kidneys, red marrow and testes. Therefore, these organs were selected as the source organs. The mean organ uptakes of ^{111}In-IgG at 4, 24 and 48 h are shown in Table 1. The mean initial activity in the liver, spleen and kidneys was 20.2, 2.1 and 7.2% ID, respectively. The mean initial uptake in the red marrow and testes was 12.1 and 0.4% ID, respectively.

The mean organ uptakes of ^{99m}Tc-HYNIC-IgG at 10 min, 4 h and 24 h are shown in Table 2. The mean initial activity in the liver, spleen and kidneys was 10.8, 2.9 and 2.1% ID, respectively. The mean initial uptake in the red marrow and the testes was 7.7 and 0.7% ID, respectively. After the initial uptake of activity, no further accumulation or release of activity from the source organs was found for either agent.

ABSORBED DOSE

The mean estimated absorbed doses to the liver, spleen and kidneys after administration of ^{111}In-IgG were 0.8, 0.7 and 1.2 mGy/MBq, respectively (Table 3).

TABLE 1

Organ uptake of ^{111}In-IgG (% ID)[a]

Organ	4 h	24 h	48 h
Liver	20.2 ± 3.1	20.4 ± 1.1	19.2 ± 0.2
Spleen	2.1 ± 0.6	1.9 ± 0.6	1.8 ± 0.6
Kidneys	7.2 ± 1.8	7.2 ± 1.8	5.6 ± 1.0
Red marrow	12.1 ± 5.1	11.2 ± 4.4	9.9 ± 3.9
Testes[b]	0.4 ± 0.1	0.5 ± 0.1	0.4 ± 0.1
Total body	100	88 ± 2.8	84 ± 2

a Data are mean ± s.d. for five subjects
b Data are mean ± s.d. for three males

TABLE 2

Organ uptake of ^{99m}Tc-HYNIC-IgG (% ID)[a]

Organ	10 min	4 h	24 h
Liver	10.8 ± 3.1	11.3 ± 2.8	11.7 ± 2.8
Spleen	2.9 ± 0.7	2.3 ± 0.7	2.4 ± 0.7
Kidneys	2.1 ± 0.7	2.1 ± 0.8	2.3 ± 0.6
Red marrow	7.7 ± 5.6	7.7 ± 5.9	6.7 ± 4.8
Testes[b]	0.7 ± 0.1	0.7 ± 0.2	0.7 ± 0.2
Whole body	100	99 ± 3	102 ± 2

a Data are mean ± s.d. for seven subjects
b Data are mean ± s.d. for three males

TABLE 3

Absorbed doses in organs[a]

Organ	^{111}In-IgG (mGy/MBq)	^{99m}Tc-HYNIC-IgG (μGy/MBq)
Liver	0.8 ± 0.24	16 ± 4
Spleen	0.67 ± 0.32	24 ± 6
Kidneys	1.24 ± 0.4	15 ± 4
Red marrow	0.32 ± 0.06	10 ± 2
Testes[b]	0.40 ± 0.13	22 ± 5
Urinary bladder wall	0.13 ± 0.03	5 ± 1

a Data are mean ± s.d. for five (^{111}In-IgG) and seven (^{99m}Tc-HYNIC-IgG) subjects
b Data are mean ± s.d. for three (^{111}In-IgG) males and three (^{99m}Tc-HYNIC-IgG) males

The calculated absorbed dose in the red marrow, testes and urinary bladder wall was 0.3, 0.4 and 0.1 mGy/MBq, respectively. The mean effective dose was 0.25 mSv/MBq. For a typical administered activity of 75 MBq ^{111}In-IgG, the calculated red marrow dose was 24 mGy, the testes dose was 30 mGy and the effective dose was 19 mSv.

For ^{99m}Tc-HYNIC-IgG, the absorbed dose to the liver, spleen and kidneys was 16, 24 and 15 μGy/MBq, respectively (Table 3). The calculated absorbed doses to the red marrow, testes and urinary bladder was 10, 22 and 5 μGy/MBq. The mean effective dose was 8.4 μSv/MBq. For a typical administered activity of 740 MBq ^{99m}Tc-HYNIC-IgG, the dose to the red marrow was 7 mGy, the testes dose was 16 mGy and the effective dose was 6 mSv.

DISCUSSION

^{111}In-IgG has demonstrated its usefulness in imaging infectious and inflammatory foci *(1-4)*. Recently, we have showed that ^{99m}Tc-HYNIC-IgG has excellent imaging characteristics for infectious and inflammatory foci *(5)*. To further characterize these radiopharmaceuticals, the pharmacokinetics and the absorbed dose to patients were estimated.

The ^{111}In-IgG dosimetric calculations were performed in healthy volunteers. The absorbed dose for ^{99m}Tc-HYNIC-IgG was derived from patients who had possible infectious or inflammatory foci. Theoretically this might have resulted in variations in metabolism of this radiopharmaceutical and therefore in the estimated absorbed dose. However, the relative uptake in infectious foci is low in patients. Thus, it is very unlikely that the metabolism differs significantly between volunteers and patients *(1)*. Moreover, in the current study, six out of seven patients showed no focal uptake, thus they may be considered as healthy volunteers with respect to dosimetry. The coefficients of variation of the absorbed dose in the various organs is somewhat higher in the ^{111}In-study when compared to the ^{99m}Tc-study (19 to 48% versus 20 to 27%, respectively, Table 3).

Various methods have been used to quantitate the *in vivo* distribution of radioactivity. These techniques include methods of background correction *(9,18)*, activity calibration, attenuation correction and scatter correction *(8,9,11,12,14,18-23)*, as well as procedures for estimating bone marrow and bone uptake *(24-30)*. In this study, the geometric mean method was used for estimation of absolute organ and whole body activity *(8,9)*. The organ activity was divided by the whole body activity to estimate the fractional uptake at all time points, the so-called 'whole body' method. Whole body activity was estimated either by overlapping static images in the ^{111}In-study, in combination with a daily profile scan on the shadow shield whole-body counter, and from

whole-body images using a dual-headed whole body gamma camera for the ^{99m}Tc-HYNIC-IgG study. Both methods are equally reliable, since in both studies uptake of activity in an organ was calculated as the percentage of the initial whole body image activity. Moreover, both techniques use similar methods for attenuation and background correction. The organ uptake of ^{111}In-IgG was also calculated using experimentally determined gamma camera efficiency and attenuation factors, related to the amount of scatter and the size of the ROI *(13,22,23)*. The calculated uptake values, expressed as the percent injected dose in the liver, spleen, kidneys and red marrow, were similar for both methods with differences of less than 10%.

In this study the partial background subtraction method was used. This method consists of subtracting a fraction only of the background ROI counts, depending on the relative organ and body thicknesses. Using this method will give a more reliable estimation of the actual organ activity, in comparison with the most commonly used method for background correction, where all the background ROI counts are subtracted from the counts in the source ROI. This latter method may result in an underestimation of the actual activity in the organ and thus of the absorbed dose in the organ *(31)*. Therefore, when comparing absorbed doses in an organ after administration of radiopharmaceuticals, it should be mandatory to report the method for background correction. In this study, application of the conventional full background subtraction method resulted in 20-40% lower values for the organ absorbed doses, when compared with the partial background correction method.

For both agents, activity was localized in the skeleton as seen on the gamma camera images (Figure 3). Therefore, estimation of the red marrow dose was based on gamma camera images. Calculating red marrow doses via extrapolation of measured activities in particular ROIs in the skeleton may lead to significant errors, due to the non-uniform distribution of red marrow over the skeleton and to differences in local metabolism *(30)*. Therefore, the dynamic distribution of ^{111}In-IgG in the skeleton was analyzed in two different parts of the skeleton: left and right iliac crest ROIs, and a lumbar spine ROI (L3+L4). Only a small difference between the two methods was found in this study and in a previous study *(13)*. However, it seems likely that the amount of activity measured in these ROIs represented a superposition of activity in the bone and in the red marrow. In calculating the red marrow uptake, all the activity found in the iliac crest ROI was assigned to the red marrow in that region. This procedure could have led to an overestimation of the red marrow dose. Direct measurement of activity in human bone and bone marrow samples after administration of ^{111}In-IgG showed that approximately 30% of the lumbar spine activity was due to bone activity *(28)*. If the same distribution of activity between bone and red marrow exists in the iliac crest ROIs, correction for such bone uptake will lower the calculated red

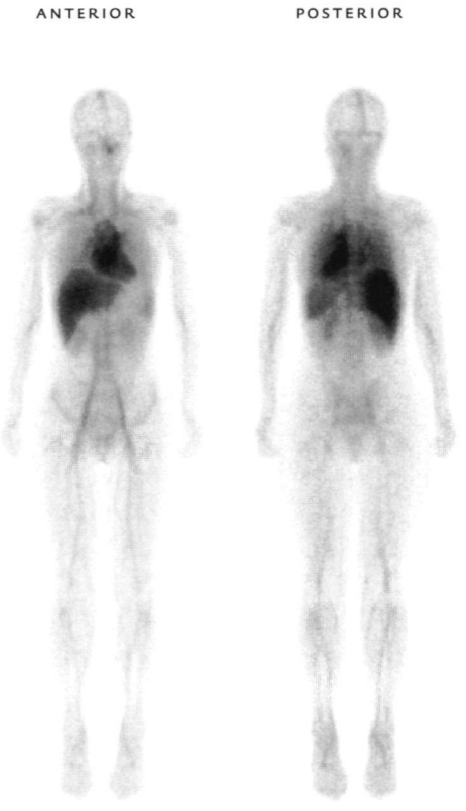

Figure 3. *Anterior and posterior whole-body ^{99m}Tc-HYNIC-IgG scintigrams showing normal distribution of the radiolabel at 4 h postinjection. Uptake of activity in the skeleton is clearly visible.*

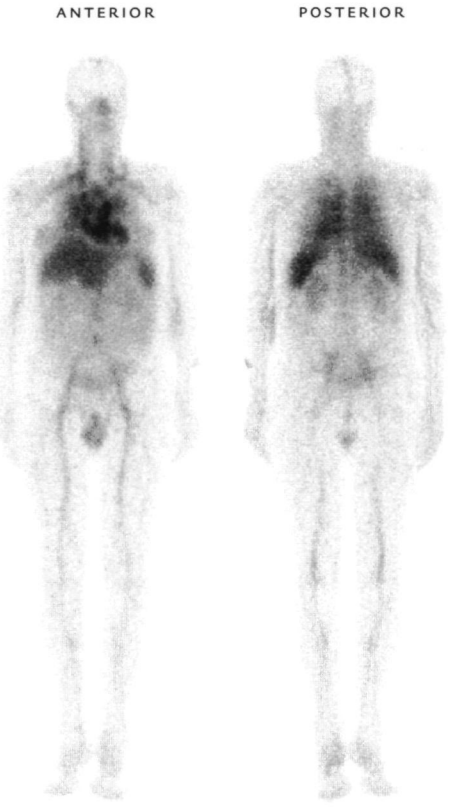

Figure 4. *Anterior and posterior whole body ^{99m}Tc-HYNIC-IgG scintigrams showing clear uptake in the testes at 24 h postinjection.*

marrow dose accordingly. The tissue risk factors for red marrow and bone surface are 0.12 and 0.01, respectively *(32)*. Therefore, the radiation risk for an ^{111}In-IgG examination will be at least 4% lower than the radiation risk derived from the calculations in this study.

Forty eight hours after injection of ^{111}In-IgG, the sum of the excreted activity and the activity accumulated in all measured source organs was 55% of the injected dose. Thus about 45% of the injected activity was still circulating in the blood or present in interstitial tissue. This finding is concordant with the blood activity data indicating that after 48 h, 38 % of the administered activity was still present in the blood. The measured total excretion of ^{111}In-IgG in urine and feces after 24 and 48 hours agreed very well with the image-based whole body retention measurements at those times, with only a 2-3 % difference between the two methods. The whole body retention of ^{99m}Tc-HYNIC-IgG was a constant 100% of the

injected dose for 24 h p i , indicating that no excretion of activity in urine or feces had occurred In contrast, C allahan et al *(33)* reported a mean excretion of 9 6 ± 2 7% ID 24 h after injection of ^{99m}Tc-HYNIC-IgG *(33)* The lack of urinary excretion of the ^{99m}Tc-HYNIC-IgG in this study may be explained by the differences in chemical and biological characteristics of the two products

From Tables 1 and 2 it can be seen that the uptake of ^{99m}Tc-HYNIC-IgG in the liver was much lower than that of ^{111}In-IgG This is most likely due to the fact that free ^{111}In, once released from the ^{111}In-IgG molecule, is retained intracellularly to a greater extent than ^{99m}Tc *(34)*

Relatively high uptake of ^{111}In-IgG and ^{99m}Tc-HYNIC-IgG in the testes was visible on the images (Figure 4) The average uptake of ^{111}In-IgG and ^{99m}Tc-HYNIC-IgG in the testes was 0 4-0 5% and 0 7% ID, respectively, leading to an absorbed dose of 0 4 mGy/MBq and 22 uGy/MBq, respectively Datz et al *(35)* found an initial uptake of 0 294% ID gradually decreasing to 0 067% ID at 120 h after the injection of ^{111}In-IgG The calculated absorbed dose in the testes was 0 3 mSv/MBq (1 17 rad/mCi), which is similar to the absorbed dose found in the current study The absorbed dose in the testes after injection of ^{111}In-IgG in the current study was also in the same range as the mean absorbed dose in the testes after injection of ^{201}Tl-chloride, calculated to be 0 245 mGy/MBq by Castronovo *(36)* and 0 35 mGy/MBq by Rao et al *(37)* The large testicular dose has a significant influence on the effective dose In the current study the contribution of the testicular dose to the effective dose was 30% and 50% for ^{111}In IgG and ^{99m}Tc-HYNIC-IgG, respectively

The absorbed dose of ^{111}In-IgG in the liver, spleen and kidneys were higher than those found by Datz et al *(35)* 0 8 0 7 and 1 2 mGy/MBq versus 0 38 0 2 and 0 2 mGy/MBq respectively This can partly be explained by the different methods for activity quantification, particularly the method of background subtraction However, in contrast to the large differences in organ doses between the study of Datz et al and the present study, the mean effective dose for ^{111}In-IgG was similar (0 21 and 0 25 mSv/MBq, respectively) This is reasonable, since the effective dose is not influenced much by the choice of the background correction method (e g , partial vs full background subtraction), as the difference in subtracted background activity will appear as "remainder of the body" uptake For an intravenous injection of 75 MBq ^{111}In-IgG, the effective dose was 19 mSv When compared to other radiopharmaceuticals used for diagnosing infections, the effective dose was in the same range as that from 30 MBq ^{111}In-labeled white blood cells (11 mSv) and for 150 MBq ^{67}Ga-citrate (17 mSv) *(38)*

Comparing the dosimetric data for ^{99m}Tc-HYNIC-IgG in this study with data from Callahan et al *(33)*, the absorbed doses in the liver and kidneys were similar 13 and 12 mGy/MBq versus 11 and 10 mGy/MBq, respectively However, the estimated absorbed dose to the spleen in the current study was twice as high

as reported by Callahan et al. This may be explained both by differences in the IgG brands and the HYNIC conjugation methods as well as the different methods for activity quantification. In the current study, the effective dose for a typical administered activity of 740 MBq ^{99m}Tc-HYNIC-IgG was 6 mSv. This is in the same range as for other ^{99m}Tc-labeled compounds used for diagnosing infections; for example, 5.5 mSv for 500 MBq ^{99m}Tc-labeled white blood cells and 3 mSv for 500 MBq ^{99m}Tc-labeled phosphonate for three-phase bone scintigraphy.

CONCLUSION

Clearance from the blood was similar for both agents. However, 14 and 19% of the injected activity of ^{111}In-IgG was excreted within 24 and 48 h post-injection respectively, whereas no excretion of ^{99m}Tc-HYNIC-IgG was seen in the first 24 hours after injection based on whole body gamma camera images. The uptake of ^{111}In-IgG in the liver, kidneys and red marrow was 80, 250 and 50% higher than the uptake of ^{99m}Tc-HYNIC-IgG in these organs. The calculated uptake in the spleen was similar and the uptake in the testes was 50% lower for ^{111}In-IgG compared to ^{99m}Tc-HYNIC-IgG. Finally, the resulting doses for both ^{111}In-IgG and ^{99m}Tc-HYNIC-IgG are low and, therefore, these radiopharmaceuticals can be administered safely from a radiation risk perspective.

REFERENCES

1 Oyen W J G Claessens R A M J van Horn J R van der Meer J W M Corstens F H M Scintigraphic detection of bone and joint infections with indium-111 labeled nonspecific polyclonal human immunoglobulin G *J Nucl Med* 1991 32 403–412

2 Oyen W J G Claessens R A M J van der Meer J W M Rubin R H Strauss H W Corstens F H M Indium-111 labeled human nonspecific immunoglobulin G: A new radiopharmaceutical for imaging infectious and inflammatory foci *Clin Infect Dis* 1992 14 1110–1118

3 Rubin R H Fischman A J Callahan R J et al In-111 labeled nonspecific immunoglobulin scanning in the detection of focal infection *N Engl J Med* 1989 321 935–940

4 Corstens F H M Oyen W J G and Becker W S Radioimmunoconjugates in the detection of infection and inflammation *Semin Nucl Med* 1993 XXIII 148–164

5 Dams F Th M Oyen W J G Boerman O C et al Technetium-99m labeled to human immunoglobulin G via the nicotinyl hydrazine derivative: a clinical study *J Nucl Med* 1998 39 119–124

6 Hnatowich D J Childs R L Lanteigne D Najafi A The preparation of DTPA-coupled antibodies radiolabeled with metallic radionuclides: an improved method *J Immunol Meth* 1983 65 147–157

7 Abrams M J Juweid M ten Kate C I et al Technetium-99m human polyclonal IgG radiolabeled via the hydrazino nicotinamide derivative for imaging focal sites of infection in rats *J Nucl Med* 1990 31 2022–2028

8 Fleming J S A technique for the absolute measurement of activity using a gamma camera and computer *Phys Med Biol* 1979 24 176–180

9 Thomas S R Maxon H R and Kereiakes J G In vivo quantitation of lesion radioactivity using external counting methods *Med Phys* 1976 3 253–255

10 Beekhuis H and Nieweg O Radiation absorbed doses from Co-57 and Co-55 Bleomycin *J Nucl Med* 1984 24 478–485

11 Rensburg A J Lotter M G Heyns A P et al An evaluation of four methods of indium-111 planar image quantification *Med Phys* 1988 15 853–861

12 Reenen O van Lotter M G Heyns A et al Quantification of the distribution of ^{111}In labeled platelets in organs *Int J Nucl Med* 1982 7 80–84

13 Buijs W Massuger L Claessens R Kenemans P and Corstens I Dosimetric evaluation of immunoscintigraphy using indium-111 labeled monoclonal antibody fragments in patients with ovarian cancer *J Nucl Med* 1992 33 1113–1120

14 Macey D J DeNardo S J DeNardo G L Goodnight J K Unger M W Uptake of indium-111 labeled monoclonal antibody 7ME-018 as a function of tumor size in a patient with melanoma *Am J Physiologic Imaging* 1988 3 1–6

15 ICRP Publication 70 *Basic Anatomical and Physiological Data for use in Radiological Protection*: The Skeleton Oxford: Pergamon Press 1995

16 Loevinger R Berman M A revised scheme for calculating the absorbed dose from biologically distributed radionuclides *Med pamphlet no 1 revised* New York: Society of Nuclear Medicine 1975

17 Stabin M G MIRDOSE: Personal computer software for internal dose assessment in nuclear medicine *J Nucl Med* 1996 37 538–546

18 Kojima M Takaki Y Matsumo M et al A preliminary phantom study on a proposed model for quantification of renal planar scintigraphy *Med Phys* 1993 20 33–37

19 Myers B M Lavender A R Oliveira J B Maseri A A simplified method of quantitating organ uptake using a gammacamera *Br J Radiol* 1981 54 1062–1067

20 Wu R K and Siegel J A Absolute quantitation of radioactivity using the buildup factor *Med Phys* 1984 11 189–192

21. Hammond ND, Moldofsky PJ, Beardsly MR, Mulhern CB. External imaging techniques for quantitation of distribution of ^{131}I-F(ab')$_2$ fragments of monoclonal antibody in humans. *Med Phys* 1984; 11:778-783.
22. Siegel JA, Wu RK, Maurer AH. The buildup factor: effect of scatter on absolute volume determination. *J Nucl Med* 1985; 26:390-394.
23. Siegel JA. The effect of source size on the buildup factor calculation of absolute volume. *J Nucl Med* 1985; 26:1319-1322.
24. Cristy M. Active bone marrow distribution as a function of age in humans. *Phys Med Biol* 1981; 26:389-400.
25. Siegel JA, Lee RE, Pawlyk DA, Horowitz JA, Sharkey RM, Goldenberg DM. Sacral scintigraphy for bone marrow dosimetry in radioimmunotherapy. *Nucl Med Biol* 1989; 16:553-559.
26. Siegel JA, Wessels BW, Watson EE et al. Bone marrow dosimetry and toxicity for radioimmunotherapy. *Antibody Immunoconj Radiopharm* 1990; 3:213-233.
27. Sgouros G. Bone marrow dosimetry for radioimmunotherapy: theoretical considerations. *J Nucl Med* 1993; 34:689-694.
28. Oyen W, Buijs W, Kampen A van, Koenders E, Claessens R, Corstens F. Intraoperative bone and bone marrow sampling: a simple method for accurate measurement of uptake of radiopharmaceuticals in bone and bone marrow. *Nucl Med Commun* 1993; 14:112-116.
29. Macey DJ, DeNardo SJ, DeNardo GL, DeNardo DA and Shen S. Estimation of radiation absorbed doses to the red marrow in radioimmunotherapy. *Clin Nucl Med* 1995; 20:117-125.
30. Sgouros G, Jureidini IM, Scott AM et al. Bone marrow dosimetry: regional variability of marrow-localizing antibody. *J Nucl Med* 1996; 37:695-698.
31. Buijs WCAM, Siegel JA and Corstens FHM. Estimation of absolute organ activity using five different methods for background correction: a phantom study. *Eur J Nucl Med* 1997; 24:931(abs).
32. ICRP Publication 60. *1990 Recommendations of the International Commission on Radiological Protection*. Oxford: Pergamon Press; 1991.
33. Callahan RJ, Barrow SA, Abrams MJ, Rubin RH and Fischman AJ. Biodistribution and dosimetry of technetium-99m-hydrazino nicotinamide IgG: comparison with indium-111-DTPA-IgG. *J Nucl Med* 1996; 37:843-846.
34. Pimm MV, Perkins AC and Baldwin RW. Differences in tumour and normal tissue concentrations of iodine- and indium-labeled monoclonal antibody. *Eur J Nucl Med* 1985; 11:300-304.
35. Datz FL, Castronovo FP, Christian PE at al. Biodistribution and dosimetry of indium-111-polyclonal IgG in normal subjects. *J Nucl Med* 1995; 36:2372-2379.
36. Castronovo FP. 201Tl-labelled TlCl dosimetry revisited. *Nucl Med Commun* 1993; 14:104-107.
37. Rao DV, Shepstone BJ, Wilkins I IB and Howell R. Kinetics and Dosimetry of Thallium-201 in Human testes. *J Nucl Med* 1995; 36:607-609.
38. ICRP Publication 62. Radiological protection in biomedical research. Includes addendum 1 to publication 53-*Radiation Dose to Patients from Radiopharmaceuticals*. Oxford: Pergamon Press; 1993.

CHAPTER 7

Intraoperative Bone and Bone Marrow Sampling: A Simple Method for Accurate Measurement of Uptake of Radiopharmaceuticals in Bone and Bone Marrow

Wim J.G. Oyen, Wilhelmina C.A.M. Buijs, Albert van Kampen, Emile B. Koenders, Roland A.M.J. Claessens, Frans H.M. Corstens.

Nucl Med Commun 1993; 14:112-116

ABSTRACT

Accurate estimation of bone marrow uptake of radiopharmaceuticals is of crucial importance for accurate whole body dosimetry In this study, a method for normal bone marrow and bone during routine surgery without inconvenience to volunteers is suggested and compared to an indirect method

In five volunteers (group 1) 4 MBq indium-111 labeled human polyclonal IgG (^{111}In-IgG) was administered 48 h before placement of a total hip prosthesis After resection of the femoral head and neck, bone marrow was aspirated from the medullary space with a biopsy needle In five patients, suspected of having infectious disease (group 2), bone marrow uptake was calculated according to a well accepted method using regions of interest over the lumbar spine, 48 hours after injection of 75 MBq ^{111}In IgG

Bone marrow uptake in group 1 (4 5 ± 1 3 %ID/kg) was significantly lower than that in group 2 (8 5 ± 2 1 %ID/kg), $p < 0.01$ Blood and plasma activity did not differ significantly for both groups

This method provides a system for directly and accurately measuring uptake and retention in normal bone marrow and bone of all radiopharmaceuticals at various time points It is a safe and simple procedure without any discomfort to the patient Since small amounts of activity are sufficient, the absorbed dose to the patient is low

INTRODUCTION

Adequate estimation of bone marrow uptake of radiopharmaceuticals is of critical importance for accurate whole body dosimetry, since bone marrow toxicity forms the dose limiting factor in many therapeutic applications with radionuclides such as radiolabeled monoclonal antibodies *(1)* However accurate estimation of bone and bone marrow uptake and retention of radiopharmaceuticals in humans remains a difficult problem Until now, bone marrow uptake was derived from techniques using regions of interest, drawn on scintigraphic images, from the activity in blood, or from whole body data *(2-8)* Because of the nature of these indirect measurements many assumptions have to be made, making the method more or less inaccurate Therefore, direct measurement is to be preferred

Direct measurement of bone marrow activity in humans, using established techniques such as sternal aspiration and iliac crest biopsy is cumbersome, since these procedures cause significant discomfort to patients Furthermore, it is difficult to obtain sufficient and representative material Moreover, these methods are not without hazards, such as perforation of the sternum and bleeding *(9)* To our knowledge no simple method for bone and bone marrow sampling with minimal or no discomfort to the patient has been reported Therefore, we looked for a common surgical procedure, in which some bone marrow and bone are exposed and removed routinely during elective surgery in otherwise healthy patients Such a method would allow direct measurement of bone and bone marrow uptake of radiopharmaceuticals, administered prior to surgery In this study, the feasibility of obtaining bone marrow samples from patients, undergoing total hip replacement for degenerative osteoarthritis was evaluated

MATERIALS AND METHODS

RADIOPHARMACEUTICALS

Since we are currently preparing a biodistribution and dosimetric study of indium-111 human nonspecific polyclonal immunoglobulin G (^{111}In-IgG) in humans, we chose this radiopharmaceutical, which is normally used for scintigraphic detection of infection and inflammation, for the study *(10)*

IgG (Sandoglobulin, Sandoz AG, Nuernberg, FRG) was conjugated to diethylenetriaminepentaacetic bicyclic anhydride (bicyclic DTPA) according to the method described by Hnatowich et al and labeled with In 111 (indium chloride, Amersham International Ltd , Buckinghamshire, UK) *(11)* Labeling efficiency was always greater than 95%

PATIENTS

GROUP 1

Direct measurement of bone and bone marrow uptake

Patients with degenerative osteoarthritis of the hip, who were already scheduled for primary total hip replacement, were eligible for the study. ^{111}In-IgG scintigraphy was by no means indicated for clinical evaluation of these patients. On the basis of history, physical examination and routine blood tests, these patients had to be considered as healthy volunteers for this study. To distinguish the patients in group 1 from the other group, the patients in group 1 are referred to as "volunteers".

Two male and three female volunteers were studied (mean age 63.0 years, range 49-76 years). A dose of approximately 0.1 mg of IgG-DTPA conjugate, radiolabeled with 4 MBq of ^{111}In was administered intravenously 48 h prior to surgery.

The study was approved by the Institutional Review Board of the University Hospital Nijmegen. Written informed consent was obtained from all volunteers.

Intraoperative procedure

The surgical procedure was a standard procedure and not modified because of this study. After resection of the femoral head and neck, a bone chip was obtained from the femoral neck. Blood and soft tissue remnants were removed from the bone sample. Thereafter, the medullary canal of the femur was opened with a chisel. Four to five ml of bone marrow were aspirated from the intertrochanteric and trochanteric region, using a 3 mm biopsy needle with a blunt trocar. After obtaining the bone marrow sample, the prosthesis was inserted according to standard procedures. From all volunteers, a venous blood sample was obtained during surgery.

GROUP 2

Calculation of bone marrow uptake from scintigrams of the lumbar spine

The uptake in bone marrow of the lumbar spine was estimated scintigraphically in five age-matched patients, in whom an ^{111}In-IgG scintigraphy was indicated clinically. To these patients a common dose of 1-2 mg of IgG-DTPA conjugate, radiolabeled with 75 MBq of ^{111}In, was administered intravenously. Three male and two female patients were studied (mean age 64.6 years, range 56-70 years). None of these had evidence of enhanced bone marrow activity due to acute infection or inflammation. From all patients, a venous blood sample was obtained 48 hours postinjection.

Scintigraphy and analysis of bone marrow uptake

A posterior planar gamma camera image of the lumbar spine was recorded 48 h after injection using a single-head gamma camera (Siemens Orbiter Siemens Inc Hoffmann Estate, IL) equipped with a parallel-hole medium-energy collimator and connected to a computer for subsequent data analysis (A^2, Medical Data Systems/ Medtronic, Ann Arbor, MI) Symmetric 20% windows were used for both the 173 and 247 keV energy peaks The image was obtained with a preset time of 10 min and stored in a 256 x 256 matrix More than 500 000 counts were acquired Patients were imaged in the supine position with the gamma camera horizontally under the trunk An aliquot of the injected dose was positioned directly on the collimator and was recorded using the same acquisition parameters to permit calculation of the uptake in the lumbar spine The scintigraphic results were analyzed by drawing a region of interest (ROI) over lumbar vertebrae 2, 3 and 4 (L2-L4), corresponding with 93 g of bone marrow *(12)* Attenuation and background correction were performed as reported earlier *(13)* For calculation of tissue attenuation, the aliquot was then recorded with 5 cm acryl (density 1 2 g/cm^3) between collimator and source A paravertebral region was chosen for background correction

MEASUREMENT OF ^{111}IN-IGG ACTIVITY IN BLOOD AND TISSUE SAMPLES

The activity in blood, plasma, bone marrow and bone samples was measured in a shielded well-type gamma counter To correct for radioactive decay and to permit calculation of the uptake of the radiopharmaceutical in each sample as a fraction of the injected dose, aliquots with a known fraction of the injected doses and the samples were counted simultaneously The measured activity was expressed as percentage of the injected dose per kg tissue (%ID/kg) The activity in plasma as a fraction of whole blood activity was calculated from the measured hematocrit and the activity in whole blood and plasma

STATISTICAL ANALYSIS

All results were expressed as mean values ± 1 s d The results were analyzed using the two-tailed Student's *t*-test

RESULTS

In all volunteers, the surgical procedure took place at the scheduled time 1 e 48 h after injection of the radiopharmaceutical Puncture of the intramedullary space and aspiration of bone marrow was an effortless procedure, taking less than two min The procedure did not at all interfere with the course of the operation No side effects or complications were observed

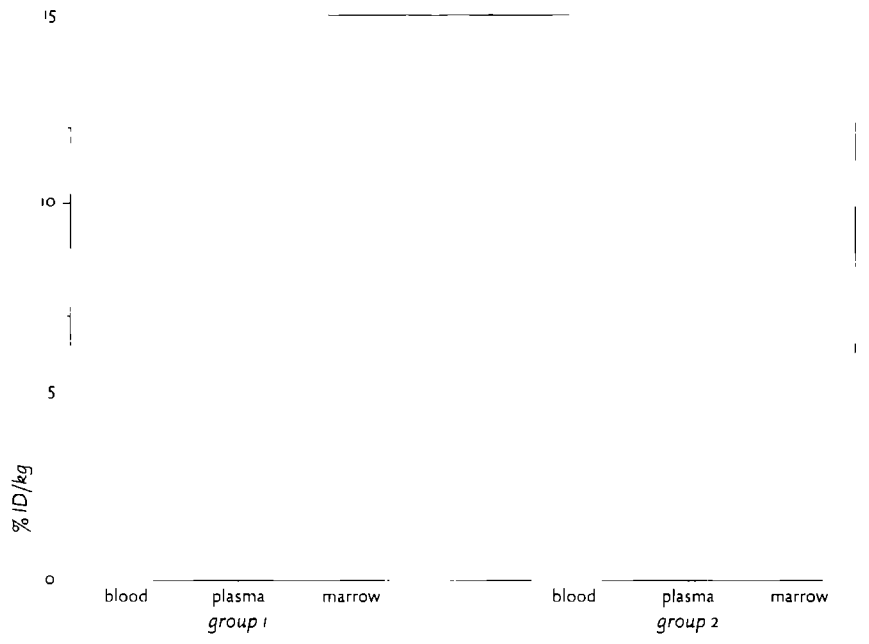

Figure 1. *Blood, tissue and bone marrow activity in the individual volunteers (group 1) and patients (group 2), expressed as percentage of dose per kg tissue. In group 1, bone marrow was measured in samples taken at surgery. In group 2, a region of interest methodology was used*

In Figure 1, the measured and calculated values of the individual patients and volunteers are given. Table 1 shows the mean ^{111}In-IgG activity in various tissues. Blood and plasma activity did not differ significantly between the two groups. No cell-associated ^{111}In-IgG activity was measured in blood. For group 1, the mean bone marrow uptake was significantly lower than that of group 2: 4.5 ± 1.3 %ID/kg and 8.5 ± 2.1 %ID/kg, respectively ($p < 0.01$). In group 1, the uptake in bone was 1.7 ± 0.4 %ID/kg. Because of the methodology used, it was not possible to differentiate bone marrow from bone uptake in group 2.

DISCUSSION

With intraoperative bone marrow sampling, sufficient quantities of bone and bone marrow can be obtained during total hip replacement without interfering with surgery and without any discomfort to the patient, thus making direct measurement of bone and bone marrow uptake possible. Accurate measurement of bone and bone marrow uptake of radiopharmaceuticals in humans is highly important for adequate calculation of the radiation burden to the body, since radiation to the bone marrow is quite often the dose limiting

TABLE 1

^{111}In-IgG activity (mean ± s d) in tissues in five volunteers and five patients at 48 h postinjection

	Volunteers (group 1)	Patients (group 2)	p
Blood (%ID/kg)	5 5 ± 1 1	6 3 ± 0 9	n s
Plasma (%ID/kg)	8 7 ± 2 4	10 2 ± 2 3	n s
Plasma associated activity (%)	98 ± 2	100 ± 1	n s
Bone marrow (%ID/kg)	4 5 ± 1 3[a]	8 5 ± 2 1[b]	< 0 01
Bone (%ID/kg)	1 7 ± 0 4[a]	–	–

%ID/kg Percentage of injected dose per kg tissue
n s Not statistically significant
a Directly measured in sample taken at surgery
b Indirect measurement using a region of interest over the lumbar spine on scintigraphic images

factor, particularly in therapeutic use of radiopharmaceuticals *(1)* This especially applies for agents which accumulate over time in the bone marrow Although not used for radioimmunotherapy, ^{111}In-IgG also accumulates in bone marrow Typically, relatively high blood pool activity and low bone (marrow) uptake is observed 4 h postinjection On the 24 and 48 h images, blood pool activity has gradually decreased while the bone structures become more prominent *(10)*

Other sampling techniques such as sternal puncture or iliac crest biopsy do cause discomfort and are not without hazards *(9)* Moreover, if bone marrow sampling is done in patients in whom a sternal puncture or iliac crest biopsy is indicated on clinical grounds it is not unlikely that abnormal bone marrow is obtained In contrast with the current bone marrow sampling technique normal bone marrow can be obtained

There is no generally accepted method for calculating the radiation burden to the bone marrow using ROIs on scintigraphic images of the lumbar spine, sacrum, and iliac crest, or activity in blood or whole body data Depending on the method of calculation used, they lead to highly variable results Whole body data and blood data are inadequate for inhomogenously distributed radiopharmaceuticals, especially for those with high affinity to bone marrow *(4,8,14)* Measurement of the bone marrow uptake on scintigraphic images appears to be more adequate However, it can easily lead to erroneous results, for example due to overlying tissues, such as blood vessels, or due to differences in background subtraction and attenuation correction *(2 7, 13)* In our study, a significant discrepancy was found between the direct measurement using bone marrow aspiration (group 1) and the indirect method using ROIs on the scintigraphic images (group 2) One explanation might be that with the ROI method the bone

uptake accounted for the difference in bone marrow uptake between group 1 and group 2 However, this methodological problem of the ROI method, which also applies to all other scintigraphic calculation methods for estimating bone marrow uptake, can not explain the total difference between the marrow uptake in the two groups, since bone uptake of ^{111}In-IgG is only approximately one third of that in bone marrow When using the data from ICRP publication no 23 "Reference Man", one can calculate that the total lumbar spine mass is 348 g, the lumbar spine mass without bone marrow 348 g minus 152 g = 196 g *(12,15)* Using the measurements in group 1, the expected uptake in the lumbar spine would then be 196 x 1 7/1000 (measured bone uptake) + 152 x 4 5/1000 (measured bone marrow uptake) = 1 01 %ID in the whole lumbar spine For L2-L4 this would be 3/5 x 1 01 = 0 61 %ID Erroneously attributing this total dose to bone marrow uptake alone would lead to a marrow uptake of 0 61 / 0 093 (marrow weight L2-L4) is 6 5 %ID/kg Although still lower, this value is more in concert with the scintigraphic calculation However, the unavoidable contribution of bone activity in the ROI, used for calculation of bone marrow activity, further emphasizes the need for direct and separate measurement of bone marrow and bone samples

One might question whether it is fair to compare bone marrow uptake in healthy volunteers suffering from degenerative osteoarthritis with those suspected of having infectious disease However, follow-up in four out of five patients revealed no evidence of infection These four patients showed a normal ^{111}In-IgG distribution on the scintigraphic images In the fifth patient, mild pathologic activity uptake was observed near an infected total hip prosthesis Moreover, all five patients had normal peripheral blood cell counts In our experience in over 600 patient studies, the degree of ^{111}In-IgG uptake in bone marrow is correlated with age, but not with the presence of infectious foci

In this study, bone marrow uptake was not calculated over the intertrochanteric region, since the proximity of the femoral blood vessels and the relatively high background activity in this area make it very difficult to identify bone marrow with sufficient accuracy on the scintigraphic images Although nonidentical areas where chosen for comparison of bone marrow uptake between the two groups, the difference in uptake in the two groups can not be explained by a variation in the red to yellow ratio in the marrow of the proximal femur and the lumber spine In these areas, this ratio is very similar (approximately 75 % red and 25 % yellow bone marrow) *(12)*

An additional advantage of the current method of bone and bone marrow sampling is that only low radioactivity doses are needed, resulting in a low absorbed dose to the volunteer The effective dose equivalent to patients, injected with the diagnostic dose of 75 MBq ^{111}In-IgG, is approximately 15 mSv *(16)* So, in group 1, the effective dose equivalent was less than 1 mSv

The method also has logistic advantages. Total hip replacement for degenerative osteoarthritis is a frequent, elective surgical procedure. This implies that bone and bone marrow sampling can be planned in advance and that sufficient volunteers can be included in a study in a relatively short period of time. Furthermore, no additional bone marrow is removed for the purpose of this study, since the bone marrow at the site of the shaft will be removed anyway.

In this preliminary study, the uptake was only measured at one time point. It is of course possible to inject different volunteers at various intervals before surgery. Thus the dynamic distribution in bone and bone marrow can be determined in a group of volunteers. This is of course necessary for dosimetric calculations.

In the present study, only samples of older volunteers were measured. However, it is possible to include younger volunteers. Firstly, patients with hip joint destruction due to fracture or rheumatoid arthritis are also candidates for total hip replacement. Secondly, bone and bone marrow samples can also be obtained with this procedure in patients who are scheduled for intertrochanteric osteotomy of the femur.

CONCLUSION

Intraoperative bone and bone marrow sampling is a new, direct, and simple procedure for accurate measurement of bone and bone marrow uptake of radiopharmaceuticals without discomfort to the patient. Since only minute doses are sufficient, the radiation burden is very low. It can contribute to the validation of the various indirect methods used for calculating bone marrow uptake. It can be especially useful for dosimetric calculations of radiopharmaceuticals labeled with pure β-emitters. It can result in more realistic calculation of biodistribution and dosimetry studies of radiopharmaceuticals in humans, since overestimation due to overlying tissue, uptake in bone and variability due to attenuation and background correction can be avoided.

ACKNOWLEDGEMENTS

We thank the orthopedic surgeons Professor T. Slooff, Dr. G. Homminga, and Dr. J. Gardeniers for their cooperation in obtaining the bone and bone marrow samples.

REFERENCES

1 Goldenberg DM Future role of radiolabeled monoclonal antibodies in oncological diagnosis and therapy *Semin Nucl Med* 1989, 19 332-339

2 Harwood SJ, Carroll RG, Webster WB et al Human biodistribution of In-111-labeled B72 3 monoclonal antibody *Cancer Res (Suppl)* 1990, 50 9328-9368

3 Gainey MA, Siegel JA, Smergel EM, Jara BJ Indium-111-labeled white blood cells dosimetry in children *J Nucl Med* 1988 29 689-694

4 Siegel JA, Pawlyk DA, Lee RE et al Tumor, red marrow, and organ dosimetry for I-131 labeled anti-carcinoembryonic antigen monoclonal antibody Cancer Res (Suppl) 1990, 50 10395-1042s

5 Siegel JA, Lee RE Pawlyk DA, Horowitz JA, Sharkey RM, Goldenberg DM Sacral scinti graphy for bone marrow dosimetry in radioimmunotherapy *Nucl Med Biol* 1989, 16 553-559

6 Marcus CS, Stabin MG, Watson EE Henneman PL, Butler JA, Kuperus JH Dosimetry of leukocytes labeled with Tc-99m-albumin colloid *Nucl Med Commun* 1988 9 249-254

7 Suey CM DeNardo GL DeNardo SJ, Goluby AH Radioimmunotherapy with monclonal antibodies *J Nucl Med Tech* 1990 18 176-183

8 Plaizier MABD van Dieren EB, van Lingen A et al Bone marrow dosimetry for In 111 and I-131 labeled antibodies (MoAbs) based on whole body data, and immunoscintigraphic data *Eur J Nucl Med* 1991, 18 603 (abstract)

9 Williams WJ, Nelson DA Examination of the marrow In Williams WJ, Beutler E Erslev AJ, Lichtman MA, eds *Hematology* 4th ed New York McGraw-Hill Publishing Company, 1990 25-26

10 Oyen WJG, Claessens RAMJ, van Horn JR, van der Meer JWM, Corstens FHM Scintigraphic detection of bone and joint infections with indium-111 labeled nonspecific polyclonal human immunoglobulin G *J Nucl Med* 1990, 31 403-412

11 Hnatowich DJ, Childs RL, Lanteigne D, Najafi A The preparation of DTPA coupled antibodies radiolabeled with metallic radionuclides an improved method *J Immunol Meth* 1983 65 147-157

12 ICRP Publication 23 *Report of the Task Group on Reference Man* Oxford Pergamon Press Ltd 1975 91

13 Buijs WCAM, Massuger LFAG, Claessens RAMJ, Corstens FHM Dosimetric evaluation of immunoscintigraphy using indium 111 labeled monoclonal antibody fragments in patients with ovarian cancer *J Nucl Med* 1992, 33 1113-1120

14 Bigler RE, Zanzonico PB Leonard R, Cosma M *Bone marrow dosimetry for monoclonal antibody therapy* In Proceedings of the Fourth International Radiopharmaceutical Dosimetry Symposium Oak Ridge, TN Oak Ridge Associated Universities 1986 535-544

15 ICRP Publication 23 *Report of the Task Group on Reference Man* Oxford Pergamon Press Ltd 1975 65

16 Buijs WCAM, Oyen WJG, Claessens RAMJ, Koenders EB, Meeuwis APW, Corstens FHM Biodistribution and radiation dosimetry of indium 111 labeled immunoglobulin G *Eur J Nucl Med* 1990, 16 433 (abstract)

CHAPTER 8

Dosimetric Evaluation of Immunoscintigraphy Using Indium-111-Labeled Monoclonal Antibody Fragments in Patients with Ovarian Cancer

Wilhelmina C.A.M. Buijs, Leon F.A.G. Massuger, Roland A.M.J. Claessens, Frans H.M. Corstens

J Nucl Med 1992, 33 1113-1120

ABSTRACT

This study reports the biodistribution and dosimetry for a monoclonal antibody against ovarian carcinoma. Eight patients received 140 MBq ^{111}In-OV TL 3 F(ab')$_2$, thereafter gamma camera imaging was performed daily up to 96 h. By using the conjugated view counting method, activity in the organs was quantitated by phantom calibration and by whole-body measurements using a whole-body counter. Red bone marrow uptake was derived from regions of interest over the lumbar vertebrae and iliac crest.

In both methods, organ uptake varied only slightly with time, having a mean value of approximately 18%, 4%, 6% and 17% of the injected dose in the liver, spleen, kidneys and red bone marrow, respectively. The mean absorbed dose to these organs was 0.9, 1.5, 1.2 and 0.5 mGy/MBq. The effective dose equivalent was 0.4 mSv/MBq.

In this study, two different methods of uptake calculations, result in similar values of organ uptake.

INTRODUCTION

Radiolabeled monoclonal antibodies (MAbs) against tumor-associated antigens have been used to detect tumor deposits with variable degrees of success *(1)* Since gamma camera imaging of patients injected with radiolabeled MAbs has demonstrated selective tumor uptake of MAbs, antibody-directed radiotherapy has gained greater interest Prior to employing antibodies for radioimmunotherapie, their biodistribution and dosimetry must be determined The different characteristics of whole antibodies and fragments and of metallic and nonmetallic radionuclides require that agents as similar as possible be used for dosimetry calculations and therapy For instance, a biodistribution study with an iodinated whole antibody does not predict the radiation burden at therapy with ^{90}Y-labeled F(ab')$_2$ fragments

We used an ovarian carcinoma-associated murine MAb OV-TL 3, for the immunoscintigraphic detection of ovarian cancer The safety and diagnostic accuracy of imaging with the ^{111}In-labeled OV-TL 3 F(ab')$_2$ was studied in 31 patients suspected for ovarian cancer *(2)* Several aspects of the biological behavior of the ^{111}In-labeled MAb fragment in patients were studied using multiple blood samples and measurements of tissues removed at surgery *(3)* The latter study concentrated on tissue distribution of the radioimmunoconjugate at the time of surgery The aim of the current study was to determine the dynamic distribution of radioactivity over a number of organs and to calculate the absorbed dose to these organs and to the total body The technique most commonly used for quantitation of absolute organ activity is the conjugate view counting method with calculation of the geometric mean of the counts in opposing views of planar images *(4,5)* Two different methods, both based on this principle, were evaluated Both methods are modifications of existing techniques In the first method, phantom based correction factors were used to quantitate organ uptake *(5,6)* In the second method, calculated organ counts were compared with the amount of counts in the total body in order to obtain the absolute organ uptake *(7)* Data obtained for the liver using these methods were compared with measurements of activity in tissue specimens taken at surgery

The absorbed dose to various organs and the effective total body dose were estimated using the standard MIRD methods

MATERIAL AND METHODS

PATIENTS

Dosimetric studies were performed in 8 of 31 patients studied under a protocol approved by the Human Research Review Committee of this institution *(2)*

Prior to study entry, each patient gave written informed consent. All eight patients were highly suspected of having primary or recurrent ovarian cancer and were scheduled to undergo subsequent surgery. The selection of these patients for inclusion in the study was based on the absence of large amounts of ascites in the abdomen and the fact that there was only minimal overlap of the liver, spleen and left kidney on the gamma camera images. The mean age of the patients was 62.1 y (range: 50-77 y). Indium-111-OV-TL 3 $F(ab')_2$ (1 mg, 140 MBq) in 5 ml of saline was intravenously infused within 5 min. The actual administered dose was carefully measured prior to injection using a dose calibrator.

IMAGING PROCEDURE

Planar gamma camera images were recorded 4, 24, 48, 72 and 96 h after injection using a single-head gamma camera (Orbiter-ZLC-Digitrac, Siemens, Hoffmann Estates, IL) equipped with a parallel-hole medium-energy collimator and connected to a computer for subsequent data analysis (A^2, Medical Data Systems/ Medtronic, Ann Arbor, MI). Symmetric 20% windows were used for both the 173 and 247 keV energy peaks. At all time points, anterior and posterior planar images of pelvis, abdomen and thorax were made with a 5-min preset time and stored in a 128 x 128 matrix. On average, a 5-min image recorded more than 500,000 events. Patients were imaged in the supine position with the gamma camera horizontally above or under the trunk.

URINE AND FECES MEASUREMENTS

For 5 days following injection of the radiopharmaceutical, urine and feces were collected in 24-h aliquots. Activity was measured in a well-type gamma counter and expressed as percent of the injected dose (%ID).

WHOLE-BODY MEASUREMENTS

In one patient, the activity distribution in the body was measured with a shadow-shield whole-body counter in scan mode in order to assess the ratio of activity in the trunk to that in the total body.

QUANTITATIVE ORGAN UPTAKE

Two methods were used to quantitate the uptake of activity in the liver, spleen and left kidney. In both methods, the conjugate view counting technique, using the geometric mean (GM) of counts in an organ, was used at various timepoints *(4,5,8-11)*. The GM of anterior and posterior images was calculated according to the formula:

$$GM = SQRT(A \times P),$$

where A is the number of counts in the anterior region and P is the number of counts in the posterior region. Prior to calculation of the GM, both anterior and

posterior measurements were corrected for background. In Method 1, the absolute uptake of activity in an organ was calculated via comparison of the net (background-corrected) GM with a calibration curve obtained from measurements of known amounts of activity in a water equivalent phantom *(5,6)*. In Method 2, the net GM in an organ was related to the GM of the total body using a combination of adjacent spot images to reconstruct a near whole-body GM *(7)*.

BACKGOUND CORRECTION

For each imaging study, regions of interest (ROIs) were manually drawn over the liver, spleen and left kidney on both anterior and posterior abdominal images. On the posterior image, the liver ROI excluded the overlying right kidney. Similar organ ROIs were chosen for all time points.

A background ROI was drawn over the area just caudally and medially of the left kidney. Background correction was performed on a counts per pixel basis. In order to avoid overcorrection, no background correction was performed for the liver, because this organ almost occupies the whole body thickness in cross section. For the spleen and kidney, only partial background correction was used *(9)*. From x-ray CT scans, it was derived that these organs occupied only 30% of the whole-body thickness in cross section, so a 70% value of the background ROI was subtracted to achieve this partial thickness compensation.

Method 1 (Calibration Phantom). In this method the organ counts were calibrated with phantom measurements to correct for attenuation and scatter *(5,6)*.

In calculating absolute organ activity, the GM of the anterior and posterior counts were corrected for gamma camera efficiency and for attenuation and scatter of gamma radiation in the patient *(4)*. Gamma camera efficiency is defined as the count rate per unit activity without attenuation. The attenuation depends on patient thickness and tissue composition. Moreover, due to the scattered radiation, the degree of attenuation depends on the window settings of the gamma camera and the size of the ROI. The transmission curve, which describes the count rate from a source as a function of depth of the source in tissue, was measured for ^{111}In using two different source sizes. Cylindrical containers with a height of 3 cm and a diameter of 8.5 and 18 cm, respectively, were filled with water containing a known amount of ^{111}In. An attenuating phantom was built using acrylic plates with a diameter of 42 cm and a thickness of 2 or 3 cm. An additional partly hollow plate was constructed with a thickness of 4 cm, in which either one of the cylindrical sources at various depths could be placed, thus making it possible to image the cylindrical sources at various depths with steps of 1 cm up to a total depth of 21 cm. Phantom measurements were performed with the same window settings used for patient imaging. For translation of acrylic thickness to tissue thickness, acrylic thickness was multiplied by 1.18, which represents the mass density of acrylic relative to tissue. The transmission factor,

defined as the quotient of the count rate from a source with attenuation and the count rate from this source without attenuation was calculated for various source depths. For a given patient thickness the GM of the transmission factors for diverse combinations of source depths was calculated. The arithmetic mean of these GM values was used as correction factor for attenuation and scatter. These correction factors were computed for various patient thicknesses ranging from 15 to 21 cm. The correction factors calculated for the large source were used to calibrate the GM counts of the liver. For the spleen, left kidney, lumbar spine and iliac crest the transmission factors for the small source were used. The thickness of the abdomen was measured from X-ray CT scans. Because the thickness of the abdomen at the site of the right liver lobe and at the site of the spleen was smaller than the maximum thickness of the abdomen, a correction factor for a body thickness of 0.89 was used for the spleen and 0.91 for the liver *(5)*. The absolute organ activity was calculated by dividing the GM of the organ counts by camera efficiency and the correction factor for attenuation and scatter. The percent uptake of the injected activity in that organ was calculated as the absolute organ uptake, corrected for physical decay and divided by the amount of injected activity.

Method 2 (Whole Body). This method calculates the percent organ uptake, relative to the total body activity, by using overlapping spot images to reconstruct near-whole body images *(7,10,12)*. Total-body activity was measured by summing the GMs of adjacent body parts (thorax, abdomen and pelvis) after correction for differences in attenuation of these body parts. The difference in attenuation between the thorax, abdomen and pelvis was estimated with an ^{111}In transmission flood source in three patients. The count rate measured from the activity in the flood source after transmission through the patient was divided by the count rate of the flood source measured without attenuation by the patient. This quotient, the so-called 'transmission factor', was similar for both abdomen and pelvis. The square root of the transmission factor for the thorax was on average 15% higher than that for both abdomen and pelvis transmissions. The thoracic contribution was multiplied by 0.85 in order to obtain correct total body counts. These calculated total body counts were further corrected for that part of the body not seen by the gamma camera, as estimated from daily total-body profile scans with the shadow shield whole-body counter in one patient. The uptake of radioactivity in an organ at each time interval could then be calculated as the net GM divided by 1% of the corrected total-body counts and expressed as a percentage of the total body counts at that time. Organ uptake as %ID was further corrected for the excretion of activity in urine and feces.

In all patients studied, subsequent surgery was performed between 5 and 7 days after infusion of the immunoconjugate. In three patients, liver biopsies of approximately 1 g of tissue were taken. All samples were weighed and ^{111}In uptake was quantitatively measured using a well-type counter. Mean liver uptake was

expressed as %ID/kg ± s d and from these results total liver uptake was calculated, assuming a mean liver weight in elderly women of 1500 g These results were compared with those obtained using ROI analysis

RED BONE MARROW

Uptake in the red bone marrow was estimated from the gamma camera images using calibration Method 1 with the small calibration source Two different parts of the skeleton were chosen for measurement of red bone marrow uptake and the uptake found in each of these areas were extrapolated to the whole-body red bone marrow, assuming a homogenous distribution of the activity over the red bone marrow A ROI was drawn around the lumbar vertebrae L3+L4 together, corresponding with 4 6% of the total red bone marrow *(13)*, and a background region of the same size was chosen adjacent to the left side of these vertebrae Moreover, ROIs were drawn over a part of the left and right iliac crest The sum of these areas represented 25% of the os coxae as calculated from X ray CT measurements, corresponding with 6 5% of total body red bone marrow *(13)* Background ROIs, the same size as those of the iliac crest, were drawn lateral to the iliac crest For the lumbar vertebrae L3+L4 and for the iliac crest, the GM was calculated from the background-corrected counts in the corresponding ROIs

ABSORBED DOSE CALCULATION

The absorbed dose to the organs was calculated with the MIRD method *(6,14)* Revision 2 of a BASIC computer program (MIRDOSE2) was used with S-factors for 15-y old people *(15)* To obtain dose calculations in accordance with this method, the residence time in the source organs must be calculated The liver, spleen, kidneys, red bone marrow, bladder and rest of the body were used as source organs The amount of activity for the rest of the body at each time point was calculated as the difference between the injected activity and the sum of the excreted activity and the activity in the liver, spleen, both kidneys and red bone marrow The residence time is defined as the cumulated activity in an organ per unit of injected activity and was calculated as the integration over time of the activity in an organ, not corrected for physical decay, divided by the amount of injected activity It was assumed that uptake after 4 h was representative as the initial uptake at time zero For the period from 0-96 h the trapezoidal method was used for the integration of activity over time After 96 h, it was assumed that there was only physical decay and no increase or decrease of activity in the organs and the rest of the body Residence times for the liver, spleen and the kidneys were calculated using the mean of the results obtained with Methods 1 and 2 For red bone marrow, the residence time was calculated as the mean of the results obtained for the vertebrae-derived red bone marrow uptake and the iliac

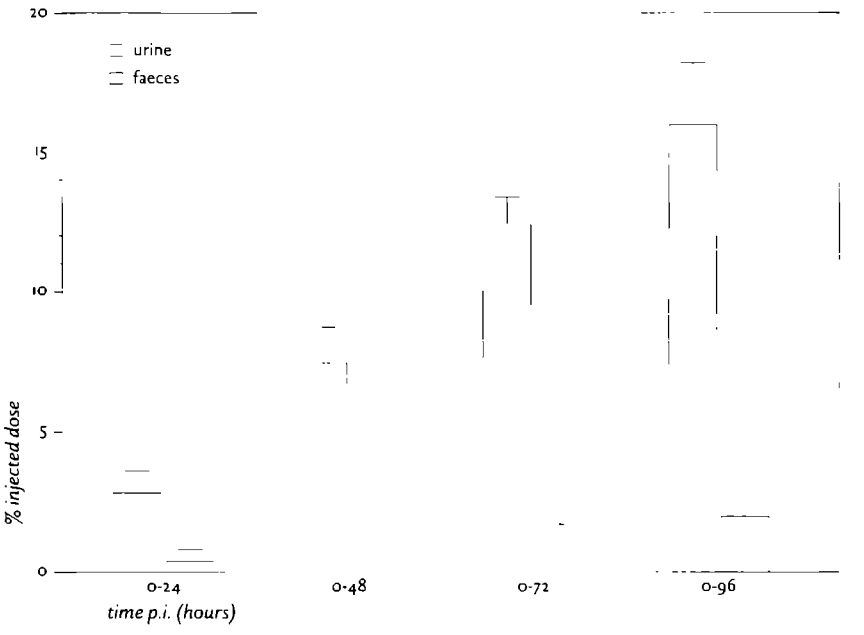

Figure 1. *Cumulative excretion of urine and feces after injection of ^{111}In-OV-TL3 F(ab')2. Mean values (n=8). Error bars represent 1 s.d.*

crest-derived red bone marrow uptake. The residence time for the rest of the body was calculated as the mean of the results for each of the four combinations of Methods 1 and 2 and both red bone uptake estimations. For the bladder, a constant urine flow and a voiding interval of 4 h was assumed. The effective dose equivalent (EDE) was computed from the absorbed doses to the organs using weighting factors for adults, which represent the relative radiation sensitivity of organ or tissue *(16)*.

RESULTS

EXCRETION IN URINE AND FECES

Urinary and feces excretion of the radiolabel were measured in all eight patients studied. Total excretion (urine + feces) was at a relatively constant rate during the entire study period, where excretion of activity in the feces was small, compared to that in the urine. At 24, 48, 72 and 96 h postinjection, the mean cumulative excretion was 3.4 ± 0.7, 8.1 ± 1.5, 13.6 ± 1.4 and 18.4 ± 3.0 %ID, respectively (Figure 1).

TABLE 1

Uptake of ^{111}In-OV-TL 3 F(ab')$_2$ in the Liver According to Methods 1 and 2 (Results Are Expressed as %ID)

Patient no	Time postinjection 4 h	24 h	48 h	72 h	96 h
			Method 1		
1	190	186	193	187	199
2	156	172	179	166	166
3	125	136	134	126	137
4	259	308	293	284	268
5	163	174	172	149	159
6	165	177	193	157	157
7	121	144	142	132	141
8	122	119	115	109	100
mean	163	177	178	164	166
sd	43	54	51	51	47
			Method 2		
1	192	180	192	182	190
2	189	199	204	191	189
3	146	156	157	147	155
4	258	311	301	287	278
5	173	179	171	161	151
6	173	199	199	185	177
7	152	178	174	169	169
8	151	150	143	132	128
mean	179	194	193	182	180
sd	34	47	45	44	42

WHOLE BODY MEASUREMENTS

During the study, there was a relative decrease in activity in those parts of the body not seen by the gamma camera. Compared with the total body, the relative amount of counts in the trunk at 4, 24, 48, 72 and 96 h was 85, 87, 88, 89 and 90%, respectively, meaning that there was a minimal shift in the distribution of the activity from the head and extremeties to the trunk. The whole-body measurements in Method 2 were corrected accordingly.

ORGAN UPTAKE

Liver. Liver uptake was calculated at five different time points during the study, using both Methods 1 and 2 (Table 1). Similar results were obtained with both methods. From 4 h onwards, liver uptake was fairly constant during the entire 96-h study period for all patients. Still, there were clear differences between patients for ^{111}In uptake levels. At 24 h, this level varied from 12% ID in Patient 8 to 31% ID in Patient 4. Mean liver uptake in all patients studied varied from 16.3% ± 4.3% to 17.8% ± 5.1% ID for Method 1 and from 17.9% ± 3.4% to 19.4% ± 4.7% ID for Method 2. Estimated liver uptake, using both ROI based methods, was confirmed by tissue measurements taken in three patients at surgery. By assuming a mean liver weight of 1500 g, mean liver uptake (n=3)

TABLE 2

Uptake of ^{111}In-OV-TL 3 F(ab')$_2$ in the Spleen According to Methods 1 and 2 (Results are expressed as %ID)

Patient no	Time postinjection				
	4 h	24 h	48 h	72 h	96 h
			Method 1		
1	49	46	42	38	36
2	77	73	55	58	47
3	64	48	39	37	42
4	42	34	31	26	27
5	39	34	35	30	31
6	36	30	37	30	32
7	79	63	59	53	50
8	55	33	29	27	30
mean	55	45	41	37	37
s d	16	15	10	11	08
			Method 2		
1	41	37	34	31	29
2	77	71	53	58	45
3	64	47	38	37	40
4	35	28	26	22	23
5	33	27	28	26	23
6	32	29	32	30	31
7	84	66	61	57	50
8	59	36	31	28	32
mean	53	43	38	36	34
s d	19	16	12	13	09

TABLE 3

Uptake of ^{111}In-OV-TL 3 F(ab')$_2$ in the Kidneys According to Methods 1 and 2 (Results are expressed as %ID)

Patient no	Time postinjection				
	4 h	24 h	48 h	72 h	96 h
			Method 1		
1	47	98	107	81	86
2	27	49	55	64	46
3	62	114	117	95	86
4	41	49	47	46	46
5	34	63	75	68	55
6	38	68	73	55	60
7	42	51	67	52	44
8	46	88	103	94	91
mean	42	74	81	69	64
s d	10	22	24	18	19
			Method 2		
1	35	70	78	58	61
2	25	42	47	56	39
3	55	101	105	86	75
4	30	44	36	35	36
5	27	48	56	55	39
6	29	56	56	48	50
7	39	47	61	49	39
8	44	84	99	88	89
mean	36	62	67	59	54
s d	09	20	23	17	18

totaled 19 1% ± 7 7% ID In these patients mean liver uptake was 20 1% ± 6 6% ID, when calculated according to Method 1 and 20 8% ± 6 3% ID when calculated according to Method 2

Spleen The calculated spleen uptake was also similar for both methods used (Table 2) Mean splenic uptake was highest at 4 h postinfusion, being 5 5% ± 1 6% ID with Method 1 and 5 3% ± 1 9% ID with Method 2 Spleen uptake decreased during the study to 3 7% ± 0 8% ID (Method 1) and 3 4% ± 0 9% ID (Method 2) at 96 h postinfusion The level of spleen uptake at 24 h postinjection varied between patients from approximately 3%-7% ID for both methods used

Kidneys Overall, calculated kidney uptake also demonstrated similar results for both methods used (Table 3) Kidney uptake for both kidneys was calculated as twice the measured uptake of the left kidney Using both methods, there was a clear increase in kidney uptake from 4 h onwards The highest mean uptake was measured at 48 h, amounting to 8 1% ± 2 4 % ID (Method 1) and 6 7% ± 2 3% ID (Method 2) After 48 h, kidney levels decreased again resulting in mean kidney levels of approximately 6% ID for both methods at 96 h postinfusion

Red bone marrow Uptake in red bone marrow was calculated using Method 1 (Table 4) Using both the iliac crest or 2 lumbar vertebrae as the ROI, similar results were obtained for total red bone marrow uptake Mean red bone marrow uptake varied between 13 9% ± 1 5% and 18 5% ± 4 6% ID using the lumbar vertebrae and between 14 4% ± 2 1% and 18 9% ± 3 1% ID using the iliac crest

ABSORBED DOSE CALCULATIONS

The residence times for the different source organs and the rest of the body are given in Table 5 The residence time for the bladder was assumed to be similar for all patients and was calculated to be 0 15 h The absorbed dose to the different organs is given in Table 6 The mean calculated dose to the liver was 0 86 ± 0 19, spleen 1 45 ± 0 36, kidneys 1 18 ± 0 27 and red bone marrow 0 52 ± 0 05 mGy/MBq For a typical administered amount of 140 MBq this leads to a mean absorbed dose of 120 ± 26 mGy to the liver 202 ± 51 mGy to the spleen, 165 ± 38 mGy to the kidneys and 73 ± 7 mGy to the red bone marrow The mean EDE was 0 40 ± 0 02 mSv/MBq, or 56 3 ± 2 9 mSv in the current study for an administered dose of 140 MBq ^{111}In-OV-TL 3 $(Fab')_2$

DISCUSSION

OV TL3, when radiolabeled with ^{111}In, already has demonstrated its usefulness as an imaging agent in patients suspected of having ovarian cancer *(2)* However, before pursuing therapeutic tumor targeting with this MAb labeled to ^{90}Y, the therapeutic analog of ^{111}In, a thorough assessment of the biodistribution in combination with dosimetry is indispensable

TABLE 4

Uptake of ^{111}In-OV-TL 3 F(ab')$_2$ in Total Red Bone Marrow Calculated via Lumbar Vertebrae and Iliac Crest (Results are Expressed as %ID)

Patient no	Time postinjection				
	4 h	24 h	48 h	72 h	96 h
			Lumbar vertebrae		
1	150	155	152	148	169
2	145	146	125	144	178
3	156	268	221	233	214
4	146	92	88	108	91
5	110	199	201	236	223
6	147	245	224	222	150
7	138	149	152	167	152
8	117	179	235	223	181
mean	139	179	175	185	170
s d	15	53	50	46	39
			Iliac Crest		
1	104	163	138	174	232
2	148	147	123	160	137
3	174	151	140	139	194
4	134	166	166	214	177
5	142	176	173	144	155
6	155	135	163	156	178
7	130	153	192	140	212
8	166	157	205	257	224
mean	144	156	163	173	189
s d	21	12	26	39	31

TABLE 5

Residence Times of ^{111}In-OV-TL 3 F(ab')$_2$ in Source Organs (Results Are Expressed in Hours)

Patient no	Source organ				
	Liver	Spleen	Kidneys	Red bone marrow	Rest of body
1	187	36	73	168	398
2	177	56	44	145	439
3	141	43	87	191	399
4	278	27	42	133	381
5	160	29	50	178	444
6	173	31	54	172	432
7	151	57	46	163	444
8	121	33	84	192	430
mean	173	39	60	168	421
s d	44	11	17	19	23

TABLE 6

Radiation Doses for ^{111}In-OV-TL 3 F(ab')$_2$ in mGy/MBq

Patient no	Organ				EDE (mSv/MBq)
	Liver	Spleen	Kidneys	Red bone marrow	
1	0 92	1 36	1 39	0 52	0 41
2	0 87	2 00	0 93	0 47	0 41
3	0 72	1 60	1 61	0 58	0 44
4	1 30	1 04	0 90	0 44	0.38
5	0 80	1 11	1 00	0.55	0 37
6	0.85	1 18	1 07	0 53	0 38
7	0.76	2 03	0 96	0 51	0.42
8	0.64	1 27	1 55	0 59	0 41
mean	0 86	1 45	1 18	0 52	0 40
s d	0 19	0 36	0 27	0 05	0 02

Patients with ascites were omitted from the study, because of activity accumulation in ascites *(3)*, making it impossible to determine the proper background activity. Furthermore, when ascites are present, lumbar vertebrae are hardly visible on anterior views. In the concept of the MIRD dose calculations, as used in this study, only a restricted number of source organs are selected. Abdominal volume with ascites cannot be defined as such. Activity in the ascites represents at the most a few percent of the injected dose. Thus, it is very unlikely that concentration of activity in the source organs is significantly influenced by the presence or absence of ascites. Therefore, with respect to dose calculations, measurements in patients without ascites seem representative for the whole group of patients.

A variety of methods have been used to quantitate in vivo distribution of radioactivity *(4-9,12,17-19)*. In most of these studies, the GM technique for conjugated views was used with one external calibration source for attenuation correction and estimation of gamma camera efficiency *(5)*. An important drawback of this technique is its lack of correction for scatter *(17,18)*. In order to overcome this problem, we used two different methods, both based on the GM technique for conjugate views.

In the first method (calibration phantom), mean organ counts were translated to activity (MBq) using two different calibration phantoms. In the second method (whole body), radioactivity in an organ was expressed as a percentage of whole body radioactivity. In the latter method, the patient provides his own calibration, making correction for tissue attenuation, patient thickness and physical decay superfluous.

Despite efforts to optimize quantitation of absolute organ uptake, certain errors will be present. For Method 1, the phantoms should closely match the dimensions of the organs they represent *(20,21)*. The phantoms we used were not

ideal in that respect. Second, to compensate for scatter, we did not explicitly use a volume-dependent buildup factor (21). Since phantoms with different source sizes were measured at different depths and for diverse patient thicknesses, these determinations partially correct for scatter. The number of pixels in the ROI over the small source was similar to that in the ROIs over spleen, kidney, lumbar spine and iliac crest, 600-700 pixels in a 128 x 128 matrix. The number of pixels in the ROI of the large source was about 2400, a similar number of pixels as found in the liver ROI. We therefore used the correction factors for attenuation and scatter of the small sources for the spleen, kidney, lumbar spine and iliac crest and the correction factors of the large source for the liver. For the small source, the correction factors for attenuation and scatter were 15%-20% lower in comparison to the large source. We thus concluded that a minor deviation in organ size, with respect to the source size used for calibration, may give an error in the estimation of absolute organ activity of no more than 5% of the calculated activity. Third, the homogeneous nonradioactive acrylic disks used as attenuation layers do not accurately reflect variations of tissue attenuation in the body. Fortunately, we were able to derive data on the thickness of the abdomen and on the individual sizes of organs from X-ray CT scans. However, in some investigations, these data will not be available.

For Method 2, several other sources of error may occur. First, accurate reconstruction of one near whole body image from three adjacent spot images is difficult to perform and time consuming. Second, the relative attenuation correction factor used for the thorax (0.85) was not assessed for each patient. The use of a special attenuation correction factor for the thorax seems adequate. However, the effect on the outcome will be relatively poor since counts in the thorax represent only a quarter (at 4 h postinjection) to one-seventh (at 96 h post-injection) of the total body counts. Third, the relative contribution of counts from parts of the body not seen by the gamma camera was measured in only one patient and used for the whole group. Another source of error may be the assumption that attenuation and scatter are similar for the total abdomen and the abdominal organs. This assumption may give an underestimation of organ uptake, because scatter contribution in the organ ROI is smaller than that for the total abdomen ROI. This effect is smaller for the liver in comparison with the other organs. Indeed, uptake in the kidneys seems to be lower, when calculated with Method 2 in comparison with Method 1.

The results were similar with both methods. From this study no preference for either method can be made. However, it should be noted, that Method 2 is much more time consuming.

The liver had the greatest uptake (approximately 19% ID). However, measurement of liver uptake can be erroneous for various reasons. Superimposition of the right kidney and/or the spleen results in a false elevation of the

counts in the region We excluded the right kidney from the liver ROI on the posterior image, thus a part of the liver does not contribute to the count rate on the posterior liver ROI, which underestimates the posterior count rate The overestimation in the anterior liver counts might balance the under-estimation of the posterior counts when calculating the GM Furthermore, the counts were not corrected for activity in the overlying red bone marrow in ribs In view of these variables, the direct measurements of tissue specimens of the liver *(3)* provided surprisingly similar results to those obtained with the gamma camera

Uptake in the spleen was lowest of all organs measured (± 4% ID) Similar to the liver, spleen uptake was rather constant with time

Because of great overlap of the right kidney with the liver on gamma camera images only the absolute uptake in the left kidney was measured and calculated, assuming that the left kidney represented half of the activity in both kidneys at any time point Increasing activity in the kidneys was found up to 48 h (± 8% ID), whereas in both liver and spleen no increase of activity was measured during the study period

The activity concentration was 0 01% ID/g for the liver and 0 02 and 0 025% ID/g for the spleen and the kidney In vitro experiments using fluorescence-assisted cell sorter analysis, have suggested a significant cross reactivity of OV TL3 with white blood cells *(3)* In vivo however, association of OV-TL3 to blood cells could never be detected in circulating blood The relatively high and similar uptake of ^{111}In-OV-TL3 $F(ab')_2$ in liver, spleen and kidneys points to uptake of liberated indium in these organs rather than significant cross reactivity of OV TL3 with leukocytes The relatively high kidney uptake may in part be attributed to the excretion route of $F(ab')_2$ fragments

Two different ROIs (iliac crest and two lumbar vertebrae) were used to assess uptake in red bone marrow Both regions resulted in similar estimations of the relative amount of uptake in the whole red bone marrow Red bone marrow uptake was rather high and increased slightly with time during the study This finding has been previously described after injection of ^{111}In-labeled $F(ab)_2$ fragments of the MAb CA 19 9 by Hnatowich et al , who noted an increase in red bone marrow uptake on gamma camera images *(22)*

Both methods used to calculate marrow uptake have disadvantages Extrapolation of the ROI data to the total amount of red bone marrow in the body can be done in different ways *(13,23)* Furthermore, lumbar vertebrae are often barely visible on anterior views and the superimposed aorta may interfere with the results The orientation of the pelvis makes it rather difficult to draw the correct regions over the iliac crest for reproducible marrow mass measurements For assessment of red bone marrow uptake, the sum of activity in bone and marrow within the ROI was used The actual marrow uptake may thus be somewhat lower

The purpose of this manuscript is to describe dose calculations for diagnostic imaging procedures and to derive an estimation of the absorbed dose in *normal* tissue. At surgery several tissue specimens of tumor and liver were taken and activity was measured. These data were previously published *(3)*. Total tumor uptake was 2%-5% of the injected activity at maximum. In this study, we did not include tumor dose calculations, due to a lack of exact knowledge of tumor mass, shape and location in the body. Moreover, in the MIRDOSE2 program we used, only a restricted selection of source organs can be used as input.

In the literature, many studies report on the scintigraphic use of MAbs to detect ovarian cancer. However, few reports provide data on the quantitative uptake of the radiolabeled immunoconjugate in liver, spleen, kidneys etc. Harwood et al. used ^{111}In-labeled B72.3 MAb which reacts with different tumors, including ovarian tumors. In their study, uptake calculations for the liver were 32.1% ID, the spleen 3.9% ID, the kidneys 3.5% ID, and the lumbar spine marrow 2.7% ID *(24)*. Uptake in the total red bone marrow can be calculated from extrapolation as 32% ID *(13)*. Compared to our data, liver and red bone marrow uptake was higher, spleen uptake the same and kidney uptake was lower. However they used an intact MAb, while we studied a $F(ab')_2$ fragment. Beatty et al. *(25,26)* studied the uptake of ^{111}In-labeled CEA MAb (Indacea) by measuring tissue samples. In two publications, within an interval of 4 y, they reported a liver uptake of 22.1% ± 3.2% and 20.3% ± 1.7% ID/kg, respectively. For a mean liver weight of 1500 g, there was a total liver uptake of 33% and 30% ID, respectively, which is higher than the liver uptake found in our study. Hnatowich *(22)*, who used the ROI method on scintigraphic images, found a mean liver uptake of 20% ± 8% ID at 24 h after injection of ^{111}In-labeled MAb (19-9) $F(ab')_2$ fragment. This is similar to our results, giving a mean liver uptake of 18% ± 5% ID (Table 1).

For the calculation of activity residence time in the organs, we assumed that the uptake at time 0 equals the measured uptake at 4 h postinjection. Early images at 10-30 min after injection were made in a few patients. The calculated uptake was similar to the uptake measured at 4 h postinjection in these patients. Therefore, the assumption seems to be valid. Moreover this assumption has only little effect on the calculated absorbed dose, due to the relatively long physical half-life of ^{111}In and the slow biological disappearance of the activity from the organs.

For dose calculations, the most recent available version (January 1988) of the MIRDOSE2 computer program was used *(27,28)*. In all patients, measurement of activity in blood samples at many time points was available. Regrettably, the program does not yet allow inclusion of the blood compartment as a separate source organ. The application of S-factors for 15-y old individuals to adult women may result in a slight overestimation of the calculated absorbed doses in the organs and the total body. Also the assumption, that there is only physical decay for the time period after 96 h postinjection may give an overestimation for

the absorbed dose in the organs This assumption seems reasonable, because for all organs except the kidneys uptake is constant over time However, data for the kidneys suggest a biological disappearance of activity between 48 and 96 h postinjection If this decrease is representative for the period after 96 h postinjection the absorbed dose to the kidneys is overestimated by 10% 15%

From the literature, very little data on absorbed dose to organs after administration of ^{111}In-labeled MAbs are available Taylor *(29)* and Macey *(30)* reported data on the MAb ^{111}In-ZME-018 The absorbed dose in the liver, spleen, kidneys and bone marrow after administration of 2 5 mg MAb was 0 6, 1 5, 0 7 and 0 2 mGy/MBq, respectively *(29)* The whole body dose was 0 13 mGy/MBq We could derive a whole body dose from our data, 0 17 mGy/MBq Our data for liver and spleen are similar with their data, while their values for the kidneys and the bone marrow are lower However, they have only limited data on bone marrow dosimetry *(29)* Fairweather *(31)* used ^{111}In-CEA and found a whole body dose of 0 135 mGy/MBq and a liver dose of 0 783 mGy/MBq These numbers are similar to our results

We calculated the EDE according to the method used in ICRP Publication 53 using the same weighting factors for adults *(16)*, which makes it easy to compare the radiation burden of the MAb described in this study with that of other radiopharmaceuticals commonly used in nuclear medicine procedures The EDE was 0 40 mSv/MBq which was more than the 0 23 mSv/MBq for ^{201}Tl-chloride and 0 12 mSv/MBq for ^{67}Ga-citrate, two radiopharmaceuticals often used for tumor detection *(16)* For a typical 75 MBq dose of ^{201}Tl-chloride, the EDE is 17 mSv, for a typical 185 MBq dose of ^{67}Ga-citrate the EDE is 22 mSv whereas for a 140 MBq dose of ^{111}In-OV-TL3 $(Fab')_2$, the EDE is 56 mSv

With respect to the therapeutic use of MAbs, several problems need to be solved The present chelators used to label MAbs with metallic radionuclides like ^{111}In and ^{90}Y do not provide optimal stability of the radio immunoconjugate *(32,33)* thus causing a relatively high uptake of activity in liver and bone (marrow) with a correspondingly high radiation burden Furthermore, suboptimal chelate stability impairs the use of ^{111}In-labeled antibodies in predicting the effect of therapy with ^{90}Y-labeled MAbs

ACKNOWLEDGEMENTS

The authors thank Mrs Evelyn Watson for her critical review of the manuscript, H Beekhuis for his advice in revising the manuscript, and E Koenders for technical assistance

REFERENCES

1 Larson SM. Clinical radioimmuno detection, 1978-1988: overview and suggestions for standardization of clinical trials. *Cancer Res* 1990, 50 (suppl).892s-898s.

2. Massuger LFAG, Kenemans P, Claessens RAMJ, et al. Immunoscintigraphy of ovarian cancer with indium-111-labeled OV-TL3 F(ab')$_2$ monoclonal antibody. *J Nucl Med* 1990, 31 1802-1810

3. Massuger LFAG, Claessens RAMJ, Kenemans P, et al Kinetics and biodistribution in relation to tumour detection with ^{111}In-labelled OV-TL3 F(ab')$_2$ in patients with ovarian cancer. *Nucl Med Commun* 1991; 12:593-609

4. Thomas SR, Maxon I HR, and Kereiakes JG. In vivo quantitaion of lesion radioactivity using external counting methods. *Med Phys* 1976; 3:253-255

5 Fleming JS A technique for the absolute measurement of activity using a gamma camera and computer. *Phys Med Biol* 1979; 24 176-180

6. Beekhuis H, Nieweg OM Radiation absorbed doses from Co-57-and Co-55 bleomycin *J Nucl Med* 1984; 25:478-485.

7 Reenen O van, Lotter MG, Heyns A, et al Quantification of the distribution of ^{111}In-labeled platelets in organs. *Eur J Nucl Med* 1982,7 80-84.

8 Hammond ND, Moldofsky PJ, Beardsley MR, et al. External imaging techniques for quantitation of distribution of I-131 F(ab')$_2$ fragments of monoclonal antibody in humans. *Med Phys* 1984, 11 778-783

9 Eary JF, Appelbaum FL, Durack L, et al Preliminary validation of the opposing view method for quantitative gamma camera imaging. *Med Phys* 1989; 16:382-387

10. Gainey MA, Siegel JA, Smergel M, et al. Indium-111-labeled white blood cells dosimetry in children *J Nucl Med* 1988, 29.689-694.

11. Moldofsky PJ, Powe J, Hammond ND. Monoclonal antibodies for radioimmunoimaging: current perspectives *Nucl Med Ann* 1986; 57-103.

12 Rensburg AJ, Lotter MG, Heyns AP, et al An evaluation of four methods of ^{111}In planar image quantification *Med Phys* 1988, 15.853-861

13 ICRP Publication 23, Report of the task group on reference man, Oxford, Pergamon Press, 1975.

14 Loevinger R, Berman M A revised scheme for calculating the absorbed dose from biologically distributed radionuclides, *MIRD Pamphlet No 1, revised* New York, Society of Nuclear Medicine; 1975

15 Vargo GJ Software review: MIRDOSE, revision 2, Watson EE, Stabin M and Bolch WE, Oak Ridge Associated Universities (ORAU), Oak Ridge, TN. *Health Physics* 1989, 57:764

16 ICRP publication 53 *Radiation dose to patients from radiopharmaceuticals* Oxford: Pergamon Press, 1988

17 Wu RK, Siegel JA. Absolute quantitation of radioactivity using the buildup factor. *Med Phys* 1984, 11 189-192.

18. Siegel JA, Wu RK, Maurer AH The buildup factor effect of scatter on absolute volume determination. *J Nucl Med* 1985; 26:390-394.

19. Myers MJ, Lavender JP, Oliveira JB, et al. A simplified method of quantitating organ uptake using a gamma camera. *British Journal of Radiology* 1981; 54;1062-1067

20. DeVito RP, Hamill JJ, Treffert JD, et al. Energy weighted acquisition of scintigraphic images using finite spatial filters. *J Nucl Med* 1989; 30 2029-2035.

21. Siegel JA. The effect of source size on the buildup factor calculation of absolute volume. *J Nucl Med* 1985, 26:1319-1322

22. Hnatowich DJ, Griffin TW, Kosciuczyk C, et al. Pharmacokinetics of indium-111-labeled monoclonal antibody in cancer patients. *J Nucl Med* 1985, 26:849-858.

23. Cristy M. Active bone marrow distribution as a function of age in humans. *Phys Med Biol* 1981; 26:389-400.
24. Harwood SJ, Caroll RG, Webster WB, et al. Human biodistribution of ^{111}In-labeled B72.3 monoclonal antibody. *Cancer Res* 1990; 50(suppl):932s-936s.
25. Beatty JD, Duda RB, Williams LE, et al. Preoperative imaging of colectoral carcinoma with ^{111}In-labeled anticarcinoembryonic antigen monoclonal antibody. *Cancer Res* 1986; 46:6494-6502.
26. Beatty JD, Williams LE, Yamauchi D, et al. Presurgical imaging with indium-labeled anti-carcinoembryonic antigen for colon cancer staging. *Cancer Res* 1990; 59:922s-926s.
27. Cloutier RJ, Watson EE, Rohrer RH, et al. Calculating the radiation dose to an organ. *J Nucl Med* 1973; 14:53-55.
28. Coffey JL, Watson EE. Calculating dose from remaining body activity: a comparison of two methods. *Med Phys* 1979; 6:307-308.
29. Taylor A, Milton W, Eyre H, et al. Radioimmunodetection of human melanoma with indium-111-labeled monoclonal antibody. *J Nucl Med* 1988; 29:329-337.
30. Macey DJ, Denardo SJ, Denardo GL, Goodnight JK, Unger MW. Uptake of indium-111-labeled monoclonal antibody ZME-018 as a function of tumor size in a patient with melanoma. *Am J Physiologic Imaging* 1988; 3:1-6.
31. Fairweather DS, Bradwell AR, Dykes PW, Vaughan AT, Watson-James SF, Chandler S. Improved tumour localisation using indium-111 labelled antibodies. *Brit Med J* 1983; 287:167-170.
32. Goldenberg DM. Future role of radiolabeled monoclonal antibodies in oncological diagnoses and therapy. *Seminars in Nuclear Medicine* 1989; XIX:332-339.
33. Roselli M, Schlom J, Gansow OA, et al. Comparative biodistributions of yttrium- and indium-labeled monoclonal antibody B72.3 in athymic mice bearing human colon carcinoma xenografts. *J Nucl Med* 1989; 30:672-682.

CHAPTER 9

Dosimetric Analysis of Chimeric Monoclonal Antibody cMOv18 IgG in Ovarian Carcinoma Patients after Intraperitoneal and Intravenous Administration

Wilhelmina C A M Buijs, Jacoba Tibben, Otto C Boerman, Carla F M Molthoff, Leon F A G Massuger, Emile B Koenders, Charles P T Schijf, Jeffrey A Siegel, Frans H M Corstens

Eur J Nucl Med 1998, in press

ABSTRACT

In this study the potential of intraperitoneal (i.p.) and intravenous (i.v.) administration of chimeric iodine-131-labeled MOv18 IgG for radioimmunotherapy was determined. The dosimetry associated with both routes of administration of cMOv18 IgG was studied in patients. Eight patients suspected of having ovarian carcinoma, received 150 MBq ^{131}I-cMOv18 IgG i.p. Blood and urine were collected and serial gamma camera images were acquired. Another group of four patients received 7.5 MBq ^{131}I-cMOv18 IgG i.v. For all patients, tissue biopsies were obtained at surgery.

Activity in the blood after i.p. administration was described by a bi-exponential curve with a mean uptake and elimination half-life of 6.9 ± 3.2 h and 160 ± 45 h, respectively. For i.v. infusion the mean half-life for the elimination phase was 103 ± 12 h. Cumulative excretion in the urine was 17% ± 3% ID and 21% ± 7% ID in 96 h for i.p. and i.v. administration, respectively. Scintigraphic images after i.p. administration showed accumulation in ovarian cancer lesions, while all other tissues showed decreasing activity with time. Tumor uptake determined in the ovarian cancer tissue specimens ranged from 3.4% to 12.3% ID/kg for i.p. administration and from 3.6% to 5.4% ID/kg for i.v. administration. Dosimetric analysis of the data indicated that 1.7 - 4.3 mGy/MBq and 1.7 - 2.2 mGy/MBq can be guided to solid or ascites cells after i.p. and i.v. administration, respectively. Assuming that an absorbed dose to the bone marrow of 2 Gy will be dose limiting, a total activity of 4.1 GBq ^{131}I-cMOv18 IgG can be administered safely via the i.p. route and 3.5 GBq via the i.v. route. At this maximal tolerated dose, a maximum absorbed dose to 1-gram tumors in the peritoneal cavity of 18 and 8 Gy can be reached after i.p. and i.v. administration, respectively. For the i.p. route of administration, dose estimates for the tumor are even higher when the electron dose of the peritoneal activity is also taken into account: total doses to the tumor of 30 Gy and 22 Gy will be absorbed at the tumor surface and at 0.2 mm depth, respectively.

In conclusion, therapeutic tumor doses can be achieved with ^{131}I-cMOv18 IgG in patients with intraperitoneal ovarian cancer lesions with no normal organ toxicity. The i.p. route of administration seems to be preferable to i.v. administration.

INTRODUCTION

Radioimmunoscintigraphy (RIS) studies in ovarian cancer patients have demonstrated preferential tumor localization of several radiolabelled anti-tumor monoclonal antibodies (MAbs) in vivo. In RIS studies with iodine-131-labeled murine MOv18 IgG an overall sensitivity of 84% was achieved *(1)*. Also the chimeric form of MOv18 (cMOv18) has been studied extensively in experimental models and in ovarian cancer patients *(2-4)*.

Several studies have focussed on guiding therapeutic doses of radioactivity to ovarian cancer tumors with anti-tumor MAbs *(5,6)*. For therapeutic purposes radiolabelled MAbs can be administered either systemically or locoregionally. After intravenous (i.v.) administration all disseminated tumor lesions can be reached *(7,8)*, while locoregional administration may be favorable in the treatment of diseases which are known to spread locally. Ovarian cancer is a malignancy whose spread initially is confined to the peritoneal cavity *(1)*. In the majority of ovarian cancer radioimmunotherapy (RIT) studies, the radiolabeled antibody has been administered intraperitoneally (i.p.) *(5)*. Dosimetric analysis of biodistribution studies in mice with ovarian cancer xenografts indicated that higher absorbed doses were guided to solid tumor deposits after i.p. administration *(9)*. Several studies in ovarian carcinoma patients indicated that therapeutic responses can be achieved in patients with small tumor deposits after i.p. administration *(5,6)*. Intraperitoneal administration of radiolabelled MAbs may reduce the toxicity to the dose-limiting organ (e.g. bone marrow), allowing the administration of higher doses *(1,9)*.

The aim of the present study was to investigate the dosimetry associated with the i.p. and i.v. administration of radioiodinated cMOv18 IgG in ovarian cancer patients. Because the potential for therapy was a major consideration, the relation between tumor and red marrow dose was analyzed for both the i.p. and the i.v. route of administration *(10,11)*. Special emphasis was given to estimation of the dose to small tumor lesions, because small tumors are considered to be an optimal target for RIT *(12,13)*.

MATERIALS AND METHODS

PATIENTS

Patients suspected of having ovarian cancer who were scheduled to undergo exploratory laparotomy were entered in the study. Patients had to be over the age of 18 years and had to have a life expectancy of at least 3 months. The study was conducted with the approval of the Internal Review Board of the University Hospital Nijmegen or the University Hospital Vrije Universiteit Amsterdam,

The Netherlands. Written informed consent was obtained from each patient prior to study entry.

STUDY DESIGN

Access to the i.p. cavity was obtained by insertion of a Verres needle under local anesthesia. If present, the ascites was withdrawn from the peritoneal cavity prior to infusion. Patients received an i.p. infusion of approximately 1.5 L of normal saline (37° C) followed by a single i.p. infusion of 150 MBq ^{131}I-cMOv18 IgG in 50 mL of saline. Protein doses of 30-80 mg were administered. The thyroid was blocked with 100 mg potassium iodide two times a day and potassium perchlorate 200 mg four times a day orally starting 4 h before the infusion and continuing for 2 weeks. Patient characteristics are summarized in Table 1. For comparison, another group of patients received 7.5 MBq ^{131}I-cMOv18 IgG by i.v. infusion during 2 h *(14)*.

Blood samples were collected just prior to the antibody administration and at various time points until surgery. The biological half-life of disappearance from the blood was calculated using non-linear least square regression analysis. To determine renal excretion, urine was collected in 24 h fractions. All activity data were corrected for physical decay.

After i.p. administration anterior and posterior whole body images were obtained at five different time points. Images were obtained with a dual-headed gamma camera (Type MultiSpect2, Siemens Inc., Hoffman Estates, Ill., USA) equipped with high-energy collimators.

Surgery was performed 6-8 days post infusion in all patients. The tumor status was carefully mapped and examined by histological techniques. Ascites and peritoneal washings were collected. Suspected tissues were either removed or biopsied. If feasible, tissue samples of muscle, skin and normal omentum were obtained. All tissues removed at surgery were weighed and the amount of radioactivity of ^{131}I was measured in a well type gamma counter. The total activity in the whole resected tumor was measured, as well as activity in selected small tumor deposits.

DOSIMETRIC ANALYSIS

Methods consistent with those recommended by the MIRD Committee of the Society of Nuclear Medicine were used to determine the absorbed dose to the normal organs, tumor and the whole body *(15)*. The absorbed doses in organs were expressed as mGy/MBq.

For quantification of activity from gamma camera images after *i.p. administration*, the conjugate view counting technique was used *(16)*. A correction for differences in attenuation between abdomen, thorax and extremities was performed based on transmission scans. After correction for physical decay, the

TABLE I

Patient characteristics

Patient no	MAb (mg)	Age (y)	FIGO stage[a]	Histology[b]	Diff grade
Intraperitoneal administration					
1	15	64	NA	Serous cystadenoma	NA
2	15	46	IIIa	Malignant mixed mullerian tumor	III
3	15	68	Ic	Corpus carcinoma	II
4	30	37	NA	Benign teratoma	NA
5	30	18	NA	Non-Hodgkin lymphoma	NA
6	30	41	NA	Serous cystadenoma	NA
9	50	45	IIIc	Serous cystadenocarcinoma	III
10	80	78	IIc	Endometrioid adenocarcinoma	III
Intravenous administration					
8	30	53	IIIc	Clear cell (coeloma)	II
11	30	45	NA	Benign	–
12	50	43	IIIc	Serous	III
15	75	55	IIIc	Serous	III

NA Not applicable,

a Stage at first diagnosis according to the Federation Internationale de Gynecology et Obstetrique

b Pathological classification of epithelial ovarian carcinoma at first diagnosis grade I, well differentiated carcinoma, grade II, moderately differentiated carcinoma, grade III, poorly differentiated carcinoma

retention of activity in the abdomen, peritoneal cavity or whole body region of interest (ROI) was expressed as a percentage of the injected dose (% ID), setting the initial total body scintigraphic recording as 100% injected dose.

It was assumed that on the first image (1 h post infusion), all activity infused via the i.p. route of administration was localized in the abdomen. During the first 24 h post infusion (p.i.) the intra-abdominal organs were surrounded by activity. During this time virtually no radioactivity had entered the circulation. The count rate data from the ROIs of the abdominal organs, such as liver, spleen and kidney, during this time do not reflect radioactivity uptake, but rather represent the radioactivity surrounding these organs. At later time points no accumulation of radioactivity in the abdominal organs was observed, and it was assumed that the radioactivity in the abdominal organs represented blood perfusion only.

The activity in the peritoneal cavity was estimated, assuming that the activity in the abdomen ROI was partly the result of blood perfusion of the organs in the abdominal region. The fractional blood volume (FBV) in the organs situated in the ROI of the abdomen was estimated from data published in ICRP23 and

TABLE 2

Fractional blood volume for organs and tissue inside the abdominal ROI

	Weight[a] (g)	Blood content[b] (ml/kg)	Fractional blood volume[b]
Liver	1800	139	0.0481
Spleen	180	500	0.0173
Gallbladder wall	11	150	0 00032
Stomach wall	150	150	0 0043
Small intestine wall	640	150	0.0185l
Large intestine wall	370	150	0.0107
Kidneys	310	226	0 0135
Urinary bladder wall	45	150	0 0013
Uterus	80	150	0 0023
Ovaries	11	150	0.00032
Muscle[c]	5600	–	0.0269
Skin[c,d]	470	–	0 018
Trabecular bone[c]	220	25	0 00158
Cortical bone[c]	497	28	0.00268
Marrow[c]	725	127	0 0177
Total fractional blood volume			0.1835

a Data derived from ICRP 23, Table 105 *(17)*

b Data derived from ICRP 53, Table A 2 *(18)*

c For muscle, skin, bone and red marrow a proportionate part of the total organ weight and organ blood content is estimated to be present in the abdomen ROI

d It was assumed that the body surface of the abdominal region was approximately 18% of the total body surface and that the total skin receives 10% of the heart minute volume

ICRP53 *(17,18)*, (Table 2). The blood content of intra-abdominal organs was assumed to be 150 ml/kg tissue in cases when published data were not available. The sum of the FBVs for the abdominal organs was 0.1835 (Table 2). Therefore 20% of the total blood activity was assumed to be present in the abdominal organs. Assuming that no activity was present in the urinary bladder at the time of imaging, the retention of radioactivity in the peritoneal cavity was calculated for each time point according the formula:

$$\textit{Retention in peritoneal cavity (\%ID)} = \textit{\%ID in the ROI of the abdomen} - 0.2 * \textit{total blood activity} - \textit{\%ID in the ROI of the tumor} \quad (1)$$

For each patient, the absorbed dose to the target organs, due to peritoneal cavity activity, was calculated as the product of the residence time (area under the activity-time curve of the peritoneal cavity) and the photon S-values for ^{131}I in the peritoneal cavity as calculated by Watson et al. *(19)*.

The absorbed doses to the target organs due to activity in the whole body minus the peritoneal cavity was calculated using the MIRDOSE3 program *(20)* selecting the anthropomorphic phantom for the "adult female" The urinary bladder, the red marrow, the ovarian tumors and the "rest of the body" were considered as source organs following i p infusion of the MAb The residence time of the "rest of the body was calculated as the residence time of the whole body minus the sum of the residence times of the peritoneal cavity, the red marrow and the ovarian tumors A uniform distribution of the activity in the "rest of the body" was assumed The residence time for the urinary bladder was calculated from the activity excreted in the urine up to 144 h p i , using a voiding interval of 4 h

For each target organ the sum of the MIRDOSE3 doses and the dose due the activity in the peritoneal cavity was calculated

For the i v *route of administration*, the urinary bladder the red marrow and the ' rest of the body ' were considered as source organs The retention in the whole body at 24 and 96 h p i was calculated as the difference between the injected activity and the cumulative urinary excretion at those time points The absorbed organ doses were calculated from the residence times of the source organs pooled for all patients, using the MIRDOSE3 program *(20)*

RED MARROW DOSIMETRY

Since no activity was visualized in the skeleton and/or the bone marrow, it was assumed that blood activity was the primary contributor to the absorbed dose in the red marrow It was also assumed that the marrow activity concentration was 25% of the blood activity concentration *(21)* For an adult female the whole blood and red marrow were assumed to weigh 4100 g and 1120 g, respectively *(17 20)* The residence time of the red marrow could therefore be calculated as 6 8% of the blood residence time In RIT with ^{131}I-labeled MAbs, the maximum amount of activity which can be administered safely is assumed to be the activity dose that results in a 2 Gy dose to the red marrow *(11,22)* The dose to all other tissues was calculated using this maximum amount of activity The absorbed dose to the red marrow was estimated using the adult female phantom in the MIRDOSE3 program *(20)*

EFFECTIVE DOSE

For the i p route of administration the effective dose was calculated from the mean values of 24 normal organ absorbed doses according to the methods given in ICRP60 *(23)* The contributions of both the activity in the peritoneal cavity and the activity in "the whole body minus the peritoneal cavity" to the organ doses were included For the i v route of administration the effective dose was calculated using the MIRDOSE3 program

TUMOR DOSE

Three different contributions to the absorbed dose in the tumors were included: penetrating radiation due to activity in the whole body, non-penetrating radiation due to activity in tumor tissue as measured ex vivo and, for the i.p. route, the electron dose due to the peritoneal cavity wall.

Due to the similarity in location and size, the ovaries were selected as the surrogate for the intraperitoneal tumors for dose estimates due to penetrating radiation. The total tumor absorbed dose from penetrating radiation was calculated as the sum of the dose from activity in the peritoneal cavity and the absorbed dose from the activity outside the peritoneal cavity as calculated with MIRDOSE3 *(20)*.

The accumulated activity in the tumor was estimated from an ROI around the tumor in the last imaging study before surgery, using the partial background correction method as described previously *(24)*. This uptake was compared with the estimated activity as measured ex vivo. It was assumed that the amount of activity in the tumor was acquired instantaneously and remained constant. Because RIT will most likely be applied after debulking surgery *(12,13)*, it is important to estimate whether residual small tumor lesions can receive therapeutic doses. Therefore, for three patients the calculated activity in large tumors, expressed as % ID/g, following i.p. administration of ^{131}I-cMOv18 IgG, was assigned to tumors of 1 g. For the 1-g tumors the absorbed dose due to self-absorption of the non-penetrating beta radiation, was calculated as the product of the residence time and the S-factor for a 1-g sphere (being 2.95E-02 mGy/MBq sec for ^{131}I) *(25)*, using the nodule module option of the MIRDOSE3 program (20).

The absorbed dose in 1-g tumors due to activity in the *peritoneal cavity fluid* was calculated as if the tumors were localized on the inner surface of the peritoneal cavity wall *(12)*. The peritoneal cavity wall was used as the surrogate for the small tumors for electron dose estimates due to activity in the peritoneal cavity fluid. The estimated dose in the tumors due to beta radiation from activity in the peritoneal cavity was calculated by multiplication of the dose rate factors for various distances from the peritoneal cavity into the cavity wall with the mean residence time of the activity in the peritoneal cavity fluid. A volume-distributed source in the peritoneal cavity was assumed, since prior to the i.p. administration of ^{131}I-cMOv18 IgG, a volume of approximately 1.5 liter of saline was infused into the peritoneal cavity *(19)*.

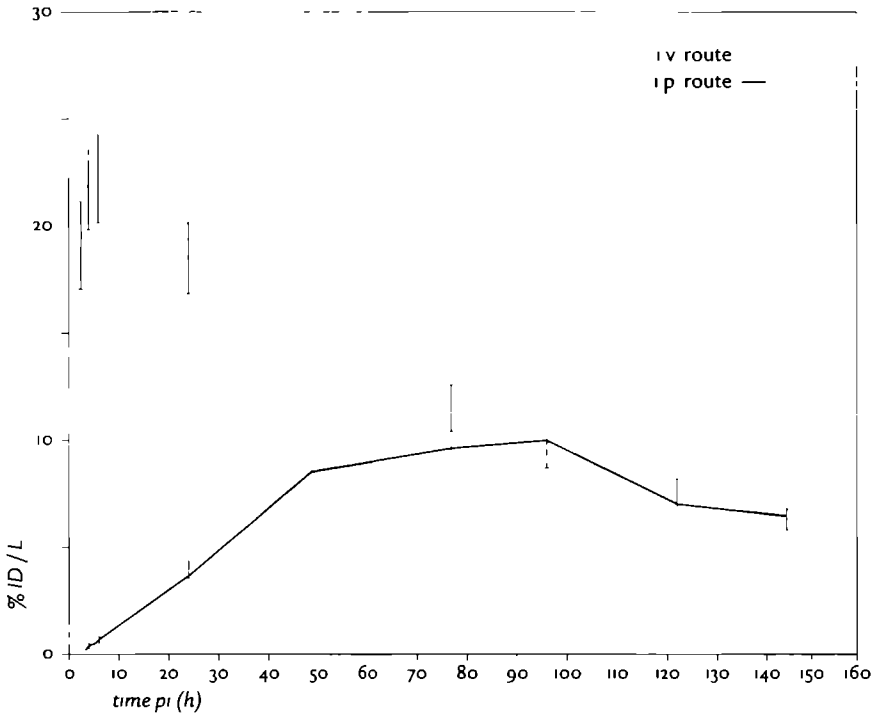

Figure 1 *Activity-time curve for the blood after i p (n=8) and i v infusion (n=4) of ^{131}I-cMOv18 IgG in patients suspected of having ovarian cancer Mean values in % ID/L Error bars indicate SEM*

RESULTS

PHARMACOKINETICS

The concentration of radioactivity in the blood (% ID/L) was not affected by the administered protein dose, therefore, the blood clearance data from all patients of each route of administration were pooled. The mean blood time-activity curves are shown in Figure 1. For the i.p. route, the peak blood activity concentration was reached between 48 and 96 h p.i and averaged 10% ± 2% ID/L. Radioactivity in the blood was described by a bi-exponential curve with a mean half-life of 6.9 ± 3.2 h p.i. for the accumulation phase and a mean half-life of 160 ± 45 h for the elimination phase. For i.v. infusion, the blood data were described by a bi-exponential curve with a biological half-life for the elimination phase of 103 ± 12 h. The peak blood concentration, 23 ± 6% ID/L, was reached at 3.0 ± 0.4 h p.i.

For both routes of administration the radioactivity appeared in the urine gradually. Maximum excretion was observed shortly after the maximum blood concentration had occurred. At 96 h after injection, the mean cumulative excretion

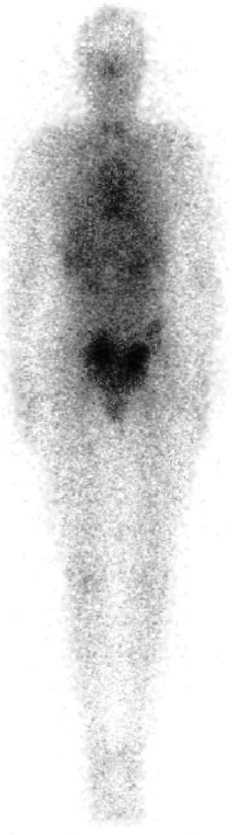

Figure 2. ↑ *Anterior planar image at 1 h p.i. showing the distribution of the radio-immunoconjugate through the peritoneal cavity*

Figure 3. → *Anterior planar image at 144 h p.i. of a patient with a serous adenocarcinoma of both ovaries showing elevated tumor uptake*

of the radiolabel in the urine was 17% ± 3% ID and 21% ± 7% ID for i.p. and i.v. administration, respectively. For the i.v. route, the mean half-life for elimination of activity from the whole body was 309 h, based on the mean excretion of activity in the urine.

RADIOIMMUNOSCINTIGRAPHY

Eight patients were imaged after i.p. administration of ^{131}I-cMOv18 IgG. Histological data of the tumors removed at surgery are summarized in Table 1. Three patients had an epithelial ovarian cancer (nos. 2, 9 and 10), two patients were diagnosed as having a non-ovarian malignancy (nos. 3 and 5) and the remaining three patients had benign gynecological tumors.

Immediately after intraperitoneal activity infusion, the estimated activity within the abdominal region was only 80% of the activity in the whole body ROI. This is probably due to scattered radiation and penetration of the high energy photons through the lead septa of the high-energy collimator. Therefore, the count rate in the abdomen ROI at the first image was set equal to 100% ID, while on subsequent images, the count rate within the abdomen ROI was divided by a factor of 0.8 in order to correct for scatter and collimator penetration.

In all patients, the radioimmunoconjugate diffused throughout the peritoneal cavity as observed on the 1-h p.i. images (Figure 2). Up until 24 h p.i., the radioactivity was confined to the peritoneal cavity. At later time points the radioactivity appeared in the circulation. All ovarian carcinoma lesions that were found at surgery were visualized in the three patients having epithelial ovarian cancer. A typical example of such an image is shown in Fig. 3. None of the benign ovarian tumors (n=3) showed elevated uptake. In addition, no elevated uptake was seen in the patient with an endometrium corpus carcinoma or the patient with a non-Hodgkin's lymphoma. After the radioimmunoconjugate had reached its maximum blood level, no retention of activity was seen in normal organs such as liver, kidneys or bone marrow.

TUMOR UPTAKE

After i.p. administration the uptake in the tumor deposits in the three patients having malignant ovarian cancer, as measured ex vivo, ranged from 3.4% to 12.3% ID/kg, corresponding with a total uptake in the resected tumors of 3.3%, 2.8% and 1.8% ID. From gamma camera images the uptake in these tumors was estimated as 3.0%, 3.1% and 2.6% ID. The uptake in benign tumors ranged from 0.5 to 1.8% ID/kg. Uptake in non-ovarian malignancies varied from 0.1% to 2.1% ID/kg. Mean uptake in muscle tissue was 1.4% ± 0.5% ID/kg. The tumor-to-muscle ratios ranged from 3 to 8 in patients with malignant ovarian tumors, whereas in the patients with benign tumors this ratio varied from 0.1 to 1.3. In the patients with a non-ovarian malignancy the tumor-to-muscle ratios ranged from 0.1 to 2.6.

For the i.v. route of administration the uptake in malignant ovarian tumor deposits ranged from 3.6% to 5.4% ID/kg. The tumor-to-non-tumor ratio ranged from 1.3 to 2.7.

ORGAN DOSES

The retention of activity in whole body, the abdomen and the peritoneal cavity for the i.p. route of administration are summarized in Table 3. Mean whole body retention was 63% ± 7 % ID at 144 h p.i. The whole-body biological half-life ranged from 104 to 590 h. The retention of activity in the peritoneal cavity was 20% ± 4% ID after 144 h p.i. The residence times of the urinary bladder and the "rest of the body" were 0.44 ± 0.16 and 80 ± 22 h, respectively. The absorbed doses for the target organs ranged from 0.35 mSv/MBq for the lungs to 1.59 mGy/MBq for the pancreas (Table 4). The contribution of the activity in the peritoneal cavity to the total absorbed doses in the abdominal organs ranged from 39% to 82% (Table 4). The absorbed dose to the target organs after i.v. administration ranged from 0.40 mSv/MBq for the skin to 0.57 mSv/MBq for the red marrow. The absorbed dose to the lungs was 0.49 mSv/MBq.

TABLE 3

Retention in whole body, abdomen and peritoneal cavity based on ROI measurements after i p administration

Time p i. (h)	No. of patients	Retention [a]		
		Total body	Abdomen	Peritoneal cavity
1	8	100	100±0	99±2
24	7	94±4	86±10	80±13
48	6	91±6	60±11	50±13
72	5	84±4	45±5	35±3
120	7	71±10	33±5	24±6
144	6	63±7	29±3	20±4

a Expressed as percentage of the whole body activity directly after i p injection (%ID)
Mean values ± s d

TABLE 4

Absorbed dose in target organs from activity in the peritoneal cavity and in the 'whole body minus peritoneal cavity' after i p administration

Organ	Dose due to activity in the peritoneal cavity (mGy/MBq)	Dose due to activity in 'whole body minus peritoneal cavity' (mGy/MBq)	Total absorbed dose (mGy/MBq)	Peritoneal contribution (%)
Adrenals	0 45±0 06	0.28±0 07	0 73±0.08	62±7
Small intestine	0 54±0.07	0.32±0.11	0 85±0.1	64±9
Stomach	0 33±0.05	0.27±0 07	0.61±0.07	55±7
Colon	0.31±0.04	0.33±0 12	0.63±0.1	50±9
Kidneys	0 36±0 05	0.27±0 06	0 63±0 07	58±7
Liver	0 30±0 04	0.27±0 06	0 57±0.07	53±7
Lungs	0.09±0.01	0.26±0 05	0.35±0.05	26±5
Ovaries [a]	0.36±0.05	0.29±0 06	0.65±0.07	55±6
Pancreas	1 31±0.16	0.28±0 06	1.59±0.17	82±4
Red marrow	0.16±0.02	0.33±0 07	0 49±0.04	32±4
Bone surfaces	0 09±0.01	0.28±0 07	0.37±0.07	25±5
Spleen	0.20±0.03	0.27±0.06	0.46±0.06	43±7
Urinary bladder	0 23±0 03	0.38±0.11	0.61±0.10	39±9

a With respect to dosimetry ovaries were used as the surrogate for tumors Only absorbed dose to the ovaries due to penetrating radiation is presented The mean absorbed dose to the ovaries is derived from the five patients having no malignant tumor For all other organs the contribution of activity in the tumor to the absorbed dose is included The absorbed dose to these organs is averaged over eight patients

RED MARROW DOSE

The mean residence time for the red marrow based on the pooled blood activity-time data was 3 05 h after 1 p administration of ^{131}I-cMOv18 IgG The mean absorbed dose in the red marrow was 0 49 ± 0 04 mGy/MBq The contribution from the activity in the peritoneal cavity to the total red marrow dose was 32% (Table 4) Assuming that an absorbed dose of 2 Gy in the red marrow is the maximum dose that will not induce grade 4 toxicity (MTD), 4 1 GBq of ^{131}I-cMOv18 IgG could be administered safely

For 1 v administration, the absorbed dose in the red marrow based on the pooled blood activity-time data was 0 57 mGy/MBq, and thus for this route of administration a maximal tolerable dose of 3 5 GBq ^{131}I-cMOv18 IgG was estimated

EFFECTIVE DOSE

Following 1 p administration, the effective dose, based on the mean organ doses, was 0 55 mSv/MBq, resulting in an effective dose of 82 mSv for the 150 MBq ^{131}I-cMOv18 IgG administered in this study For the 1 v route of administration the effective dose was 0 52 mSv/MBq, resulting in an effective dose of 3 9 mSv after administration of 7 5 MBq ^{131}I-cMOv18 IgG

TUMOR DOSE

For the 1 p route of administration the tumor absorbed dose due to penetrating radiation was 0 65 ± 0 07 mGy/MBq (Table 4) For 1 v administration the tumor absorbed dose due to activity in the whole body was 0 57 mSv/MBq Thus, the additional dose to the tumor due to penetrating radiation after 1 p administration of 4 1 GBq of ^{131}I-cMOv18 IgG will be 2 7 Gy, while the additional dose to the tumor following 1 v administration of 3 5 GBq of ^{131}I-cMOv18 IgG will be 1 9 Gy

For 1 p administration, the residence time of the large tumors, as measured ex vivo, ranged from 9 4 to 34 0 h/kg, and thus from 0 0094 to 0 034 h for 1-g tumors The absorbed doses to 1-g lesions due to non-penetrating radiation ranged from 1 0 to 3 6 mGy/MBq For an administered activity of 4 1 GBq a maximum of 15 Gy could be delivered to these tumor lesions due to self-absorption of the beta radiation For the 1 v route, the residence time for large tumors ranged from 10 to 15 h/kg, based on an initial uptake varying from 3 6% to 5 4% ID/kg The absorbed dose to the 1-g tumors ranged from 1 1 to 1 6 mGy/MBq, due to self-absorption Therefore, 3 5 GBq ^{131}I-cMOv18 IgG administered intravenously would result in a maximum absorbed dose of 5 6 Gy to these tumors for self-absorption only

The dose rate from *electrons* emitted by the activity present in the peritoneal cavity surrounding the tumor ranged from 3 0 ± 0 4 mGy/MBq at the tumor

TABLE 5

Electron doses in the tumor wall from volume distributed sources of ^{131}I after i.p. administration

Distance from peritoneal cavity into peritonial cavity wall[a] (cm)	Volume source electron dose (mGy-g/MBq-s)	Dose rate for volume 1500 g[b] (mGy/MBq)	Absorbed dose for 4 1 GBq (Gy)
0.000	0.015	3 00	12.3
0.001	0 014	2 80	11 4
0.003	0 011	2 20	9.0
0.006	0.009	1.80	7.4
0.018	0.005	1 00	4 1
0.030	0 0028	0 56	2 3
0.050	0 00105	0.21	0.86
0.080	0.00015	0.03	0.12

a Data in columns 1 and 2 were derived from Watson et al *(19)*

b For each distance, data in column 3 were calculated using the formula
(data column 2) * (mean residence time for peritoneal cavity. 83 3 h) * (3600 [s/h]) / (1500 [g])

surface to 1.0 ± 0.1 mGy/MBq at a distance of 0.2 mm from peritoneal cavity into the tumor. At a distance of 1 mm from the peritoneal cavity into the tumor the dose rate was less than 0.03 mGy/MBq (Table 5). For an administered activity of 4.1 GBq ^{131}I-cMOv18 IgG via the i.p. route, the absorbed electron dose ranged from 12.3 Gy at the tumor surface to 4.1 Gy at a distance of 0.2 mm from the intraperitoneal cavity into the tumor.

The total dose to the tumor was calculated as the sum of the dose from penetrating radiation and non-penetrating radiation in the tumor due to self-absorption of the activity in the tumor itself. For the i.p. route of administration the total dose ranged from 1.7 - 4.3 mGy/MBq. For the i.v. route of administration this range was 1.7 to 2.2 mGy/MBq. At MTD (4.1 GBq i.p.) a maximum dose of 18 Gy could be delivered to the tumor. If the electron dose to the tumor from peritoneal activity is also taken into account, a total absorbed dose of 30 Gy can be reached at the tumor surface and a dose of 22 Gy at 0.2 mm depth.

For the i.v. route of administration a maximum absorbed dose of 8 Gy could be delivered to the tumor after injection of 3.5 GBq ^{131}I-cMOv18 IgG.

DISCUSSION

The aim of the present study was to investigate the dosimetry associated with the i p and i v administration of radioiodinated cMOv18 IgG in ovarian cancer patients

PHARMACOKINETICS AND BIODISTRIBUTION

Planar images showed good distribution throughout the peritoneal cavity in all patients following i p administration of ^{131}I-cMOv18 IgG

The mean whole-body retention measured 84% and 80% ID at 96 h p i after i p and i v injection, respectively Crippa et al reported a much faster whole-body excretion of the murine MOv18 MAb after i p administration 20% ID was present in the whole body at 96 h p i *(1)* Crippa et al used a 1-mg protein dose, while in the present study 15-80 mg was administered This suggests that at very low protein doses the whole-body clearance may be enhanced We have observed this same phenomenon with the cG250 antibody This antibody also cleared faster when 2 mg was administered as a protein dose as compared to doses ≥ 5 mg *(26)* Immunohistological studies in experimental tumor models have shown that higher protein doses of antibody may enhance the tumor penetration Therefore, unless antigen saturation occurs, high protein doses may be more optimal for RIT *(12)*

TUMOR UPTAKE

Comparison of tumor uptake derived from gamma camera images and uptake determined ex vivo after i p administration showed an excellent correlation in three patients an uptake of 3 0%, 3 1% and 2 6% ID was derived from gamma camera ROIs, while the ex-vivo measurements of these tumors indicated an uptake of 3 3%, 2 8% and 1 8% ID, respectively

TUMOR DOSIMETRY

After completing the course of chemotherapy, ovarian cancer patients may undergo second-look laparotomy (SLL) to assess their disease status Persistent disease diagnosed by SLL has been observed in 45%-80% of patients with advanced disease *(27)* However, negative findings at SLL are not a definitive sign of tumor eradication Within 5 years, 24% of the patients with a negative SLL presented recurrent disease *(28)* In these situations small tumors or metastases may be present in the peritoneal cavity, on the peritoneal cavity wall or in the small intestine Therefore, for the i p route of administration, special attention was given to estimate the absorbed dose to small tumors *(12,13)*

The absorbed dose estimations were based on the assumptions that the tumor uptake level and the tumor residence time per gram tissue in small tumor

deposits will be the same as in large tumors. This is a conservative approximation: several studies have shown that antibody uptake is higher in small tumors *(12,13,29)*. Comparing tumors of different sizes (e.g. 1 - 1000 g), but with equal uptake of activity (^{131}I) per gram, the dose to small tumors will be 25% lower than that to large tumors, due to a higher self-absorption of photon energy in the large tumors *(25)*. Moreover, in micrometastases with clusters of tumor cells (10 μm radius spheres) part of the beta-energy from activity in the tumor will not be absorbed in the small spheres, resulting in lower doses, depending on the radionuclide used *(12,25)*. However, cross-radiation from the beta radiation emitted by the activity in the peritoneal cavity after i.p. administration of ^{131}I-cMOv18 IgG may increase the absorbed dose in these small tumors.

In the present study, the absorbed dose in the tumors varied from 1.7 to 4.3 and 1.7 to 2.2 mGy/MBq after i.p. and i.v. administration, respectively. This is in the same range as was reported by Behr et al (2-4 mGy/MBq) after i.v. administration of ^{131}I-labeled IgG anti-CEA antibodies in CEA-expressing cancers *(10)*. For the i.p. route of administration the tumor dose may be enhanced with 3 mGy/MBq at the tumor surface and 1 mGy/MBq at 0.2 mm depth in the tumors, due to the electron dose from activity in the peritoneal cavity *(19)*. Thus, including the electron dose due to activity in the peritoneal cavity in the dose estimates, absorbed doses of 30 and 22 Gy can be reached at the tumor surface and at 0.2 mm depth in the tumor, respectively.

INTRAPERITONEAL VERSUS INTRAVENOUS ADMINISTRATION.

The area under the blood-activity time curve from time of administration to time of surgery (AUC, biological) was estimated as 10 and 21 h/L for the i.p. route and the i.v. route, respectively. If MAb blood level were the driving force for antibody accumulation in tumors, the tumor uptake would be expected to be at least as high or even a factor of 2 higher after i.v. administration than after i.p. administration. However, such a relation was not found in our study: the uptake in ovarian carcinoma tumors, measured ex vivo, ranged from 3.4% to 12.3% ID/kg and from 3.6% to 5.4 % ID/kg for the i.p. and i.v. routes of administration, respectively. The tumor uptake data in the current study are in accordance with findings of previous clinical studies reporting higher tumor uptake after i.p. administration as compared to i.v. injection *(1,9)*. Crippa et al. *(1)* also found a more favorable biodistribution after i.p. administration of murine ^{131}I-MOv18 than after i.v. administration. These data suggest that possibly direct tumor uptake after i.p. administration (non-systemic supply) causes the major part of the uptake of the antibody in the tumor. Another main advantage of locoregional administration is the reduced uptake in normal tissues, e.g. lungs and red marrow. In this study, the mean estimated radiation doses to the lungs were 0.35 and 0.49 mGy/MBq after i.p. administration and i.v. administration, respecti-

vely For the red marrow the absorbed doses were 0 49 and 0 57 mGy/MBq, respectively In addition, in the case of RIT the relatively long retention in the peritoneal cavity may result in an increased absorbed dose to small tumor nodules on the peritoneal wall and on the intestine due to the prolonged bathing in a radiolabelled MAb fluid

In general, the accuracy of tumor dose calculations is limited due to factors such as assumption of uniform distribution of activity throughout a tumor and the inaccurate assumption of initial uptake *(30)* In the current study it was assumed that the activity in the tumor, found at surgery, was instantaneously present at the time of administration *(31)* Only physical decay was considered For the i p route of administration the count rate in the tumor ROI on the gamma camera images increased during the first 24-48 h after injection and was stable on later images Thus, the assumption of initial uptake in the tumor may have lead to a minor overestimation of the absorbed dose Such an overestimation may be counteracted by a likely increase of activity in the period after 7 days p i if no surgery would be performed

In summary, the data from this study suggest that the i p route of administration is preferable to the i v route

USE OF TRACER DOSE IMAGES TO PREDICT THERAPY DOSES

Tumor uptake and, consequently, the absorbed dose to the tumor seem to vary considerably between patients *(10,11,31)* Based on the dosimetric analysis of the data obtained after i p injection of ^{131}I-labeled B72 3 IgG in ten patients with adenocarcinoma, Larson et al recommended that the absorbed dose should be estimated on an individual basis using a diagnostic dose in order to determine the efficacy of a therapeutic dose *(31)* Other authors have confirmed the necessity of this approach *(32-35)* Haematopoietic toxicity is usually the dose-limiting factor in RIT *(21,31,35,36)* For bone marrow, 2 Gy is considered to be the maximum tolerated dose *(31)* Our calculations indicate that the absorbed dose to the marrow will amount to an MTD of 2 Gy, after administration of 4 1 or 3 5 GBq for i p and i v administration, respectively Extrapolating the dosimetric data of the tumors measured ex-vivo in the current study, the maximum absorbed dose to 1-g tumor deposits was estimated to be 18 Gy at a 4 1 GBq dose for the i p route and 8 Gy at a 3 5 GBq dose for the i v route of administration After i p administration of 4 1 GBq, an additional dose of 12 and 4 Gy can be absorbed at the tumor surface and at a depth of 0 2 mm, respectively

An absorbed dose of 20 Gy is considered a tumor-sterilizing level for tumors with a diameter of 0 3 mm *(12)*, and thus ^{131}I-cMov18-IgG could potentially induce therapeutic response, especially upon i p administration

In clinical patient management it is usually impractical to collect data for blood, urine and tissue uptake for more than a few days The calculation of the

residence times in the organs or tumors was therefore based on the limited data for uptake of activity in the organs during the sampling period, which will result in inaccurate estimates of the absorbed dose. If the sampling period is less than or equal to the effective half-life of the radiopharmaceutical, the error in the estimated dose may exceed 100%. To reduce these errors, application of physical, biological or mathematical models for the activity-time curves *(37,38)* and use of special computer programs *(39)* may be helpful, permitting more accurate determination of the residence times and absorbed doses.

CONCLUSION

The concept of targeting radiolabelled antibodies towards tumor cells remains an attractive therapy concept for ovarian cancer patients. The i.p. route of administration seems to be preferable to i.v. administration: tumor uptake is at least as high after i.p. administration while haematopoietic toxicity is reduced. Chimeric MOv18 IgG seems to offer a therapeutic advantage particularly in patients with small tumor deposits.

ACKNOWLEDGMENTS

We are grateful to Dr. K.G.G. Keijser, gynecologist, and the nursery staff of the Gynecology ward for their excellent care of the participating patients.

We would like to thank A. Meeuwis, D.J. Immerzeel and P. Kok for imaging.

REFERENCES

1 Crippa F, Buraggi GL, Di Re E, et al Radioimmunoscintigraphy of ovarian cancer with the MOv18 monoclonal antibody *Eur J Cancer* 1991, 27 724-729
2 Molthoff CF, Buist MR Kenemans P Pinedo HM, and Boven E Experimental and clinical analysis of the characteristics of a chimeric monoclonal antibody, MOv18, reactive with an ovarian cancer-associated antigen *J Nucl Med* 1992 33 2000-2005
3 Buist MR, Kenemans P, den Hollander W, Vermorken JB, et al Kinetics and tissue distribution of the radiolabeled chimeric monoclonal antibody MOv18 IgG and $F(ab')_2$ fragments in ovarian carcinoma patients *Cancer Res* 1993, 53 5413-5418
4 Boerman OC, van Niekerk CC Makkink K, Hanselaar AGJM, Kenemans P, Poels LG A comparative immunohistochemical study of four monoclonal antibodies directed against ovarian carcinoma-associated antigens *Int J Gynaecol Pathol* 1991, 10 15 25
5 Epenetos AA, Munro AJ, Stewart S, et al Antibody-guided irradiation of advanced ovarian cancer with intraperitoneally administered radiolabeled monoclonal antibodies *J Clin Oncol* 1987, 5 1890-1899
6 Stewart JSW, Hird V, Snook D, et al Intraperitoneal yttrium-90-labeled monoclonal antibody in ovarian cancer *J Clin Oncol* 1990, 8 1941-1950
7 DeNardo DA, DeNardo GL, O'Donell RT, et al Imaging for Improved Prediction of Myelotoxicity after Radioimmunotherapy *Cancer* 1997, 80 2558-2566
8 Eary JF Fundamentals of Radioimmunotherapy *Nucl Med Biol* 1991, 18 105 108
9 Tibben JG, Massuger LFAG, Boerman OC, Borm GF, Claessens RAMJ, Corstens FHM Effect of the route of administration on the biodistribution of radioiodinated OV-TL3 $F(ab')_2$ in experimental ovarian cancer *Eur J Nucl Med* 1994, 21 1183-1190
10 Behr TM, Sharkey RM, Juweid ME et al Variables influencing tumor dosimetry in radioimmunotherapy of CEA-expressing cancers with anti-CEA and antimucin monoclonal antibodies *J Nucl Med* 1997, 38 409-418
11 Siegel JA, Pawlyk DA, Lee RE et al Tumour, red marrow, and organ dosimetry for ^{131}I-labeled anti-carcinoembryonic antigen monoclonal antibody *Cancer Res* 1990, 50 10395-10425
12 Britton KE, Mather SJ and Granowska M Radiolabelled monoclonal antibodies in oncology III Radioimmunotherapy *Nucl Med Comm* 1991, 12 333-347
13 Behr TM, Sharkey RM, Juweid ME, et al Phase I/II clinical radioimmunotherapy with an iodine 131 labeled anti-carcinoembryonic antigen murine monoclonal antibody IgG *J Nucl Med* 1997, 38 858-870
14 Molthoff CFM, Prinssen HM, Kenemans P, van Hof AC, den Hollander W and Verheijen RHM Escalating protein doses of chimeric monoclonal antibody MOv18 Immunoglobulin G in ovarian carcinoma patients a phase I study *Cancer* 1997, 80 2712-2720
15 *MIRD Primer For Absorbed Dose Calculations* Prepared by Robert Loevinger, Thomas F Budinger and Evelyn E Watson The Society of Nuclear Medicine 1988
16 Buijs WCAM, Massuger LFAG Claessens RAMJ, Kenemans P, Corstens FHM Dosimetric evaluation of immunoscintigraphy using indium 111-labeled monoclonal antibody fragments in patients with ovarian cancer *J Nucl Med* 1992, 33 1113-1120
17 ICRP Publication 23 *Report of the task group on reference man* Oxford, Pergamon Press, 1975
18 ICRP Publication 53 *Radiation dose to patients from radiopharmaceuticals* Oxford, Pergamon Press, 1988
19 Watson EE, Stabin MG, Davis JL, Eckerman KF A model of the peritoneal cavity for use in internal dosimetry *J Nucl Med* 1989, 30 2002-2011
20 Stabin MG MIRDOSE Personal computer software for internal dose assessment in nuclear medicine *J Nucl Med* 1996, 37 538-546

21 Siegel JA, Wessels BW, Watson EE, et al Bone marrow dosimetry and toxicity for radioimmunotherapy Antibody Immunoconj Radiopharm 1990, 3 213-233

22 Buijs WCAM, Steffens MG, Boerman OC, Oosterwijk E, Siegel JA, Corstens FHM Estimation of absorbed red marrow dose after administration of 131-I-cG250 *Eur J Nucl Med* 1997, 24 868s

23 ICRP Publication 60 *1990 Recommendations of the International Commission on Radiological Protection* Oxford Pergamon Press 1991

24 Buijs WCAM, Siegel JA, Boerman OC, Corstens FHM Absolute Organ Activity Estimates by Five Different Methods of Background Correction *J Nucl Med* 1998, 39 in press

25 Siegel JA, Stabin MG Absorbed fractions for electrons and beta particles in spheres of various sizes *J Nucl Med* 1994, 35 152-156

26 Steffens MG, Boerman OC, Oosterwijk Wakka JC et al Targeting of renal cell carcinoma with iodine-131-labeled chimeric monoclonal antibody G250 *J Clin Oncology* 1997, 15 1529 1537

27 Copeland LJ, Gershenson DM, Wharton JT et al Microscopic disease at second look laparotomy in advanced ovarian cancer *Cancer* 1985, 55 472-478

28 Gershenson DM, Copeland LJ, Wharton JT et al Prognosis of surgically determined complete responders in advanced ovarian cancer *Cancer* 1985, 55 1129-1135

29 Van Hof AC, Molthoff CFM, Davies Q et al Biodistribution of ^{111}In-labeled engineered human antibody CTMO1 in ovarian cancer patients influence of protein dose *Cancer Research* 1996, 56 5179-5185

30 Flower MA, McCready VR Radionuclide therapy dose calculations what accuracy can be achieved? *Eur J Nucl Med* 1997, 24 1462 1464

31 Larson SM, Carrasquillo JA, Colcher DC et al Estimates of radiation absorbed dose for intraperitoneally administered iodine-131 radiolabeled B72 3 monoclonal antibody in patients with peritoneal carcinomatoses *J Nucl Med* 1991 32 1661-1667

32 Juweid M, Sharkey RM, Goldenberg DM Patient specific (PS) estimates of red marrow dose result in improved correlation with myelotoxicity *J Nucl Med* 1998 39 112P

33 Erdi AK, Erdi YE, Yorke ED, Wessels BW Treatment planning for radio-immunotherapy *Phys Med Biol* 1996, 41 2009-2026

34 Kaminski MS, Fig LM, Zasadny-KR et al Imaging, dosimetry and radioimmunotherapy with iodine 131 labeled anti-CD37 antibody in B-cell Lymphoma *J Clin Oncol* 1992, 10 1696 1711

35 Fary JF, Krohn KA, Press OW, Durack L, Bernstein ID Importance of pre treatment radiation absorbed dose estimation for radioimmunotherapy of non-Hodgkin s lymphoma *Nucl Med Biol* 1997 24 635-638

36 Fisher DR Radiation dosimetry for radioimmunotherapy *Cancer* 1994,73 905-911

37 Selikson MH, Jaggi J, Mozley PD, et al A proposal for minimum detectable compartment in MIRD dosimetry modeling *Phys Med Biol* 1997, 42 1605-1617

38 Sgouros G, Graham MC, Divgi CR, Larson SM, Scheinberg DA Modeling and dosimetry of monoclonal antibody M195 (anti-CD33) in acute myelogenous leukemia *J Nucl Med* 1993, 34 422-430

39 Herzog H, Zilken H, Niederbremer A, Friedrich W, Muller-Gartner HW Calculation of residence times and radiation doses using standard PC software Excel *Eur J Nucl Med* 1997, 24 1514-1521

CHAPTER 10

Effective Doses in Nuclear Medicine

The absorbed doses and the effective dose for a nuclear medicine procedure depend on the administered activity, on the age and size of the patient, on the clinical condition and the metabolic state of the patient, on the chemical and biological characteristics of the radiopharmaceutical and on the physical aspects of the radionuclide. With respect to dosimetry, the most important physical aspects are the physical half-life ($T_{1/2}$), and the type of emitted radiations with their associated energy. The physical characteristics of the most frequently used radionuclides are shown in Table 1, including the exposure rate at 1 meter distance of a point source. The biological behaviour and distribution of the radiopharmaceutical in the body is also very important, especially when radio-

TABLE 1

Frequently applied radionuclides in nuclear medicine

Radionuclide	$T_{1/2}$	Photon energy (keV)	β–energy average [a] (keV)	Ambient dose equivalent rate [b] ($\mu Sv\ m^2\ MBq^{-1}\ h^{-1}$)
Diagnostic				
^{18}F	110 min	511	β^+, 245	0 166
^{57}Co	272 d	122	Au	0 023
^{67}Ga	78.2 h	93,185 en 300	Au	0.025
^{81m}Kr	13 s	190	Au	–
^{99m}Tc	6 02 h	141	Au	0 023
^{111}In	2 83 d	171, 241	Au	0 088
^{123}I	13.2 h	159	Au	0 046
^{201}Tl	3.04 d	167, (Ro. 70)	Au	0 018
Therapy				
^{32}P	14 3 d	–	695	Bremsstrahlung [c]
^{90}Y	84 1 h	–	935	Bremsstrahlung
^{89}Sr	50 5 d	–	583	Bremsstrahlung
^{131}I	8.04 d	365	192	0.066
^{186}Re	90 7 h	137, 123	309, 362	0.004

a Au Auger-electrons

b Ambient dose equivalent rate taken from reference *(1)*

c Ambient dose equivalent rate for Bremsstrahlung < 0 001 $\mu Sv\ m^2\ MBq^{-1}.h^{-1}$

TABLE 2

Absorbed dose for diagnostic procedures

Effective dose for adults with normal uptake and excretion

Radiopharmaceutical	Procedure	Recommended activity [a] (MBq)	Effective dose ICRP-62 (mSv/MBq)	Effective dose per procedure (mSv)
F-18-FDG	PET-study	370	0 02	7.4
Co-57-Cyanocobalamine	Schillingtest	0.02	2.1	0.04
Ga-67-Citrate	Detection of infection	185	0.11	20
Kr-81m	Lung ventilation scintigraphy	–	0.001	<0.1
Tc-99m-DMSA	Renal study,	80	0.009	0 72
Tc-99m-DTPA	Renal study	80	0 005	0 4
Tc-99m-Erythrocytes	Gated blood pool study	500	0 007	3 5
Tc-99m-Phosphonates	Bone scintigraphy	500	0 006	3 0
Tc-99m-HIDA	Biliary scintigraphy	40	0 015	0.6
Tc-99m-Leucocytes	Detection of infection	500	0 011	5.5
Tc-99m-MAA	Lung perfusion scintigraphy	100	0.011	1 1
Tc-99m- Pertechnetate	Thyroid scintigraphy	100	0.012	1 2
Tc-99m-MAG3	Renography	100	0.007	0 7
Tc-99m-MIBI	Myocardial perfusion	600	0.009	5 4
In-111-Leucocytes	Detection of infection	30	0.36	11
In-111 Thrombocytes	Thrombocyte kinetics	10	0 39	3 9
I-123-Hippurate	Renography	20	0 012	0 24
I-123-Iodide [b]	Thyroid scintigraphy	20	0.22	4.4
I-123-MIBG	MIBG scintigraphy	300	0.014	4.2
I-131-Iodide [b]	Thyroid uptake	0.2	24	4.8
I-131-MIBG	MIBG scintigraphy	30	0.14	4.2
Tl-201-Chloride	Myocardial perfusion	100	0.23	23

a Administered activity, recommended by the Dutch Society of Nuclear Medicine (NVNG), 1996
b Thyroid uptake 35 %

nuclides with relatively long half-lives are involved. In order to get adequate information to make diagnoses, it may often be necessary to estimate the accumulation of the radiopharmaceutical in a lesion focus during a period of several consecutive days. In these cases radionuclides such as ^{111}In or ^{131}I with relatively longer half-lifes should be used as radiolabel. Unfortunately, these radionuclides have higher gamma energies when compared with the most frequently used radionuclide ^{99m}Tc, resulting in relatively high absorbed doses. Moreover, ^{131}I not only emits γ-radiation, but also β-radiation. The latter will be totally absorbed in the tissue or organ where the radionuclide is concentrated. The activity to be administered is limited: on the one hand the activity should be

as low as possible in order to minimize the absorbed dose (ALARA), on the other hand, because of statistical reasons, a minimal number of counts should be acquired in each view for adequate imaging In Table 2 the recommended activity per procedure, the effective dose per unit of administered activity for each examination and the effective dose per procedure, are shown It is clear that effective doses of various procedures may vary widely from < 0 01 to 23 mSv

The collective effective dose per year, defined as the summation of the product of the effective dose for a certain examination and the yearly number of that examination for all different nuclear medicine diagnostic examinations in the Netherlands, was reported to be 540 man Sievert per year *(2)*, resulting in a yearly effective dose equivalent per capita of 0 037 mSv *(3)* This estimation was based on the number of investigations as performed in 1984 and 1985 Over last 15 years, the yearly number of examinations raised from 200 000 to 250 000 In addition there was a shift to more complex procedures, relatively more cardiac and brain SPECT, PET, and infection detection These studies are often associated with higher absorbed doses per procedure Using the most recently available frequency data for nuclear medicine procedures in the Netherlands *(4)*, the data of the relative frequency of procedures in the United States in this decade *(5)* and the effective doses reported in ICRP 62 *(6)*, a yearly collective dose of 800 man Sievert due to nuclear medicine procedures was estimated for the Netherlands anno 1998, resulting in an average dose of 0 05 mSv/year per capita The average annual absorbed dose per head of the Dutch population, due to all sources of radiation sums up to 2 7 mSv *(7)* Thus the contribution of nuclear medicine procedures to the yearly effective dose is less than 2%

The effective dose for the diagnostic examinations or tracer studies as described in this thesis are as follows

- 19 mSv for 75 MBq ^{111}In-IgG and
  6 mSv for 740 MBq ^{99m}Tc-HYNIC-IgG *(chapter 6)*
- 36 mSv for 140 MBq ^{111}In-OV-TL3 F(ab')$_2$ *(chapter 8)*
- 82 mSv for 150 MBq ^{131}I-cMOv18 IgG via the i p route of administration and
  4 mSv for 7 5 MBq ^{131}I-cMOv18 IgG via the i v route of administration *(chapter 9)*

These data indicate that the radiation dose for these procedures are relatively high when compared to routinely used nuclear medicine procedures However, the contribution to the yearly collective effective dose will be minimal, since these procedures are performed relatively infrequent

REFERENCES

1 Keverling Buisman AS *Handboek Radionuclden* 1996 ISBN 90 75441 02 3 Bergen [N H] Betatext

2 Vaas LH Blaauboer RO and Leenhouts HP Radiation sources, doses and dose distributions in the Netherlands *Radiation Protection Dosimetry* 1991, 36 89-92

3 Beekhuis H Population radiation absorbed dose from nuclear medicine procedures in the Netherlands *Health Physics* 1988, 54 287 291

4 Bakker WH In vivo Nucleaire Geneeskunde in Nederland 1984-1988 *Nucl Geneeskd Bull* 1990, 12 88-98

5 NCRP Report No 124 Sources and magnitude of occupational and public exposures from nuclear medicine procedures *National Council on Radiation Protection and Measurements* 1996, 124 2-8

6 ICRP Publication 62 Radiological Protection in Biomedical Research Includes Addendum 1 to Publication 53- Radiation Dose to Patients from Radiopharmaceuticals Oxford Pergamon Press *Annals of the ICRP* 1991 22 25-28

7 Geleijns J Patient Dosimetry In Diagnostic Radiology *Thesis AZL Leiden* June 13 1995

Summary

In the past few decades, research in nuclear medicine has focussed on the development and application of new radiopharmaceuticals for diagnosis and therapy on the one hand and on improvements of instrumentation on the other hand For example the development of monoclonal antibodies (MAbs) and receptor binding peptides has induced the introduction of new classes of radiopharmaceuticals for diagnosis and therapy of cancer Another major research effort focussed on the development of radiopharmaceuticals for positron imaging

The combination of both new radiopharmaceuticals and the implementation of improved instrumentation, such as for SPECT (Single Photon Emission Tomography) and for PET (Positron Emission Tomography) have led to more adequate diagnostic examinations and to higher quality of medical decision making The highly improved spatial resolution of the imaging systems made it feasible to detect and localize smaller neoplastic lesions and to visualize brain or cardiac pathology more accurately

PET and/or SPECT- images now can be combined with digital MRI- or CT-images thus facilitating matching of metabolic disorders, as visualized by the gamma camera with high resolution anatomic delineation These approaches have enhanced the diagnostic accuracy of the procedures

During the past decade, the research program of the department of Nuclear Medicine of the University Hospital at Nijmegen (AZN) focussed on development and optimization of radiopharmaceuticals for diagnosis and therapy of cancer and for diagnosis of infection and inflammation The radiation risks after administration of these new radiopharmaceuticals to patients have been estimated The second part of this thesis deals with dosimetric calculations for some of these new radiopharmaceuticals

For diagnostic examinations the radiation risks for the patient are undesirable side effects (chapters 6-9) However the radiation risks are low the absorbed dose for a nuclear medicine diagnostic procedure on average is 3 mSv, which is associated with a total health detriment of 2 per 10 000 examinations For therapeutic applications, radiation damage to pathological tissue is the objective, as for example in the treatment of thyroid disease (chapter 5) However, undesired damage to the surrounding tissue should be kept as low as possible To determine whether specific treatment of a tumor or its metastases with radiopharmaceuticals is safe and/or useful, the radiation dose and radiation risks

should be estimated. Preferably this could be carried out based on a tracer study in the patient to be treated. At various time points after administration of the tracer dose of the radiopharmaceutical the distribution of radioactivity in the different organs, the disappearance of activity from the blood, the uptake of activity in the tumor and the disappearance of activity from the body should be estimated. From these kinetic data the absorbed dose in organs, tissues or the tumor can be calculated (chapter 5, 8 and 9). One of the prerequisites on which a decision for treatment is based, is that the potentially therapeutic radiation dose in the tumor (>30 Gy) can be obtained without exceeding a threshold dose for deterministic effects in any organ. In most radionuclide therapies the dose-limiting organ is the red bone marrow.

In *chapter 1* the importance of dosimetric calculations in nuclear medicine is stipulated.

In *chapter 2* the concepts of the methods in dosimetry (terminology, quantities and units) are described. Radiation effects and radiation risks are reviewed.

In *chapter 3* methods for acquisition, analysis and processing of data from biodistribution studies in patients are summarized. These methods allow estimation of the radiation dose. In recent years standardization of the methods and techniques has been introduced by the Medical Internal Radiation Dosimetry Committee of the Society of Nuclear Medicine (MIRD Schema).

In *chapter 4* phantom experiments are described in which the accuracy of the actual activity in a source organ was estimated using different methods for background correction. After administration of the radiopharmaceutical to patients the activity will spread throughout the body. To determine the exact amount of radioactivity in an organ at a particular time point, an adequate correction for background activity in surrounding tissues has to be applied.

A phantom filled with activity and simulating two kidneys in the abdomen was imaged with the gamma camera at variable source-to-background activity concentration ratios. The results of five different methods for background correction showed that – if no background correction was applied – an overestimation of 400% may occur, while for two methods (Kojima method and Buijs method) a difference of less than 10% was found between the estimated and actual activity. These studies showed that the choice of an adequate method for background correction is of vital importance when determining the absolute activity in an organ.

In *chapter 5* dosimetric aspects of radioiodine (^{131}I) treatment for volume reduction of large multinodular goiters are discussed. In patients who suffer from an enlarged thyroid (multinodular goiter), most often a large part of the thyroid is removed surgically. Such surgery carries the risk of substantial

bleeding, vocal cord paralysis and hypoparathyreoidism An alternative way to reduce thyroid volume is treatment with radioactive iodide (Na-^{131}I) This radionuclide emits electrons that are able to destroy thyroid cells Because in these patients the thyroid tissue mass is relatively large, a high dose of radioactive ^{131}I has to be administered Therefore it is important to determine the risks of the radiation burden for the rest of the body

Part of the orally or intravenously administered ^{131}I will accumulate in the thyroid In humans with normal thyroid function (euthyreoidism), the uptake in the thyroid is 5 30% of the administered dose 3 h after administration of iodine and 10 59% after 24 h In humans with thyroid hyperfunction (hyperthyroidism), the uptake after 3 h is more than 30% of the administered dose (up to 80%) The administered activity that does not accumulate in the thyroid is excreted in the urine with a half-life of 8 h This rapid excretion of activity from the body has a positive impact on the radiation burden for the rest of the body The ^{131}I in the thyroid will be incorporated in the thyroid hormones, which are well retained in the thyroid

In this study the administered activity varied from 0 8 to 4 GBq ^{131}I The mean absorbed dose in the thyroid was 94 Gy The mean absorbed doses in the other organs ranged from 60 mGy to 1 Gy The effective dose for the combined organs and tissues outside the thyroid gland was on average 0 27 and 0 19 Sv for euthyreoid and hyperthyroid patients with large goiter respectively Using the total health detriment of 7 3%/Sv given in ICRP Publication 60 and excluding the risk of severe hereditary effects, the life time risk of cancer for the combined organs and tissues outside the thyroid can be estimated as 1 8% and 1 3% for both groups of patients, respectively For patients over the age of 65 years, the life time risk of radiation induced cancer was approximately 0 5% Thus for older people the risk of inducing cancer due to the ^{131}I-treatment is low Therefore, this non-invasive approach is the treatment of choice However, for young people the risk of inducing cancer due to this treatment may be a factor 2 to 3 higher Therefore, for younger patients (<40 y), usually surgery is advised

In *chapter 6* the radiation dose from radiopharmaceuticals for the detection of focal infection and inflammation is calculated Patients may have focal pathology or fever of unknown origin The patients are referred to the department of nuclear medicine to determine the presence or source of the inflammation By means of various nuclear medicine techniques, suspected focal inflammation can be traced and located

Several studies have demonstrated the utility of human immunoglobulin G (IgG), labeled with ^{111}In or ^{99m}Tc to localize infection and inflammation The radiation burden after injection of these radiopharmaceuticals was calculated using the scintigraphic images of five healthy volunteers (^{111}In-IgG)

and seven patients (^{99m}Tc HYNIC -IgG) On the gamma camera images, it was clearly shown that a relatively large amount of ^{111}In was absorbed in the liver and the testes After administration of ^{99m}Tc-HYNIC-IgG accumulation of activity in the testis was shown as well With both radiopharmaceuticals accumulation of activity in the skeleton was observed, this activity was attributed to uptake in the bone marrow (in contrast to uptake in the bone) Due to the differences in physical characteristics between ^{111}In ($T_{1/2}$= 67 3 h and dual gamma energies of 171 and 245 keV) and ^{99m}Tc ($T_{1/2}$= 6 h and a gamma energy of 141 keV), the radiation burden per unit of administered activity was much higher for ^{111}In-IgG than for ^{99m}Tc-HYNIC-IgG For a typical dose of 75 MBq ^{111}In-IgG, the effective dose was estimated to be 19 mSv The effective dose for a typical administered amount of 740 MBq ^{99m}Tc-HYNIC-IgG was 6 mSv These estimates showed that both radiopharmaceuticals can be administered safely from a radiation safely point of view, but that the radiation burden after administration of ^{99m}Tc-HYNIC-IgG was significantly lower than for ^{111}In-IgG

The study described in *chapter 7* concerns the estimation of the relative distribution of activity in bone and red marrow after administration of ^{111}In-labeled radiopharmaceuticals The radiation sensitivity of bone marrow is relatively high a probability of approximately 1% per Gy for the induction of cancer Also the risk of a deterministic effect exists myelosuppression with a threshold dose of 2 Gy Therefore, it is very important to estimate the absorbed dose in the bone marrow accurately If ^{111}In-IgG is administered, for scintigraphic localization of infection or inflammation usually some activity is observed in the skeleton This may be due to uptake of activity in the bone as well as in the red marrow To estimate the uptake of activity in the bone marrow, Regions Of Interest (ROI) were drawn around the lumbar vertebrae and the pelvic bone However, from these images it is not possible to determine whether the measured activity is located in the bone, the red marrow or both Since the riskfactor for inducing cancer in the bone surface is 0 07%/Gy, thus approximately a factor of 15 lower than for the red marrow, it is important to determine the relative activity distribution between red marrow and bone To estimate the distribution of ^{111}In between bone and red marrow, ^{111}In-IgG was administered intravenously to five patients 48 hours prior to a scheduled total hip replacement During surgery a bonechip was removed from the femoral-neck and 4 to 5 ml of red marrow was aspirated from the femoral bone The actual activity in the red marrow and in the bone was 4 5% of the injected dose per kg tissue (ID/kg) and 1 7% ID/kg, respectively Assuming a similar relative distribution in the lumbar spine, an uptake of 0 61% ID could be expected in the vertebrae L2-L4 Erroneously, assigning the total activity to the red marrow, would lead to a total red

marrow uptake of 6 5 %ID/kg being an overestimation of 30%

After administration of ^{111}In-IgG a mean activity of 8 5% ID/kg in the red marrow was found, based on gamma camera images, using the ROI over L2-L4 and assigning all measured activity to the red marrow These studies showed that if one would attribute bone uptake on ^{111}In-IgG scans solely to red marrow, the red marrow dose may be overestimated by a factor of two

In *chapter 8* the absorbed dose of ^{111}In OV-TL3 (Fab')$_2$, a monoclonal antibody-based radiopharmaceutical for the detection of ovarian cancer, is estimated The absorbed doses in the source-organs liver spleen, kidneys and red marrow were estimated based on scintigraphic images The results of two different methods for quantification of absolute activity in organs were similar The average uptake of activity in the liver, spleen, kidneys and red marrow was 18%, 4%, 6% and 17% of the injected activity, respectively The mean absorbed doses in these organs was 0 9, 1 5, 1 2 and 0 5 mGy/MBq, respectively For a typical dose of 140 MBq ^{111}In-OV-TL3 (Fab')$_2$, the effective dose was 56 mSv This dose is higher as compared to the effective doses for two other radiopharmaceuticals that are routinely used for the localization of tumors and/or metastases (17 mSv for 75 MBq ^{201}Tl-chloride and 22 mSv for 185 MBq ^{67}Ga-citrate)

Chapter 9 deals with pharmacokinetics and dosimetric analysis of the anti-ovarian tumor monoclonal antibody ^{131}I-cMOv18 IgG The aim of this study was to evaluate the pharmacokinetics and dosimetry after intraperitoneal or intravenous administration of this MAb Such an analysis would show whether a sufficient absorbed dose can be guided to ovarian tumors to reach a tumor sterilizing effect without unacceptable red marrow toxicity The radiopharmaceutical was administered one week prior to surgery During the preoperative period, gamma camera images were acquired and blood and urine samples were taken Various tissue samples were obtained during surgery The activity in the resected tumor and tissue-samples were measured After intraperitoneal administration of 4 1 GBq ^{131}I cMOv18 IgG an absorbed dose of 30 Gy and 22 Gy can be absorbed at the tumor surface and at 0 2 mm depth in the tumor, respectively, while the red marrow dose remains below the maximum acceptable dose level of 2 Gy For intravenous administration an absorbed dose of 8 Gy in the tumor could be obtained after administration of 3 5 GBq while the dose to the bone marrow would not exceed a dose of 2 Gy

The intention of radioimmunotherapy is to transfer a high absorbed dose to the tumor On the other hand a threshold dose of 2 Gy for deterministic effects in the red marrow (myelosuppression) should be considered This study showed that ^{131}I-cMOv18 IgG could potentially induce a therapeutic response especially if administered intraperitoneally

In *chapter 10* data for effective doses in nuclear medicine diagnostic procedures are summarized. The dose estimations reported in this thesis were similar to the doses calculated for routinely diagnostic used radiopharmaceuticals.

In summary, in this thesis new methods for more accurate estimation of radiation doses for patients have been developed. Furthermore, using the newly developed methods, the absorbed doses for several experimental radiopharmaceuticals for diagnostic use (^{111}In-IgG, ^{99m}Tc-IgG, ^{111}In-OV-TL3 and ^{131}I-cMOv18 IgG) were estimated. The absorbed doses of these new radiopharmaceuticals appeared to be in the same range as those that are currently in routine use in nuclear medicine.

Samenvatting

In de laatste decennia heeft het wetenschappelijk onderzoek in de Nucleaire Geneeskunde zich geconcentreerd op de ontwikkeling en toepassing van nieuwe radiofarmaca voor diagnostiek en therapie. Bijvoorbeeld, de ontwikkeling van monoclonale antilichamen (MAbs) en receptor bindende peptiden heeft geleid tot de introductie van nieuwe klassen van radiofarmaca voor diagnose en therapie. Een andere belangrijke research inspanning betreft de ontwikkeling van radiofarmaca voor Positronen Emission Tomografy (PET).

De combinatie van zowel nieuwe radiofarmaca als het beschikbaar komen van nieuwe beeldvormende technieken, zoals SPECT (Single Photon Emission Tomography) en PET, hebben geleid tot betere en meer adequate diagnostische onderzoeksmethoden en tot een hogere kwaliteit bij medische beslissingen. De sterk verbeterde ruimtelijke resolutie van de beeldvormende systemen maakte het mogelijk om kleinere tumor uitzaaiingen op te sporen en de plaats ervan nauwkeurig te bepalen. Ook kunnen hersen- of hartafwijkingen nauwkeuriger zichtbaar gemaakt worden.

PET- en/of SPECT beelden kunnen nu samengevoegd worden met digitale MRI- of CT-beelden, zodat metabole afwijkingen, die gevonden zijn op de gammacamera beelden, afgebeeld kunnen worden op een anatomische achtergrond van zeer hoge resolutie. Deze benaderingswijze heeft de diagnostische nauwkeurigheid van de onderzoeken sterk verbeterd.

Gedurende het afgelopen decennium is het onderzoeksprogramma van de afdeling Nucleaire Geneeskunde van het Academisch Ziekenhuis in Nijmegen (AZN) toegespitst op het ontwikkelen en optimaliseren van radiofarmaca voor diagnostiek en therapie bij kanker en voor diagnostiek van infecties en ontstekingen. De stralingsrisico's na toediening van deze nieuwe radiofarmaca aan patiënten zijn geschat. De tweede helft van dit proefschrift beschrijft de dosimetrische berekeningen voor enkele van deze nieuwe radiofarmaca.

Voor diagnostische toepassingen, zoals het opsporen van ontstekingen is het stralingsrisico een ongewenst neveneffect (hoofdstuk 6-9). Echter de risico's zijn laag: de geabsorbeerde dosis voor een nucleair geneeskundig onderzoek is 3 mSv, hetgeen overeenkomt met een risico op enige vorm van gezondheidsschade van 2 op de 10.000 onderzoeken. Voor therapeutische toepassingen is het toebrengen van stralingsschade aan het door ziekte aangedaan weefsel juist het doel, zoals bijvoorbeeld bij behandeling van schildklier ziekten (hoofdstuk 5).

Echter, de ongewenste schade aan de overige weefsels dient zo laag mogelijk te zijn. Om te kunnen beoordelen of een speciale behandeling van een tumor met radiofarmaca veilig en/of zinvol is, moet de stralingsdosis en het stralingsrisico geschat worden. Bij voorkeur kan dit gedaan worden aan de hand van een tracerstudie bij de te behandelen patient. Op verschillende tijdstippen na toediening van een tracerdosis van het radiofarmacon wordt de verdeling van de radioactiviteit over de verschillende organen, de verdwijning van de activiteit uit het bloed, de opname van activiteit in de tumor en de verdwijning van de activiteit uit het lichaam bepaald. Uit deze metabole gegevens kan de stralingsdosis voor organen, weefsels of de tumor berekend (hoofdstuk 5, 8 en 9). Eén van de voorwaarden waarop een besluit tot behandeling wordt gebaseerd is dat de gewenste therapeutische stralingsdosis in de tumor (>30 Gy) bereikt kan worden, zonder dat de dosislimiet voor deterministische effecten in enig orgaan overschreden wordt. Bij de meeste therapieen met radiofarmaca is het rode beenmerg het dosis beperkend orgaan.

In *hoofdstuk 1* wordt de betekenis van dosimetrie in de Nucleaire Geneeskunde toegelicht.

In *hoofdstuk 2* worden de principes van de dosimetrische methoden (terminologie, grootheden en eenheden) beschreven. Tevens wordt er een overzicht van de stralingseffecten en stralingsrisico's gegeven.

In *hoofdstuk 3* worden methoden voor data-acquisitie, analyse en bewerken van gegevens van biodistributie studies in patienten samengevat. Met behulp van deze methoden kan de geabsorbeerde dosis geschat worden. De afgelopen jaren is een zekere mate van standaardisatie van deze methoden en technieken ingevoerd door het Medical Internal Radiation Dosimetry Committee of the Society of Nuclear Medicine: het MIRD schema.

In *hoofdstuk 4* worden fantoom experimenten beschreven, waarin de nauwkeurigheid van de werkelijke hoeveelheid activiteit in een orgaan wordt geschat, gebruik makend van verschillende methoden voor achtergrond correctie. Na toediening van het radiofarmacon aan patienten zal de activiteit zich verspreiden over het hele lichaam. Om de exacte hoeveelheid radioactiviteit in een orgaan op een zeker moment te kunnen bepalen moet er een geschikte methode voor correctie van achtergrond activiteit in het omliggende weefsel toegepast worden.

Van een met radioactiviteit gevuld fantoom, dat twee nieren in de buik simuleert, werden opnamen gemaakt met de gamma camera bij diverse verhoudingen tussen de activiteitsconcentratie van bronorgaan en achtergrond. De resultaten van vijf verschillende methoden voor achtergrondcorrectie toonden aan dat – indien geen achtergrondcorrectie toegepast zou worden – een overschatting van 400% zou kunnen ontstaan,

terwijl voor twee methoden (Kojima methode en Buijs methode) een verschil van minder dan 10% tussen de geschatte en de werkelijke activiteit gevonden werd Uit deze studie bleek dat de keuze van een adequate methode voor achtergrond correctie van essentieel belang is bij de bepaling van de absolute activiteit in een orgaan

In *hoofdstuk* 5 worden de dosimetrische aspecten van een behandeling met radioactief jodium (^{131}I) voor volume verkleining van grote multinodulaire strumata beschreven Bij patienten die lijden aan een vergrote schildklier (multinodulair struma), wordt meestal een groot deel van de schildklier operatief verwijderd Het risico bij een dergelijke operatie kan bestaan uit ernstig bloedverlies, verlamming van de stembanden en hypoparathyreoidie Een andere mogelijkheid om het schildklier volume te verkleinen is een behandeling met radioactief jodium (Na ^{131}I) Dit radionuclide zendt elektronen uit die de schildklier cellen kunnen vernietigen Omdat het gewicht van het schildklierweefsel bij deze patienten relatief groot is moet er een hoge dosis radioactief ^{131}I toegediend worden Daarom is het belangrijk om een schatting te maken van de risico's van de stralingsbelasting voor de rest van het lichaam

Een gedeelte van het ^{131}I dat oraal of intraveneus wordt toegediend wordt in de schildklier opgenomen Bij personen met een normaal functionerende schildklier (euthyreoidie) is de opname in de schildklier 5 tot 30% van de toegediende activiteit na 3 uur en 10 tot 60% na 24 uur Bij patienten met een te hard werkende schildklier (hyperthyreoidie) is de uptake na 3 uur meer dan 30 % van de toegediende dosis, oplopend tot 80% De toegediende activiteit die niet in de schildklier wordt opgenomen wordt via de urine uitgescheiden met een halveringstijd van 8 uur Deze snelle uitscheiding van de activiteit uit het lichaam is gunstig voor de stralingsbelasting van de rest van het lichaam Het ^{131}I in de schildklier wordt ingebouwd in de schildklier hormonen, die slechts langzaam vrij komen uit de schildklier

De in deze studie toegediende hoeveelheid activiteit varieerde van 0 8 tot 4 0 GBq ^{131}I De gemiddelde geabsorbeerde dosis in de schildklier was 94 Gy De gemiddelde geabsorbeerde dosis in de andere organen varieerde van 60 mGy tot 1 Gy De effectieve dosis voor alle organen en weefsels buiten de schildklier was gemiddeld 0 27 en 0 19 Sv, respectievelijk voor euthyreote en hyperthyreodie patienten Uitgaande van een totale kans op gezondheidsschade van 7 3%/Sv zoals gegeven in ICRP publikatie 60 en wanneer geen rekening gehouden wordt met de kans op ernstige erfelijke effecten kan de kans op het ontstaan van kanker gedurende de rest van het leven tengevolge van de geabsorbeerde doses in deze organen voor beide groepen geschat worden op respectievelijk 1 8% en 1 3% Voor patienten boven de leeftijd van 65 jaar was het risico op ontstaan van kanker gedurende de rest van het leven

bij benadering 0.5%. Daarom heeft deze niet-operatieve behandeling de voorkeur. Echter bij jonge mensen is de kans op het ontstaan van kanker door deze behandeling een factor twee tot drie hoger. Daarom wordt voor jonge patiënten (< 40 jaar) meestal een operatie geadviseerd.

In *hoofdstuk 6* wordt de stralingsdosis van radiofarmaca voor het opsporen van lokale infectiehaarden en ontstekingen berekend. Patienten kunnen onbekende pathologische haarden of koorts van onbekende oorzaak hebben. De patiënten worden verwezen voor scintigrafisch onderzoek om de aanwezigheid of bron van de ontsteking te bepalen. Via diverse nucleair geneeskundige onderzoeken is het mogelijk om verdachte ontstekingshaarden te traceren en te lokaliseren.

Verscheidene studies hebben het nut van humaan immunoglobuline (IgG), gelabeld met of ^{111}In of ^{99m}Tc voor de lokalisatie van infecties en ontstekingen aangetoond. De stralingsbelasting na injectie van deze radiofarmaca werd berekend aan de hand van scintigrafische opnamen van vijf gezonde vrijwilligers (^{111}In-IgG) en zeven patiënten (^{99m}Tc-HYNIC-IgG). Op de gammacamerabeelden was duidelijk te zien, dat er relatief veel ^{111}In in de lever en de testes werd opgenomen. Ook na toediening van ^{99m}Tc-HYNIC-IgG werd stapeling van activiteit in de testes aangetoond. Bij beide radiofarmaca werd er stapeling van activiteit in het skelet waargenomen; deze activiteit werd beschouwd als beenmerg opname in plaats van opname in het bot. Vanwege het verschil tussen de fysische eigenschappen van het ^{111}In ($T_{1/2}$ = 67.3 uur en gamma energieën van 171 en 245 keV) en ^{99m}Tc ($T_{1/2}$ = 6 uur en gamma energie van 141 keV) is de stralingsbelasting per eenheid van toegediende radioactiviteit voor ^{111}In-IgG veel groter dan voor ^{99m}Tc-HYNIC-IgG. Bij intraveneuze toediening van een standaarddosis van 75 MBq ^{111}In-IgG werd de effectieve dosis geschat op 19 mSv. Voor een standaarddosis van 740 MBq ^{99m}Tc-HYNIC-IgG werd de effectieve dosis geschat op 6 mSv. Deze schattingen toonden aan dat beide radiofarmaca met betrekking tot stralingsrisico veilig toegepast kunnen worden, maar dat de stralingsbelasting tengevolge van ^{99m}Tc-HYNIC-IgG onderzoek significant lager is dan bij een ^{111}In-IgG onderzoek.

In *hoofdstuk 7* wordt een studie beschreven, waarin een schatting gemaakt wordt van de relatieve verdeling van activiteit in bot en beenmerg na injectie van ^{111}In-gelabelde radiofarmaca. De stralengevoeligheid voor beenmerg is relatief hoog: een kans van ruim 1% per Gray op de inductie van kanker. Maar daarnaast is er kans op een deterministisch effect: myelosuppressie met een drempeldosis van 2 Gy. Daarom is het erg belangrijk om de geabsorbeerde dosis in het beenmerg nauwkeurig te bepalen. Wanneer ^{111}In-IgG toegediend wordt voor scintigrafische lokalisatie van infectie of ontsteking wordt meestal enige opname van activiteit in het skelet waargenomen. Dit kan

duiden op opname van activiteit zowel in het bot als in het beenmerg of in beide Om de opgenomen activiteit in het beenmerg te bepalen werden er Regions Of Interest (ROI) over de lumbale wervels en over de bekkenkam getrokken Echter op deze beelden is het niet te onderscheiden of de gemeten activiteit zich in de botmassa of in het beenmerg bevindt of in beide Aangezien de risicofactor op het ontstaan van kanker van het botoppervlak 0 07%/Gy is, dus ongeveer een factor 15 lager dan voor het beenmerg, is het belangrijk de relatieve activiteitsverdeling tussen beenmerg en bot te kennen Om de verdeling van het ^{111}In tussen bot en beenmerg te kunnen schatten, werd er ^{111}In-IgG toegediend aan vijf patienten 48 uur voor aanvang van een voorgenomen operatie ter vervanging van een totale heup Tijdens de operatie werd een botchip verwijderd van de dijbeen-hals Tevens werd er 4 tot 5 ml rood beenmerg uit het dijbeen gehaald De opname van activiteit in het rode beenmerg en in het bot was respectievelijk 4 5 % van de toegediende dosis per kg weefsel (ID/kg) en 1 7% ID/kg Aannemende dat een dergelijke relatieve verdeling ook bij de lumbale wervelkolom bestaat, zou dat betekenen dat de uptake in de lumbale wervels L2-L4 (beenmerg plus bot) 0 61% van de toegediende dosis bedraagt Als deze activiteit, ten onrechte, geheel zou worden toegekend aan het beenmerg dan zou hieruit een beenmerg opname volgen van 6 5 % ID/kg, dus een overschatting van 30%
Na toediening van ^{111}In-IgG werd een gemiddelde activiteit van 8 5% ID/kg in het beenmerg gevonden, gebaseerd op gammacamera beelden, waarbij ROI's over L2-L4 getrokken waren en waarbij de gemeten activiteit in het geheel aan beenmerg werd toegekend Deze studies toonden aan, dat indien men de uit ^{111}In IgG scans geschatte activiteitsopname in het skelet geheel aan het beenmerg zou toekennen, de beenmerg dosis een factor 2 overschat zou kunnen worden

In *hoofdstuk 8* wordt de geabsorbeerde dosis van ^{111}In-OVTL3 (Fab')$_2$ een op een monoclonaal antilichaam gebaseerd radiofarmacon voor detectie van ovarium kanker, berekend De geabsorbeerde dosis in de lever, milt, nieren en rode beenmerg werd geschat aan de hand van scintigrafische beelden verkregen met een gammacamera De resultaten van twee verschillende methoden voor kwantificering van de absolute activiteit in organen waren gelijk De gemiddelde activiteitsopname in de lever, milt, nieren en rode beenmerg was respectievelijk 18%, 4%, 6% en 17% van de geinjecteerde activiteit De gemiddelde geabsorbeerde dosis in die organen was respectievelijk 0 9, 1 5 1 2 en 0 5 mGy/MBq Voor een typische dosis van 140 MBq ^{111}In-OVTL3 (Fab')$_2$ was de effectieve dosis 56 mSv Deze dosis is hoger dan de effectieve doses bij twee andere radiofarmaca, die in de routine toegepast worden voor de lokalisatie van tumoren (17 mSv voor 75 MBq ^{201}Tl-chloride en 22 mSv voor 185 MBq ^{67}Ga-citraat)

In *hoofdstuk 9* wordt de farmacokinetiek en de dosimetrie van het anti-ovarium tumor monoclonale antilichaam ^{131}I cMOv18 IgG beschreven Het doel van deze studie was om de therapeutische mogelijkheden van het monoclonaal antilichaam na toediening in de buikholte (intra-peritoneaal) of na intraveneuze toediening te evalueren Een dergelijke analyse zou kunnen aantonen of er een zodanige geabsorbeerde dosis in de ovarium carcinomen kan worden verkregen, die voldoende is om de tumor te steriliseren zonder dat er een onaanvaardbare schade aan het rode beenmerg berokkend wordt

Het ^{131}I-cMOv18 IgG werd een week voorafgaande aan de operatieve verwijdering van de tumor toegediend Gedurende deze periode werden er dagelijks gammacamera opnamen gemaakt en werden bloed en urine monsters verzameld Tijdens de operatie werden diverse weefselmonsters genomen De activiteit in de uitgenomen tumor en in weefsel monsters werd gemeten Uit dosimetrische analyse bleek dat bij intraperitoneale toediening van 4 1 GBq ^{131}I-cMOv18 IgG een stralingsdosis van 18 Gy bereikt zou kunnen worden in de tumor, terwijl de beenmerg dosis beneden de maximaal tolereerbare dosis van 2 Gy zou blijven Bij intraveneuze toediening zou een dosis van 8 Gy in de tumor kunnen worden geabsorbeerd na toediening van 3 5 GBq, terwijl de beenmerg dosis van 2 Gy niet overschreden zou worden

Het doel van radioimmunotherapie is een hoge geabsorbeerde dosis naar de tumor te leiden, bij een zo laag mogelijke stralingsdosis voor normaal weefsel Er moet rekening gehouden worden met een drempeldosis van 2 Gy voor deterministische effecten in het beenmerg (myelosuppressie) Uit deze studie bleek dat ^{131}I cMOv18 IgG mogelijk een therapeutische reactie kan induceren, met name na intraperitoneale toediening

Samenvattend, in dit proefschrift worden nieuwe methoden beschreven, voor het nauwkeurig schatten van de stralingsbelasting voor de patient Vervolgens werd, gebruik makend van deze nieuw ontwikkelde methodes, de geabsorbeerde doses voor een aantal experimentele radiofarmaca (^{111}In-IgG, ^{99m}Tc IgG, ^{111}In-OVTL3 en ^{131}I-cMOv18 IgG) berekend De stralingsbelasting van deze nieuwe radiofarmaca blijkt in dezelfde orde van grootte te zijn als gebruikelijk in de huidige nucleair geneeskundige praktijk

Dankwoord

Vanaf deze plaats wil ik gaarne allen bedanken die mij tijdens de voorbereiding van dit proefschrift hebben ondersteund, gestimuleerd geadviseerd en geassisteerd

Dr H Beekhuis, waarde Henk Jij hebt me de eerste beginselen van de dosimetrie in de nucleaire geneeskunde bijgebracht en mijn belangstelling voor dit deel van het vakgebied aangewakkerd Zonder jouw voorbeeld, toewijding en kennis zou ik niet op dit spoor van de dosimetrie en dit proefschrift terecht gekomen zijn Daarvoor ben ik je zeer erkentelijk

Prof Dr F H M Corstens, waarde promotor, beste Frans Wij hebben reeds 25 jaar samengewerkt, maar pas in de sfeer van het huidige research programma van de afdeling nucleaire geneeskunde dat het afgelopen decennium onder jouw bezielende leiding is opgebouwd, ontstond een klimaat, waarin het mogelijk werd dat ik ook zelf een promotieonderzoek kon afronden Eindelijk kon je de wens van je eigen promotor vervullen, die jou destijds de raad gaf mij de gelegenheid te geven ook te promoveren Ik ben je er dankbaar voor dat je me tijdens de voorbereiding van dit proefschrift zeer nadrukkelijk en intensief ondersteund en gestimuleerd hebt

Dr O C Boerman, waarde co-promotor, beste Otto Jij introduceerde en ontwikkelde de meeste van de radiofarmaca waarvoor in dit proefschrift de stralingsbelasting is berekend en waaraan ik de fysische en mathematische methodes kon toetsen Jouw ervaring in research, je interesse en je positieve instelling waren een grote steun voor me, de afgelopen jaren Heel hartelijk bedankt

Dr Leon Massuger, Dr Wim Oyen, Dr Dyde Huysmans, Dr Coby Tibben, Dr Carla Molthoff en bijna Dr Els Dams Tijdens onze samenwerking bij jullie promotie onderzoek aan patienten, hebben jullie vaak extra data moeten verzamelen zodat ik de dosimetrische analyses kon uitvoeren Zonder deze welwillendheid had ik dit proefschrift niet kunnen schrijven

Dr Jeffry Siegel, dear Jeff It was nice to work with you during the past two years I learned a lot about quantitative and dosimetric methods concerning radiopharmaceuticals You introduced me to your colleagues in the United States and showed me the world of physics in your country Our discussions by E-mail were very useful and always I received an answer within 24 hours Once again I want to apologize for my English

Beste collega's van de afdeling nucleaire geneeskunde: Adrienne, Antoi, Conny, Dirk-Jan, Dorie, Eddy, Elsen, Emile, Frans, Gonnie, Jo, Magda, Marcel, Marjo, Marjon, Martin, Martijn, Otto, Paul, Peters, Roel, Sandra en Wimmen, bedankt voor jullie loyaliteit gedurende de voorbereiding van dit proefschrift. Enerzijds moest ik soms een beroep doen op jullie inventiviteit, zoals bij de fantoomproeven, anderzijds was ik afhankelijk van jullie metingen bij patienten en tenslotte stelde ik jullie geduld vaak op de proef als mijn hulp of advies gevraagd werd.

Lieve Renz. Ook jij kwam de laatste tijd aandacht te kort. Maar je hebt me altijd aangezet tot promoveren en je hebt me voortdurend gesteund tijdens het bewerken van dit proefschrift. Hartelijk bedankt hiervoor.

Tot slot, veel dank aan mijn ouders, die mij zo stimuleerden tijdens mijn studie. Helaas hebben ze deze door hen zo zeer gewenste gebeurtenis niet meer mogen meemaken.

Curriculum vitae

Wilhelmina Buijs

Is geboren 9 juli 1943 te Hoeven

Behaalde op 1 juli 1961 het eindexamen Hogere Burgerschool aan het Sint Gertrudislyceum te Roosendaal

Verwierf op 8 november 1968 het doctoraalexamen Natuurkunde aan de Faculteit Wiskunde en Natuurkunde van de Universiteit Nijmegen

Is sinds 1 september 1968 als wetenschappelijk medewerker werkzaam aan de Medische Faculteit en Sint Radboudziekenhuis van de Nijmeegse Universiteit, aanvankelijk bij de afdeling Radiologie/Radiotherapie (Hoofd Prof Dr W Penn), vervolgens op het isotopenlaboratorium van de afdeling Interne Geneeskunde (hoofd Prof Dr C L H Majoor) en, sinds 1 april 1984, op de afdeling Nucleaire Geneeskunde (hoofd Prof Dr F H M Corstens)

Behaalde het Diploma "Deskundigheid Stralingsbescherming", Niveau III op 14 juni 1973

Behaalde het diploma "Deskundigheid die benodigd is voor een veilig beheer van een B-laboratorium", Niveau II, op 24 april 1981

Is sinds 8 september 1987 geregistreerd als klinisch fysicus in het register van de Nederlandse Vereniging voor Klinische Fysica voor het Werkterrein Nucleaire Geneeskunde

Was vanaf 1 januari 1985 tot 1 november 1990 eerste voorzitter en van 1 november 1990 tot 1 september 1997 lid van de Commissie Kwaliteitsbevordering (oorspronkelijk "Protocollencommissie") van de Nederlandse Vereniging voor Nucleaire Geneeskunde (NVNG)

Is sinds 3 april 1995 namens de NVNG bestuurslid van de Nederlandse Commissie voor Stralingsdosimetrie (voorzitter Prof Dr J J Broerse)

List of Publications

PUBLICATIONS IN INTERNATIONAL SCIENTIFIC JOURNALS

1 Nadorp J, Vos M, Buijs W, van Munster P, van Tongeren J, Aalberse R, van Loghem E The Significance of the presence of Anti-IgA Antibodies in Individuals with an IgA deficiency *Eur J Clin Invest* 1973, 3 317-23

2 Yap S, Hafkenscheid J, Goossens C Buijs W, Binkhorst H, van Tongeren J Estimation of radiation dosage and transmutationeffect of ^{14}C involved in measuring rate of albumin synthesis with ^{14}C-Carbonate *J Nucl Med* 1975, 16 642-8

3 Boerbooms A, Buijs W Rapid Assessment of ^{99m}Tc-pertechnetate uptake in the knee joint as a parameter of inflammatory activity *Scand J Rheum* 1975, 8 16-01

4 Boerbooms A, Buijs W Rapid Assessment of ^{99m}Tc-pertechnetate uptake in the knee joint as a parameter of inflammatory activity *Arthritis and Rheumatism* 1978, 21 348-52

5 Boerbooms A, Buijs W Assessment of inflammatory activity in knee joint *The Lancet* 1978 II 323 (Letter)

6 Boerbooms A van den Broek W, Buijs W Assessment of ^{99m}Tc-pertechnetate uptake in the joints as a parameter of inflammation activity In *Proceedings of the V th ISRA Symposium* Feltkamp T, van der Korst J, eds Alphen aan den Rijn Stafleu 1979

7 Corstens F, Buijs W, Drayer J, Kloppenborg P Treatment of hyperthyroidism due to Graves' disease with a combination of fractionated low doses of ^{131}I-Iodine and antithyroid drugs In *"Radioactive Isotope in Klinik und Forschung"* 14 Band, Gasteiner Internationales Symposium 1980, herausgegeben von Hofer R, und Bergmann H Wien Egermann, 1980 213-223

8 Van Beusekom H, van den Broek W, van de Putte L, Buijs W, van den Berg W ^{99m}Tc-pertechnetate uptake measurement in the rabbit knee-joint I Standardization of the method and measurements in experimental arthritis *J Rheumat* 1981, 8 31-9

9 Van Beusekom H, van de Putte L, van den Berg W, van den Broek W, Buijs W Antigen handling in antigen-induced joint inflammation kinetics of a second intra-articularly injected dose of antigen in an already established antigen-induced joint inflammation *Immunology* 1981, 44 153-161

10 Van Beusekom H van de Putte L, Buijs W, van den Broek W, van den Berg W ^{99m}Tc pertechnetate uptake measurement in the rabbit knee-joint II Kinetics of $^{99m}TcO_4$ in Normal and Arthritic Rabbit knee-joint *Scand J Rheumat* 1983, 12 59-63

11 Benraad H, Benraad Th, Buijs W, Kloppenborg P "Spironolactone in Essential Hypertension Effects on Kidney Function and Plasma Electrolytes in Relation To Salt Intake" In *Mineralocorticoids and hypertension*, Proceedings of the Boekinger Mannheim Symposium "Mineralocorticoids and Hypertension" in Keulen 1-2 October 1982, Kaufman W, Wamback G, Heller A, Meuren K eds Springer-Verlag, 1983

12 Hermus A Pieters G Pesman G, Buijs W, Smals A, Benraad T, Kloppenborg P Differential Effects of ovine and human corticotrophin releasingfactor in human subjects *Clinical Endocrinology* 1984, 21 589-95

13 Corstens F, Smals A, Buijs W, Kloppenborg P Thyroid function after treatment of solitary autonomous thyroid nodules *The New Eng J Med* 1984, 310 1394
14 Corstens F, Smals A, Buijs W, Kloppenborg P Incidence of hypothyroidism after I-131 treatment of solitary autonomous thyroid nodules *The New Eng J Med* 1984, 319 1393
15 Boerbooms A, Buijs W, Danen M, van de Putte L, Vandenbroucke J Radio-synovectomy in chronic synovitis of the knee joints in patients with reumatoid arthritis *Eur J Nucl Med* 1985, 10 446-449
16 Buijs W, Beentjes L, Corstens F Long term elimination of bismuth from the human body after injection of ^{206}Bi *Health Physics* 1985 49 1267-1269
17 Geven W, Monnens L, Willems H, Buijs W, ter Haar B Renal Magnesium wasting in two families with autosomal dominant inheritance *Kidney International* 1987, 31 1140-1144
18 Geven W, Monnens L, Willems J, Buijs W, Hamel C Isolated autosomal recessive renal magnesium loss in two sisters *Clinical Genetics* 1987, 32 398-402
19 Engels L, Hamer C van de, Buijs W, van Tongeren J Metabolism of orally administered ^{69m}Zn in patients with short bowel syndrome as compared to control subjects *Trace Elements in Medicine* 1987, 4 67-71
20 Beentjes L, Buijs W, Corstens F, Duysings J Radioactive Contamination of Kiev Vacationers after the Tsjernobyl Accident Biological Half life of Cs *Nucl Med Biol* 1988, 15 171-175 *Int J Rad Appl Instrum Part B*
21 Nagengast F, Hectors M, Buijs W, van Tongeren J Inhibition of secondary bile acid formation in the large intestine by lactulose in healthy subjects of two different age groups *Eur J of Clin Invest* 1988, 18 56-61
22 Nagengast F, Werf van der S, Lamers H, Hectors M, Buijs W, van Tongeren J Influence of age, intestinal transit time and dietary composition on fecal bile acid profiles in healthy subjects *Dig Dis Sci* 1988, 33 673-678
23 Van Hengstum M, Festen J, Beurskens C, Hankel M, Van den Broek W, Buijs W, Corstens F The Effect of Positive Expiratory Pressure versus Forced Expiration Technique on Tracheobronchial Clearance in Chronic Bronchitics *Scand J Gastr* 1988, 23 114 118
24 Franssen M, Boerbooms A, Karthaus R, Buijs W, Putte van de L Treatment of pigmented villonodular synovitis of the knee with yttrium-90 silicate prospective evaluations by arthroscopy, histology and ^{99m}Tc pertechnetate uptake measurements *Annals of the Rheumatic Diseases* 1989, 48 1007-1013
25 Van Hengstum M, Festen J Buijs W, Van den Broek W, Corstens F Reproducibility of tracheobronchial clearance in healthy non-smoking subjects *Respiration* 1989, 56 94-102
26 Laan RFJM, van Riel PLCM, van Erning LJTHO, Lemmens JAM, Buijs WCAM, Corstens FHM, Ruijs SHJ and van de Putte LBA Generalized osteoporosis in patients with rheumatoid arthritis Osteoporosis 1990 Proceedings of the Third International Symposium on Osteoporosis Christiansen C, Overgaard K (eds) 1990 Osteopress ApS, Copenhagen
27 Massuger L, Claessens R, Kenemans P, Verheijen R, Boerman O, Meeuwis A, Schijf Ch, Buijs W, Hanselaar T, Corstens F Kinetics and biodistribution in relation to tumour detection with ^{111}In-labelled OV-TL 3 F(ab')$_2$ in patients with ovarian cancer *Nucl Med Commun* 1991, 12 593-609
28 Buijs W, Massuger L, Claessens R, Kenemans P, Corstens F Dosimetric evaluation of immunoscintigraphy using Indium-111-labeled monoclonal antibody fragments in patients with ovarian cancer J of Nucl Med 1992, 33 1113-1120
29 Corten F, Van t Hof M, Buijs W, Hoppenbrouwers P, Kalk W, Corstens F Measurement of mandibular bone density ex vivo and in vivo by dual energy X-ray absorptiometry precision of method *Archives of Oral Biology* 1993, 38 215 219

30 Laan R, Buijs W, Van Erning L, Lemmens J, Corstens F, Ruijs S, Van de Putte L, Van Riel P Differential effects of glucocorticoids on cortical appendicular and cortical vertebral bone mass in patients with rheumatoid arthritis *Calcified Tissue International* 1993, 52 5-9

31 Oyen W, Buijs W, Van Kampen A, Koenders E, Claessens R, Corstens F Intraoperative bone and bone marrow sampling a simple method for accurate measurement of uptake of radiopharmaceuticals in bone and bone marrow *Nucl Med Commun* 1993, 14 112-116

32 Laan R, Buijs W Verbeek A, Draad M, Corstens F, Van de Putte L, Van Riel P Bone mineral density in patients with recent onset rheumatoid arthritis influence of disease activity and functional capacity *Ann Rheum Dis* 1993, 52 21-26

33 Boerbooms A, Buijs W Efficacy and safety of radiation synovectomy with Yttrium-90 a retrospective long term analysis of 164 applications in 82 patients *Brit J Rheumatol* 1993 Dec, 32(12) 1114-5

34 Boerbooms AM, Buijs WC Synovectomy for haemophilic arthropathy 6-21 years of follow-up in 16 patients *J Intern Med* 1994 Oct, 236(4) 479 81

35 Van Dooren-Greebe R Kuijpers A, Buijs W, Kniest P, Corstens F, Nagengast F, De Boo Th, Willems J, Duller P, Van de Kerkhof P The value of dynamic hepatic scintigraphy and serum aminoterminal propeptide of type III procollagen for early detection of methotrexate-induced hepatic damage in psoriasis patients *Br J Dermatol* 1996, 134 481-487

36 Boerbooms AM, Buijs WC Evaluation of Disease Activity in Rheumatoid Arthritis and Other Arthritides Using ^{99m}Technetium Labeled Nonspecific Human Immunoglobulin *J Rheumatol* 1996, 23 405-406 (Letter)

37 Huysmans DAKC, Buijs WCAM, van de Ven MTP, van den Broek WJM, Kloppenborg PWC, Hermus ARMM, and Corstens FHM Dosimetry and Risk Estimates of Radioidine Therapy for Large, Multonodular Goiters *J Nucl Med* 1996, 37 2072-2079

38 Franssen MJAM, Koenders EB, Boerbooms AMTh, Buijs WCAM, Lemmens JAM and van de Putte LBA Does Application of Radiographic Contrast Medium in Radiation Synovectomy Influence the Stability of Yttrium-90 Colloid? *Brit J Rheumat* 1997, 36 506-507 (Letter)

40 Hoogen van den F, Buijs W, Boerbooms A, Putte van de L and Corstens F Quantitative Esophageal Scintigraphy How Reproducible Is This Test? *J Nucl Med* 1997, 38 1665 (Letter)

41 Steffens MG, Boerman OC, Oosterwijk-Wakka JC, Oosterhof GON, Witjes JA, Koenders EB Oyen WJG, Buijs WCAM, Debruyne FMJ, Corstens FHM and Oosterwijk E Targeting of Renal Cell Carcinoma With I-131-Labeled Chimeric Monoclonal Antibody G250 *J Clin Oncol* 1997, 15 1529 1537

42 Buijs WCAM, Siegel JA, Boerman OC and Corstens FHM Absolute Organ Activity Estimated by Five Different Methods of Background Correction *J Nucl Med* 1998, 39 in press

43 Buijs WCAM, Oyen WJG, Dams EThM, Boerman OB, Siegel JA, Claessens RAMJ, van der Meer JWM and Corstens FHM Dynamic Distribution and Dosimetric Evaluation of Human Non-specific Immunoglobulin G labelled with In 111 or Tc-99m *Nucl Med Commun* 1998, 19 743-751

44 Buijs WCAM, Tibben JG, Boerman OC, Molthoff CFM, Massuger LFAG, Koenders EB, Schijf CT, Siegel JA and Corstens FHM Dosimetric Analysis of Chimeric Monoclonal Antibody cMOv18 IgG in Ovarian Carcinoma Patients after Intraperitoneal and Intravenous Administration *Eur J Nucl Med* 1998, in press

STELLINGEN

behorende bij het proefschrift
van
W.C.A.M. Buijs

Patient Dosimetry in Nuclear Medicine

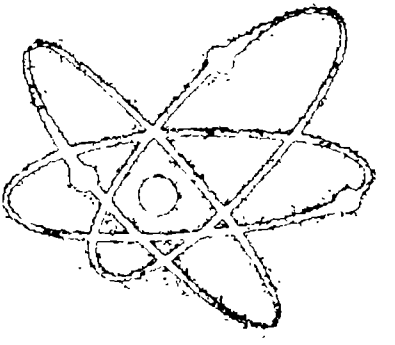

Katholieke Universiteit Nijmegen, 4 december 1998

1 Voor een betrouwbare schatting van de stralingsdosis op basis van de opname van activiteit verkregen van gammacamerabeelden is een juiste keuze van de methode voor achtergrondcorrectie zeer belangrijk. Daarmee kan worden voorkomen dat er afwijkingen tot 400% voor de berekende activiteit ten opzichte van de werkelijke activiteit kunnen ontstaan (dit proefschrift)

♦

2 Het hanteren van de effectieve dosis bij therapie met radionucliden als maat voor de stralingsbelasting van de patient is over het algemeen onjuist. Het is alleen zinvol bij speciale toepassingen (dit proefschrift).

♦

3 Als maat voor de stralingsbelasting wordt vaak de whole body dose opgegeven. Helaas bestaat er geen goede definitie van deze grootheid, zodat soms de effectieve dosis ten onrechte geinterpreteerd wordt als whole body dose.

♦

4 De invoering van de effectieve dosis als vervanging van het effectief dosisequivalent voor de stralingsbelasting leidt in de nucleaire geneeskunde over het algemeen tot lagere waarden voor de dosis, met uitzondering van enkele jodiumverbindingen. Getallen veranderen dan weliswaar, maar dit betekent natuurlijk niet dat de werkelijkheid in de zin van risico's ten gevolge van straling dan ook verandert.

♦

5 Sinds de officiele invoering van het SI-eenhedenstelsel, 20 jaar geleden, is de eenheid van activiteit omgezet van curie naar bequerel en de eenheid van geabsorbeerde dosis van rad naar gray. Het nog steeds naast elkaar toepassen van de oude en nieuwe eenheden geeft aanleiding tot verwarring.

♦

6. Het beperken van doseringen van radiofarmaca voor diagnostiek van individuele patienten middels vergunningen in het kader van de Kernenergiewet is onaanvaardbaar. Een betere benadering is het verwijzen naar de door de Nederlandse Vereniging voor Nucleaire Geneeskunde uitgebrachte bundel 'Aanbevelingen Nucleaire Geneeskunde'.

7 Bij klinisch met ^{131}I behandelde patiënten die geen huisgenoten hebben jonger dan 60 jaar, kunnen, rekening houdend met de voor deze personen geldende risicofactoren, de ontslagnormen aanzienlijk worden verruimd.

♦

8 De adviezen in het onlangs door de Gezondheidsraad uitgebrachte rapport 'Deskundigheidseisen voor medische stralingstoepassingen' dienen, voor wat betreft de basisopleiding geneeskunde, zo snel mogelijk te worden geïmplementeerd in het reguliere medisch curriculum. Een betere kennis van de risico's van straling bij artsen die een rontgen- of nucleair geneeskundig onderzoek aanvragen kan de collectieve dosis door medische toepassingen aanzienlijk verlagen.

♦

9 Kleine hoeveelheden straling zijn weldadig voor de mensheid.

♦

10 Een dedicated 3D PET scanner is niet alleen voordeliger in aanschaf dan een universele 2D-3D PET scanner, maar ook de exploitatiekosten per onderzoek zijn lager. Een bijkomend voordeel is, dat de stralingsbelasting voor de patient en het personeel per onderzoek lager is.

♦

11 Indien de adviezen van zogenaamde beleggingsadviseurs werkelijk waarde zouden hebben, zou hun persoonlijke welstand veel hoger moeten zijn.

♦

12. Vanaf het begin is de natuurkunde een door mannen beheerste wetenschap. De oorzaak hiervan is de religieuze oorsprong van natuurwetenschap; daardoor is de natuurkunde nauw verbonden met de instituten van het christelijk geloof en als gevolg daarvan gesloten voor vrouwen.

(uit: Margareth Wertheim, De broek van Pythagoras, God, Fysica en de strijd tussen de seksen, 1997)

ISBN 90 9012 177 3